Ros9

SPACE
TELESCOPE
SCIENCE
INSTITUTE

Hubble Space Telescope

Faint Object Spectrograph

Instrument Handbook

Version 5.0
May 1994

Revision History

Handbook Version 1.0	October 1985; edited by Holland C. Ford
Handbook Version 1.1	May 1990; edited by Holland C. Ford; supplement by G. F. Hartig
Handbook Version 2.0	April 1992; edited by Anne L. Kinney
Handbook Version 4.0	February 1993; edited by Anne L. Kinney
Handbook Version 5.0	May 1994; edited by Anne L. Kinney

The Space Telescope Science Institute is operated by the Association of Universities for Research in Astronomy, Inc., for the National Aeronautics and Space Administration.

FAINT OBJECT SPECTROGRAPH

INSTRUMENT HANDBOOK

A.L. Kinney

Space Telescope Science Institute
3700 San Martin Drive
Baltimore, MD 21218

Version 5.0
May 1994

Table of Contents

List of Figures

List of Tables

INTRODUCTION

The Faint Object Spectrograph and its use are described fully in the Version 1.0 FOS Instrument Handbook (Ford 1985), and in the supplement to the Instrument Handbook (Hartig 1989), from which much of this handbook is drawn. The detectors are described in detail by Harms *et al.* (1979) and Harms (1982).

This version of the FOS Instrument Handbook is for the refurbished telescope, which is affected by an increase in throughput, especially for the smaller apertures, a decrease in efficiency due to the extra reflections of the COSTAR optics, and a change in focal length. The improved PSF affects all exposure time calculations due to better aperture throughputs, and increases the spectral resolution. The extra reflections of COSTAR decrease the efficiency by 10–20%. The change in focal length affects the aperture sizes as projected on the sky. The aperture designations that are already in use both in the Exposure Logsheets and in the Project Data Base (PDB) have not been changed. Apertures are referred to here by their size, followed by the designation used on the Exposure Logsheet. For example, the largest circular aperture is referred to as the 0.9″ (1.0) aperture, while the largest paired aperture is referred to as the 0.9″ paired (1.0-PAIR) aperture.

Section 1 presents the information that is needed for proposing to observe with the FOS, *i.e.*, for filling out Phase I Proposals. The overall instrument capabilities are described and presented in Table 1.0.1. The spectral resolution is given in Section 1.1 as a function of grating and aperture. The data for calculating exposure times are listed in Section 1.2 in three different ways. The easiest way to calculate exposure time is by simply reading off the detected counts s^{-1} diode^{-1} for a disperser illuminated by a constant input spectrum $F_\lambda = 1.0 \times 10^{-14}$ erg cm^{-2} s^{-1} Å^{-1} (Figure 1.2.3). The count rate can then be scaled to the incident flux expected from the object of interest. The limits for the brightest objects that can be observed with FOS are listed in Section 1.3. A discussion of time resolution with the FOS, *i.e.*, ACCUM, RAPID, and PERIOD modes, is given in Section 1.4. Polarization is discussed in Section 1.5. The FOS noise and dynamic range are discussed in Section 1.6.

Section 2 presents the information that is needed for observing with the FOS after winning HST time, *i.e.*, for filling out Phase II Proposals. The acquisition of targets is described in Section 2.1. Examples of Exposure Logsheets that have been validated by the Remote Proposal Submission System (RPSS) are given for target acquisition modes (for example, ACQ/BINARY), for the standard data taking mode (ACCUM), for the time resolved mode (RAPID), and for spectropolarimetry (observed in ACCUM mode with the optional parameter STEP-PATT = POLSCAN). The example Exposure Logsheets can be copied via anonymous ftp from stsci.edu or 130.167.1.2 (STEIS). The Logsheets are in the subdirectory proposer/documents/props_library, and are called fos_handbook5_example. Caveat emptor.

Section 3 describes briefly the current calibrations for wavelength, absolute photometry, and flat field calibrations of the FOS. See Chaper 16 of the *HST Data Handbook* for a detailed description of FOS calibration. The *HST Data Handbook* is available through the User Support Branch, and is available on-line on STEIS.

Section 4 describes how to simulate FOS spectra with the "synphot" package, which runs in the ST Science Data Analysis System (STSDAS) under IRAF. The simulator, developed by K. Horne, allow input of a large variety of spectra, and incorporate the current calibration files for the FOS.

The details of data taking are given in Appendix A, along with the FOS observing parameters both in the nomenclature of Exposure Logsheets, and in the nomenclature of FOS headers. Appendix A gives also the equations for calculating the start time of any time resolved exposure. Appendix B lists the dead diode tables of December 6, 1993. Appendix C, by M. Rosa, gives a method to estimate the scattered light contribution for a number of spectral types. Appendix D, by C.D. Keyes, supplies line lists and spectra of comparison lamps for wavelength calibration. Appendix E is a compendium of recent FOS calibration reports, including science verification reports. Calibration reports can be obtained by requesting copies from Bonnie Etkins (see below). Appendix F contains Exposure Logsheet examples for different FOS modes.

The FOS Instrument Scientists and relevant ST ScI contacts are:

Tony Keyes, I.S.	410-338-4975	keyes@stsci.edu
Anne Kinney, I.S.	410-338-4831	kinney@stsci.edu
Anuradha Koratkar, I.S.	410-338-4470	koratkar@stsci.edu
Bonnie Etkins, Secretary	410-338-4955	etkins@stsci.edu
User Support Branch	410-338-4470	usb@stsci.edu
Research Support Branch	410-338-1082	analysis@stsci.edu

The procedures for creating a Phase II proposal are being reviewed and revised as this is written. We strongly recommend that users check the Phase II documentation carefully. We also recommend checking on STEIS at that time for a revised version of this Instrument Handbook.

1. INSTRUMENT CAPABILITIES

The Faint Object Spectrograph has wavelength coverage on the blue side from 1150Å to 5400Å (FOS/BL), and on the red side from 1620Å to 8500Å (FOS/RD). There are both low spectral resolution ($\lambda/\Delta\lambda \approx 250$) and high resolution ($\lambda/\Delta\lambda \approx 1300$) modes, as discussed with examples in Section 1.1. The brightest objects observable with FOS have magnitudes from $V \approx 6$ (for a G2V star) to $V \approx 8$ (for a B0V star or for an object with spectral shape of $f_\nu \propto \nu^{-1}$; see Table 1.3.1 for brightness limits of all gratings and spectral types. For magnitudes $V \approx 20$, the target counts are approximately the same as the detector dark counts (0.007 counts s^{-1} diode^{-1} on the blue side, and 0.01 counts s^{-1} diode^{-1} on the red side) for a G2V star observed with the red side or for a B0V star observed with the blue side.

These general traits of FOS blue side (FOS/BL) and red side (FOS/RD) are given in Table 1.0.1.

The Faint Object Spectrograph has two Digicon detectors with independent optical paths. The Digicons operate by accelerating photoelectrons emitted by the transmissive photocathode onto a linear array of 512 diodes. The individual diodes are 0.31″ wide along the dispersion direction and 1.21″ tall perpendicular to the dispersion direction. The detectors span the wavelength range on the blue side from 1150Å to 5400Å (FOS/BL) and on the red side from 1620Å to 8500Å (FOS/RD). The quantum efficiency of the two detectors is shown in Figure 1.0.1. The optical diagram for the FOS is given in Figure 1.0.2. The FOS entrance apertures are 3.6′ from the optical axis of HST.

Dispersers are available with both high spectral resolution (1 to 6Å diode^{-1}, $\lambda/\Delta\lambda \approx 1300$) and low spectral resolution (6 to 25Å diode^{-1}, $\lambda/\Delta\lambda \approx 250$). The actual spectral resolution depends on the point spread function of HST, the dispersion of the grating, the aperture used, and whether the target is physically extended.

The instrument has the ability to take spectra with high time resolution (≥ 0.03 seconds, RAPID mode), and the ability to bin spectra in a periodic fashion (PERIOD mode). Although FOS originally had polarimetric capabilities, the post-COSTAR polarimetry calibrations were not exercised before the writing of this document, so the capabilities post-refurbishment are as yet unknown. See STEIS postings for the most up to date information on the status of polarimetry.

There is a large aperture for acquiring targets using on-board software (3.7″ × 3.7″, designation 4.3). A variety of science apertures are available; a large aperture for collecting the maximum light (effectively 3.7″ × 1.2″, designation 4.3); several circular apertures with sizes 0.86″ (1.0), 0.43″ (0.5), and 0.26″ (0.3); and paired square apertures with sizes 0.86″ (1.0-PAIR), 0.43″ (0.5-PAIR), 0.21″ (0.25-PAIR), and 0.09″ (0.1-PAIR), for isolating spatially resolved features and for measuring sky. In adition, a slit and several barred apertures are available (see Figure 1.1.1).

The blue side sensitivity decreased at a rate of about 10% from launch until 1994.0 but now appears to be more stable. The red side sensitivity is generally stable to within 5%, but was observed to decrease more rapidly in cycles 1 and 2 in a highly wavelength dependent fashion between 1800Å and 2100Å, affecting gratings G190H, G160L, and to a lesser degree G270H. The flat fields for these 3 gratings have changed little since early 1992. Flat fields will be obtained in the large 3.6″ × 1.2″ aperture (4.3) for the G190H, G160L, and the G270H gratings quarterly begining March, 1994 to continue to monitor this affect. The sensitivity of both the blue and the red detectors is being monitored approximately every 2 months in cycle 4.

1.1 Spectral Resolution

The spectral resolution depends on the point spread function of the telescope, the dispersion of the grating, the diode width, the spacecraft jitter, the aperture, and whether the target is extended or is a point source. Table 1.1.1 lists the dispersers, their wavelengths, and their dispersions (Kriss, Blair, & Davidsen 1991). All available FOS apertures are listed in Table 1.1.2 with their designation as given in HST headers, their size and shape. Figure 1.1.1 shows the FOS entrance apertures overlaid upon each other, together with the diode array. The positions of the apertures are known accurately and are highly repeatable.

The spectral resolution (FWHM) is given as a function of aperture in Table 1.1.3 in units of diodes for a point source at 3400Å and for a uniform, extended source. The FWHM does not vary strongly as a function of wavelength, so that this FWHM, together with the dispersion of the gratings given in Table 1.1.1, can be used to approximate the effective spectral resolution.

• **Example.** Observing a point source using the red side with the G270H grating in the 3.7″ × 1.2″ aperture (`4.3`) gives a spectral resolution of

$$\mathrm{FWHM} = 0.96 \text{ diode} \times 2.05\text{Å diode}^{-1},$$

$$\mathrm{FWHM} = 1.97\text{Å}.$$

The same observation with the 0.26″ (`0.3`) slit would have a spectral resolution of

$$\mathrm{FWHM} = 0.92 \text{ diode} \times 2.05\text{Å diode}^{-1},$$

$$\mathrm{FWHM} = 1.89\text{Å}.$$

Line spread functions computed from a model point spread function at 2250Å through the FOS apertures are shown in Figure 1.1.2 in units of microns, where 1 diode width = 50 microns. FOS line spread functions are available in the HST Archive.

1.2 Exposure Time Calculations

The information necessary to calculate exposure time is given here in several forms. First, the HST + COSTAR + FOS efficiencies (Figure 1.2.1), aperture throughputs (Figure 1.2.2), and wavelength dispersions (Table 1.1.1), are given together with a series of relations between count rate and input spectra (Table 1.2.1). Then, count rate per diode at the wavelength corresponding approximately to the peak sensitivity of the given grating is provided in tabular form for a number of spectral types for objects with V=15 (Table 1.2.2). Finally, the count rate per diode is shown in Figure 1.2.3 for both detectors and all gratings, assuming a flat input spectrum ($F_\lambda \propto \lambda^0 = 1.0 \times 10^{-14}$ erg cm^{-2} s^{-1} Å^{-1}) observed throught the 0.9″ aperture (`1.0`).

• **Example using Table 1.2.1.** The count rate for a point source with flux of $F_\lambda = 3.5 \times 10^{-15}$ erg cm^{-2} s^{-1} Å^{-1} at 3700Å using the red detector, in the 0.9″ aperture (`1.0`), with the G400H grating, is given by equation 1 in Table 1.2.1,

$$N_\lambda = 2.28 \times 10^{12} F_\lambda(\lambda\Delta\lambda)E_\lambda T_\lambda.$$

where $F_\lambda = 3.5 \times 10^{-15}$ erg cm^{-2} s^{-1}, $\lambda = 3700$Å, $\Delta\lambda = 3.0$Å (from Table 1.1.1), the efficiency is $E_\lambda = 0.052$ (from Figure 1.2.1), and the throughput is $T_\lambda = 0.95$ (from Figure 1.2.2), so that

$$N_\lambda = 4.4 \text{ counts s}^{-1}\text{diode}^{-1}.$$

The exposure time for a desired signal-to-noise ratio per resolution element is then given by

$$t = \frac{SNR^2}{N_\lambda},$$

which for $SNR = 20$ (for example), gives $t = 400/4.4$ counts sec^{-1} diode^{-1} = 91 s. For a source with a count rate comparable to the dark count rate d, this equation becomes

$$t = \frac{SNR^2}{N_\lambda}\left(\frac{1 + N_\lambda/d}{N_\lambda/d}\right).$$

• **Example using Table 1.2.2.** As a comparison, count rates for objects of representative spectral type with V=15.0 are given in Table 1.2.2 at the wavelengths corresponding to the peak response of a given grating. The example given above corresponds to an object with power law $F_\nu \propto \nu^{-2}$, V=15.0, observed with the G400H grating on the red side.

• **Example using Figure 1.2.3.** Alternatively, the count rate for observations in the 0.9″ (`1.0`) aperture can be read directly from Figure 1.2.3 and scaled to the appropriate flux. For the example given above, with $F_\lambda = 3.5 \times 10^{-15}$erg cm^{-2}s^{-1}Å^{-1}, the count rate per diode at 3700 Å is given by $N_\lambda = (3.5 \times 10^{-15}/1.0 \times 10^{-14}) \times n_\lambda$counts sec^{-1} diode^{-1}, where n_λ is the count rate as given in Fig. 1.2.3. $N_\lambda = 0.35 \times 12.0 = 4.2$ counts s^{-1} diode^{-1}. To calculate the count rate in other science apertures, the count rate must be corrected according to the relative throughputs according to aperture, in Figure 1.2.2.

When observing in time resolved modes, the total observing time can become dominated by the read–out time for FOS data. Section 1.4 below discusses the time to read–out the FOS in the context of RAPID observations.

1.3 Brightness Limits

The photocathode can be damaged if illuminated by sources that are too bright. The brightness limits of the detectors have been translated into a limit of total counts detected in 512 diodes per 60 seconds—the overlight limit. If the overlight limit is exceeded in a 60 second interval, the FOS automatically safes—*i.e.*, the FOS shuts its aperture door, places all wheels at their rest position, and stops operation. The overlight protection limit is 1.2×10^8 counts per minute summed over the 512 diodes for the gratings and 3×10^6 counts per minute for the mirror. The visual magnitudes for unreddened stars of representative spectral types corresponding to this limiting count rate are given in Table 1.3.1 for all grating settings. The restrictions on target brightness are also found in the Bright Object Constraints Table of the Proposal Instructions (Table 5.15).

1.4 Time Resolution

The manner in which FOS data are obtained depends on which of the modes (*e.g.* ACCUM, RAPID, or PERIOD) are used.

FOS data are acquired in a nested manner, with the innermost loop being livetime plus deadtime (see Appendix A for a full description of data taking). The next loop sub–steps the diode array along the dispersion direction (X direction), with steps one-quarter of the diode width (12.5 micron, or 0.076″). To minimize the impact of dead diodes, this loop of data–taking is continued by sub–stepping in steps of one-quarter of the diode width, but starting at the adjacent diode. This over–scanning is repeated until spectra are obtained over 5 continuous diodes, or a total of 20 sub–steps.

A typical data taking sequence would divide the exposure time into twenty equal bins, and then perform the sequence of (livetime + deadtime), stepped four times. That sequence would be performed 5 times, each time stepping to the next diode. As each of the 5 over-scanned spectra are obtained, they are added to the same memory locations of the previous spectra, so that the over–scanning does not increase the amount of data. The data taking is then performed as (livetime + deadtime) × sub–stepping × over–scanning, or

$$(\mathrm{LT} + \mathrm{DT}) \times 4 \times 5.$$

1.4.1 ACCUM

FOS observations longer than a few minutes are automatically time resolved. Spectra taken in a standard manner in ACCUM mode are read out at regular intervals. The red side (FOS/RD) is read out at ≤ 2 minute intervals, while the blue side (FOS/BL) is read out at ≤ 4 minute intervals. The standard output data for ACCUM mode preserve the time resolution in "multi–group" format. Each group of data has associated group parameters with information that can be used to calculate the start time of the interval, plus a spectrum for each 2 minute (for red side, 4 minute for blue side) interval of the observation. Each consecutive spectrum (group) is made up of the sum of all previous intervals of data. The last group of the data set contains the spectrum from the full exposure time of the observation. For details on data formats, see Part VI of the HST Data Handbook (ed. Baum 1994).

1.4.2 RAPID

For observations needing higher time resolution, RAPID mode reads out FOS data at a rate set by the observer with the parameter READ-TIME. The shortest READ-TIME is 0.036 seconds. RAPID data is also in group format but contains a header only at the beginning of the data. Each group then contains group parameters with FOS related information followed by the spectrum for one time segment. (Of particular interest among the group parameters is FPKTTIME, which is used to derive the start time for each individual exposure, as given in Appendix A.)

READ-TIME is equal to livetime plus deadtime plus the time to read out FOS (see Appendix A and Welsh, Keyes, & Chance 1994),

$$\begin{aligned}\mathrm{READTIME} &= (\mathrm{LT} + \mathrm{DT}) \times \mathrm{INTS} \times \mathrm{NXSTEPS} \times \mathrm{OVERSCAN} \times \mathrm{YSTEPS} \times \mathrm{SLICE} \\ &\quad \times \mathrm{NPATT} + \mathrm{ROT}.\end{aligned}$$

where NXSTEPS=SUBSTEP, and is usually set to 4, OVERSCAN=COMB=MUL, and is usually set to 5, YSTEPS=Y-SIZE, and is almost always set to 1, and where ROT refers to the Read-Out Time. The Read–Out Time for FOS is dependent on the telemetry rate, and on the amount of data to be read out, which is dependent on number of diodes (*i.e.,* , the wavelength range) being observed, as well as on the sub–stepping.

$$ROT = \frac{15}{14} \times \frac{1024}{RATE} \times \mathrm{NSEG(WORDS)} \times \mathrm{SUBSTEPS} \times \mathrm{YSTEPS}$$

where RATE is the telemetry rate, and NSEG(WORDS) is given by

$$\text{NSEG} = 1 \text{ if } (\text{WORDS} - 50) < 61$$

$$\text{NSEG} = 1 + 1 + \text{INTEGER}\left(\frac{\text{WORDS} - 50}{61}\right) \text{ otherwise}$$

where WORDS = (NCHNLS + OVERSCAN − 1), NCHNLS is the number of diodes to be read out (with a maximum of 512 and a minimum of 46 for an OVERSCAN of 5), and INTEGER truncates to the next lowest integer. To achieve the fastest READ-TIMES, the RATE of reading data can be increased from the default telemetry rate of 32kHz to 365kHz, the wavelength region can be decreased, and sub–stepping set to 1. The amount of data being taken by FOS must be decreased to achieve the fastest READ-TIME because a smaller amount of data can be read out in a faster time. The relation between number of diodes read out and wavelength coverage can be derived from Table 1.1.1. (Table 1.1.1 is accurate to within a few Ångstroms since it is based on data that was not corrected for the geomagnetically induced image drift, Kriss, Blair, & Davidsen 1991).

The observer should be aware of the fact that the percentage of time spent accumulating data in RAPID can be very small depending on how the parameters are set. Figure 1.4.1, from Welsh *et al.* (1994) shows the duty cycle, or ratio of time spent accumulating data over READ-TIME as a function of READ-TIME. Given the two values of telemetry rate (32,000, and 365,000) and the three possible values of SUBSTEP (4, 2, and 1), there are six curves for duty cycle. The parameters should be set to maximize duty cycle, while maintaining the resolution and wavelength coverage necessary for the scientific objectives.

• **Example** For an FOS RAPID observation requiring a READ-TIME of 0.2 seconds, Figure 1.4.1 shows that to achieve this short READ-TIME, the SUB-STEP must be set equal to 1, and that the telemetry rate is automatically set to the high (365kHz) rate. This results in $WORDS = 512 + 5 - 1$, and $NSEG = 1 + 1 + INT([516 - 50]/61) = 9$, leading to a ROT given by

$$ROT = 15/14(1024/365000) \times 9$$

$$ROT = 0.02705.$$

Thus the READ-TIME, made up of Read-Out Time plus (LT+DT) times the multiplicative factors given above can be obtained by setting SUB-STEP=1, and READ-TIME=0.2.

1.4.3 PERIOD

For objects that have a well known period, FOS data can be taken in PERIOD mode in such a way that the period is divided into BINS, where each bin has a duration of Δt = period/BINS. The period of the object is specified by the parameter CYCLE-TIME. The spectrum taken during the first segment of the period, Δt_1, is added into the first memory location. The spectrum taken during the second segment, Δt_2, is added to a contiguous memory location, and so on. The number of segments that a period can be divided into depends on the amount of data each spectrum contains, which depends on the number of sub-steps, whether or not the data are overscanned, and how large a wavelength region is to be read out. If the full range of diodes are read out, and the default observing parameters are used, 5 BINS of data can be stored. PERIOD mode data are single group, with a standard header followed by the spectra stored sequentially, where there are BINS spectra.

The data size, which cannot exceed 12,288 pixels, is given for PERIOD by

$$\text{Data size} = (\text{NCHNLS} + \text{MUL} - 1) \times \text{SUBSTEP} \times \text{BINS}$$

where BINS applies to PERIOD mode only. BINS is the number of time–segments into which the periodic data are divided. If the observer needs a larger number of BINS than 5, the wavelength range can be decreased, or the sub–stepping can be decreased to 2 or 1. (See Table 1.1.1 for relation between number of diodes [NCHNLS], and wavelength dispersion.)

1.5 Polarization

The deployment of COSTAR resulted in two extra reflections for light entering the FOS. These extra reflections introduce instrumental polarization so that polarization measurements have become difficult and possibly infeasible with the FOS. However, the section on polarization is included here because the FOS team felt that the G190H and the G270H grating may be used for polarization observations if it can be recalibrated properly. Calibrations in Cycle 4 will be used to quantify the polarimetric capability. Thus, proposals for the use of FOS polarimetric capabilities can be submitted, and GO's are recommended to survey updates to polarimetric capabilities on STEIS (see chapter 4 for logging onto STEIS).

A Wollaston prism plus rotating waveplate can be introduced into the light beam to produce twin dispersed images of the slit with opposite senses of polarization at the detector (Allen & Angel 1982). Although there are two waveplates available, only waveplate B is currently recommended for use, and only in the G190H and the G270H gratings. (See Allen & Smith 1992 for polarization calibration results.)

Although the "A" waveplate was designed to do well at Lyα λ 1216Å, the split spectra are not well separated by the "A" waveplate, so that the polarization at Lyα cannot be observed. Linear polarization observations should use the "B" waveplate and gratings G130H, G190H, and G270H.

The sensitivity of the polarizer depends upon its throughput efficiency. The detector can observe only one of the two spectra produced by the polarizer at one time, so that another factor of two loss in practical throughput occurs. The count rate is given by

$$\text{Count rate(pol)} = \text{Count rate(FOS)} \times \eta_{thr} \times 0.5,$$

where η_{thr} is found in Figure 1.5.1.

1.6 FOS Noise and Dynamic Range

The minimum detectable source levels are set by instrumental background, while the maximum accurately measurable source levels are determined by the response times of the FOS electronics.

When the FOS is operating outside of the South Atlantic Anomaly, the average dark count rate is roughly 0.01 counts s^{-1} diode^{-1} for the red detector and 0.007 counts s^{-1} diode^{-1} for the blue detector (Rosenblatt *et al.* 1992). However, Rosenblatt *et al.* note that the background count rate varies with geomagnetic latitude so that higher rates are observed at higher latitudes. Furthermore, there is some evidence that the above dark rates systematically underestimate the actual dark counts by $\approx$ 30%.

The detected counts s^{-1} diode^{-1} plots given in Figure 1.2.3 for an input spectrum with constant flux of $F_\lambda = 1 \times 10^{-14}$ erg cm^{-2} s^{-1} Å^{-1} can be compared with the observed dark count rate to determine the limiting magnitude for the FOS.

• **Example.** For an object observed at 2600Å with the red side G270H grating in the 0.9″ (1.0) aperture, an incident flux of $F_\lambda = 4.7 \times 10^{-17}$ erg cm^{-2} s^{-1} Å^{-1} would produce a count rate comparable to the red side dark rate. For an object observed at 2600Å with the blue side G270H grating in the 0.9″ (1.0) aperture, an incident flux of $F_\lambda = 4.7 \times 10^{-17}$ erg cm^{-2} s^{-1} Å^{-1} would produce a count rate comparable to the blue side dark rate.

In the other extreme, for incident count rates higher than approximately 100,000 counts s^{-1} diode^{-1}, the observed output count rate does not have an accurate relation with the true input count rate. Figure 1.6.1 shows a determination of the relation between true count rate and observed count rate, as measured by Lindler & Bohlin (1986, measured for high count rates for the red side only). For observed count rates above 50,000 counts s^{-1} diode^{-1}, the correction exceeds a factor of 2 and the accuracy decreases drastically. By the time a true count rate of 200,000 counts s^{-1} diode^{-1} is reached, the error in the correction to the true rate is of order 50%. A correction is applied in the pipeline processing to account for this detector non-linearity at high count rates.

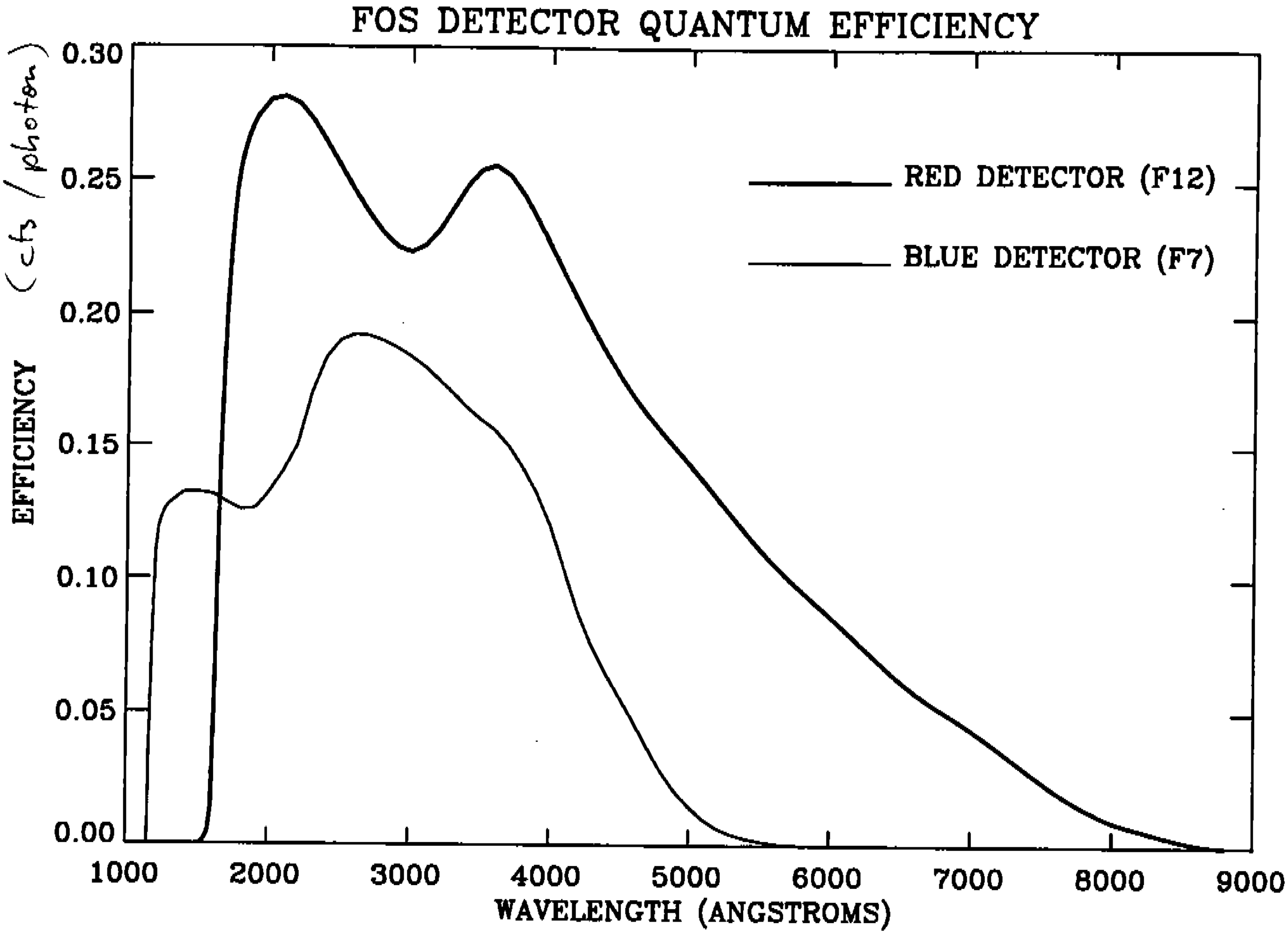

Figure 1.0.1: Quantum efficiency of the FOS Flight detectors.

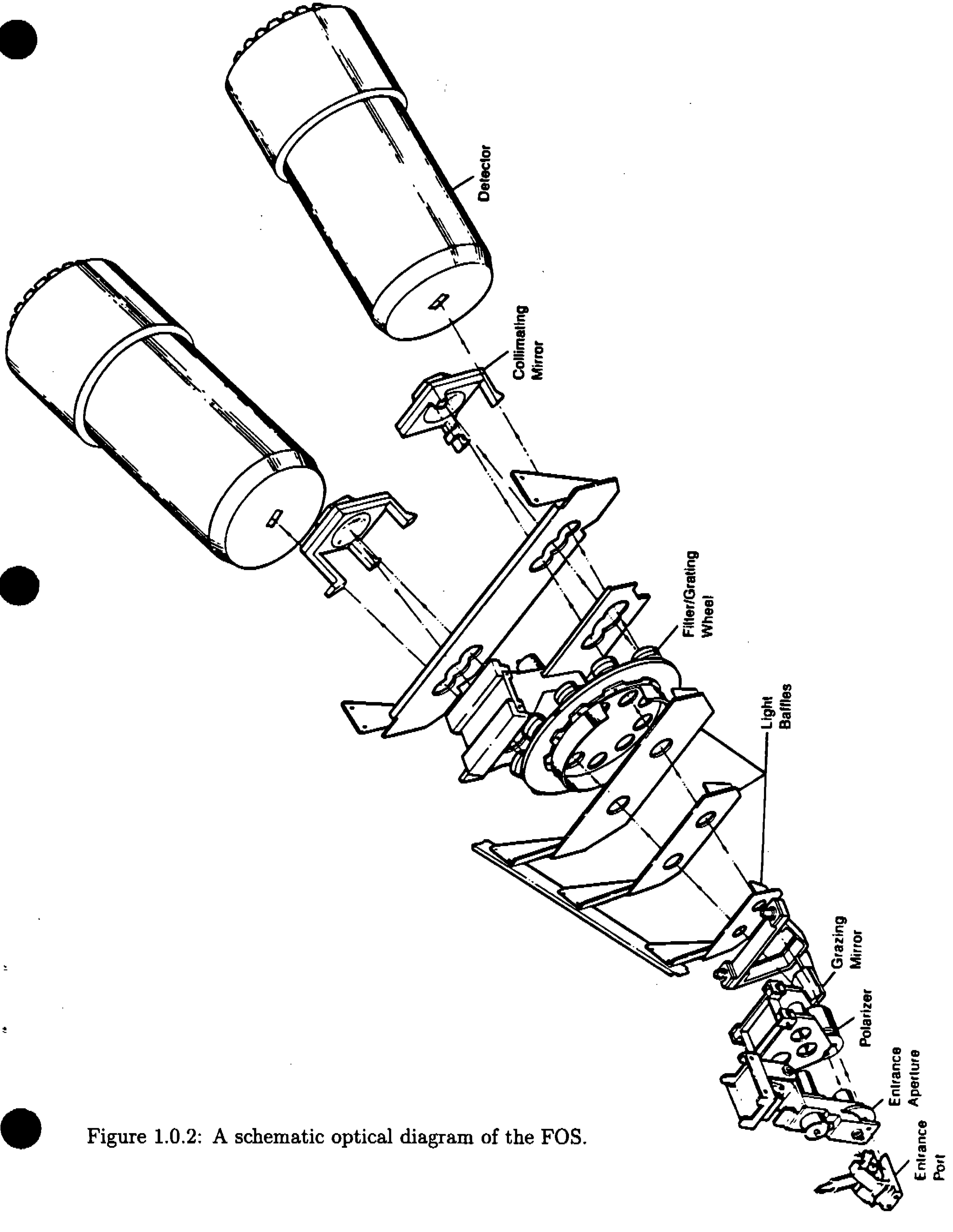

Figure 1.0.2: A schematic optical diagram of the FOS.

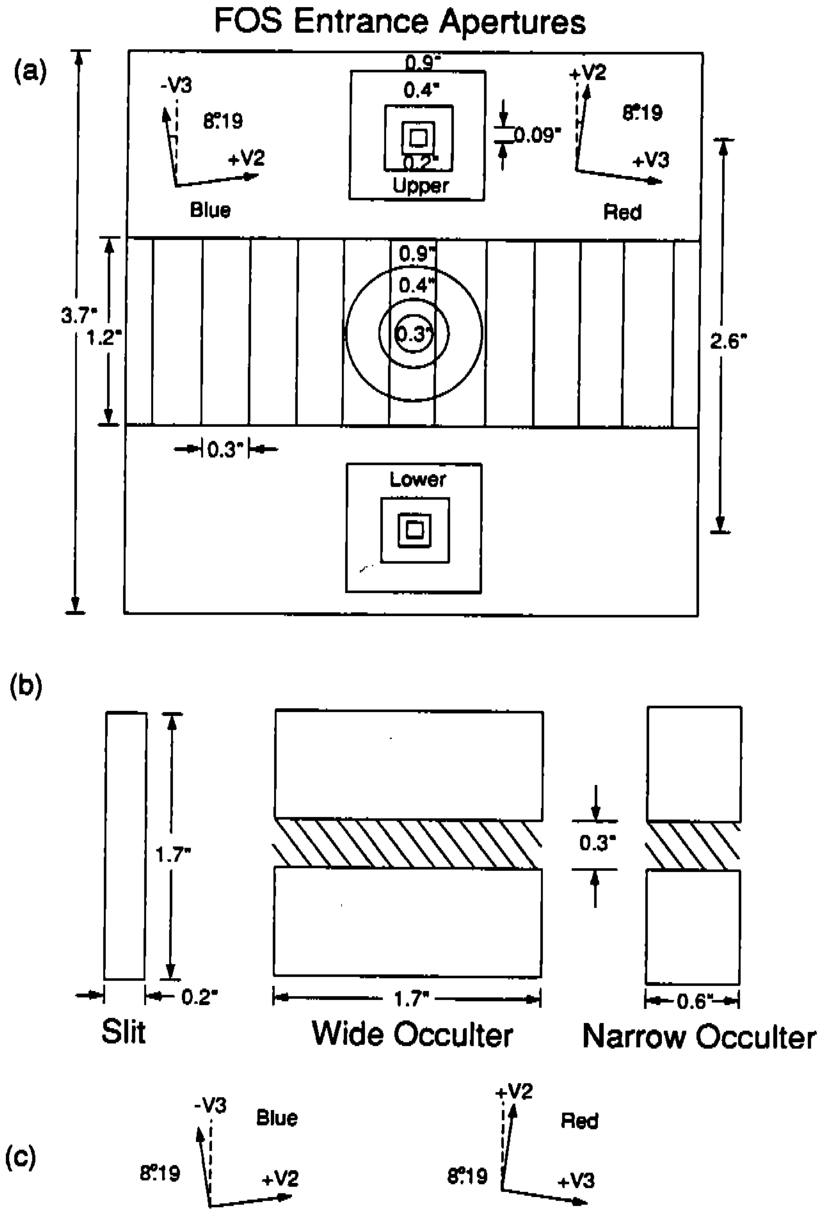

Figure 1.1.1: A Schematic of the FOS Apertures projected onto the sky. The upper panel (a) shows the array of 0.30″ × 1.21″ diodes projected across the center of the 3.66″ × 3.71″ target acquisition aperture. The target acquisition aperture and the single circular apertures position to a common center. The pairs of square apertures position to common centers with respect to the target acquisition aperture as shown in the figure. Either the upper aperture (the "A" aperture, which is furthest from the HST optical axis) or the lower aperture (the "B" aperture, which is closest to the HST optical axis) in a pair can be selected by an appropriate y-deflection in the Digicon detectors. The lower panel (b) shows three more slits that position to the center of the target acquisition aperture. The bottom of the figure (c) shows the orientation of the direction perpendicular to the dispersion (shown as a dashed line) relative to the HST V2, V3 axes. The FOS x-axis is parallel to the diode array and positive to the left; the y-axis is perpendicular to the diode array and positive toward the upper aperture. The angle between the FOS/BLUE and the FOS/RED slit orientation is 73.6 degrees.

FOS Line Spread Function at 2250Å

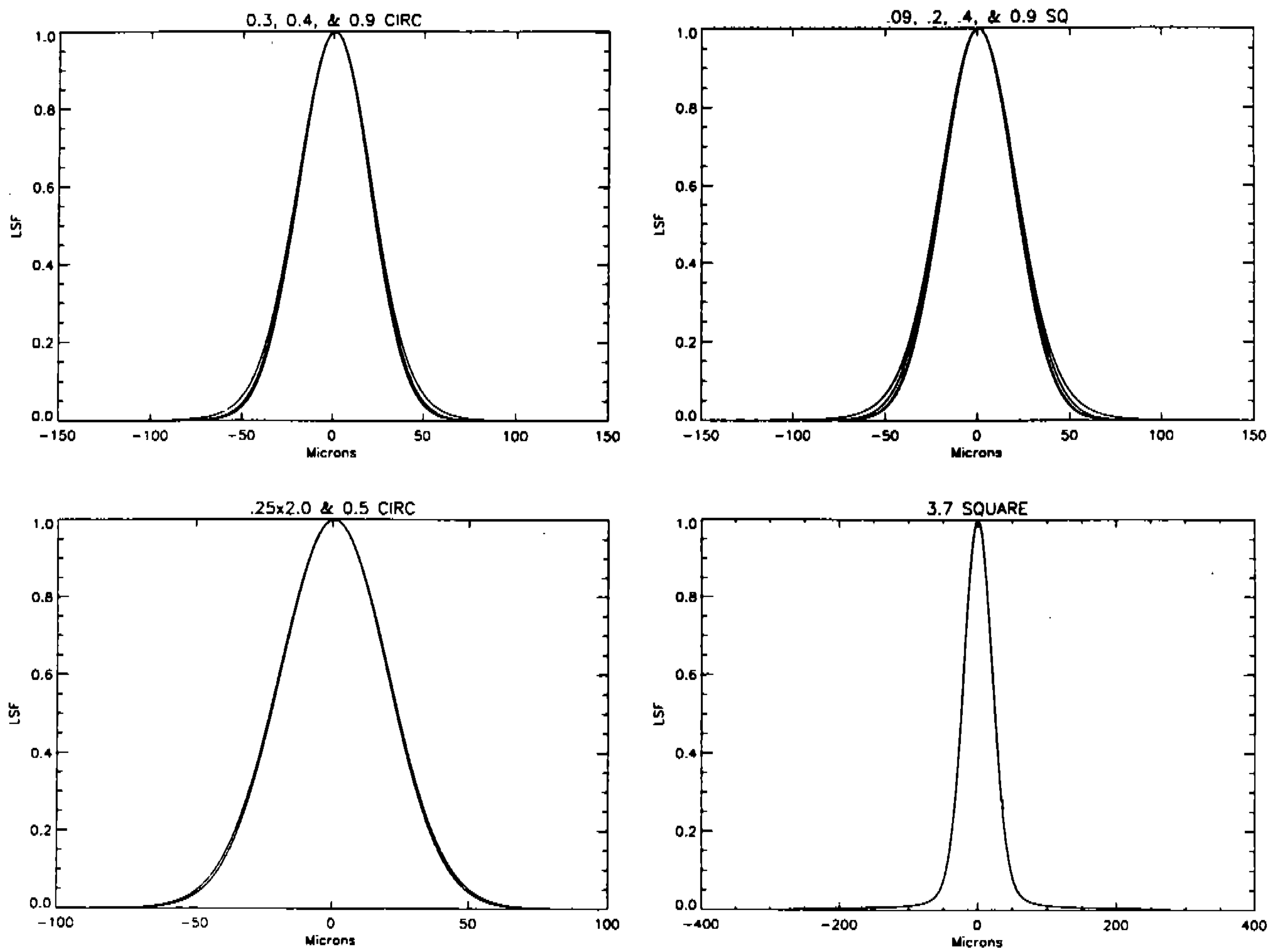

Figure 1.1.2: The solid curves are spectral line spread functions for various FOS apertures. Ordinate shows relative intensity versus distance in the dispersion direction in microns (one diode, equal to one nominal spectral resolution element, is 50 microns).

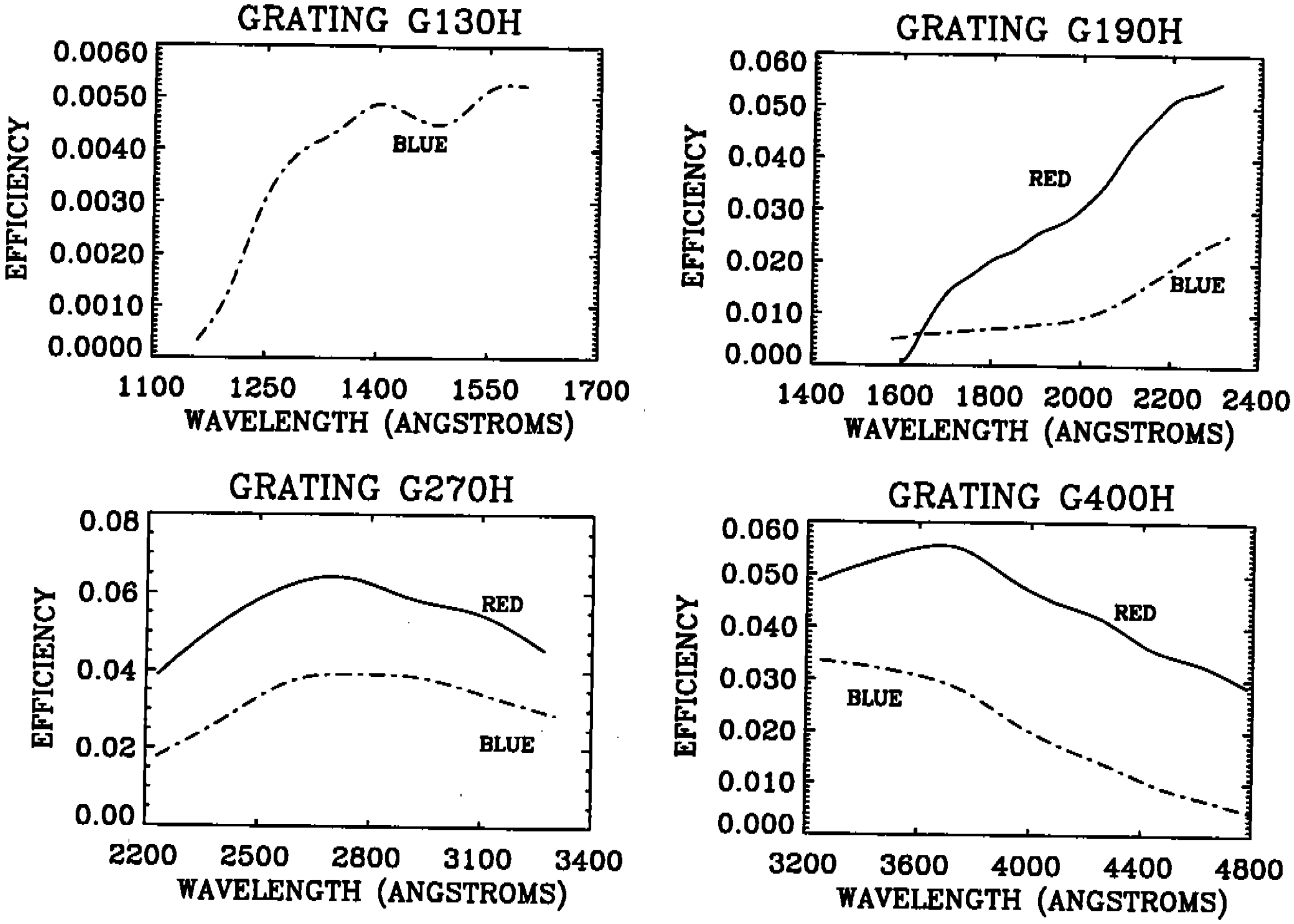

Figure 1.2.1: HST + FOS + COSTAR Efficiency, E_λ vs. λ.

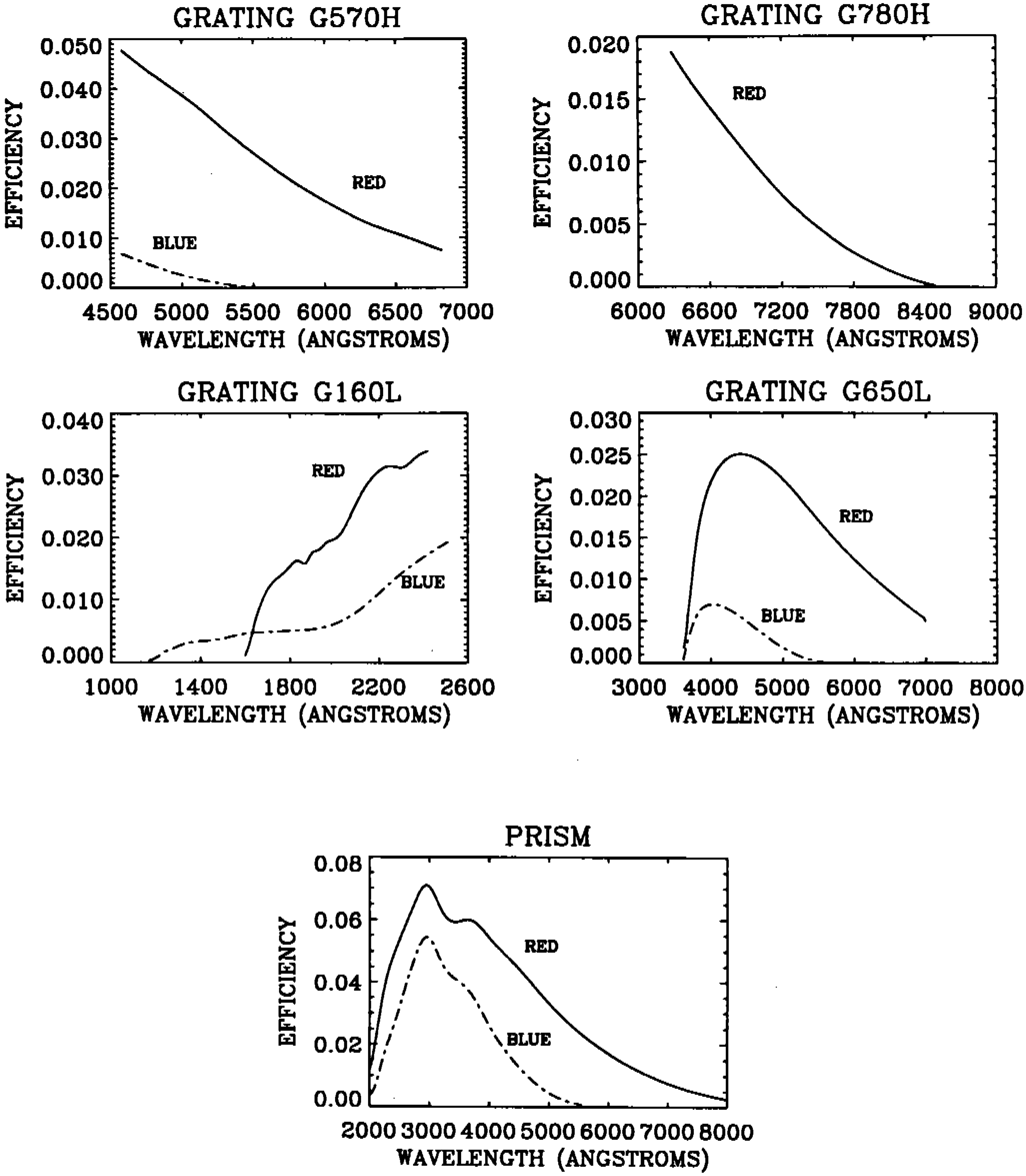

Figure 1.2.1 (cont.): HST + FOS + COSTAR Efficiency, E_λ vs. λ.

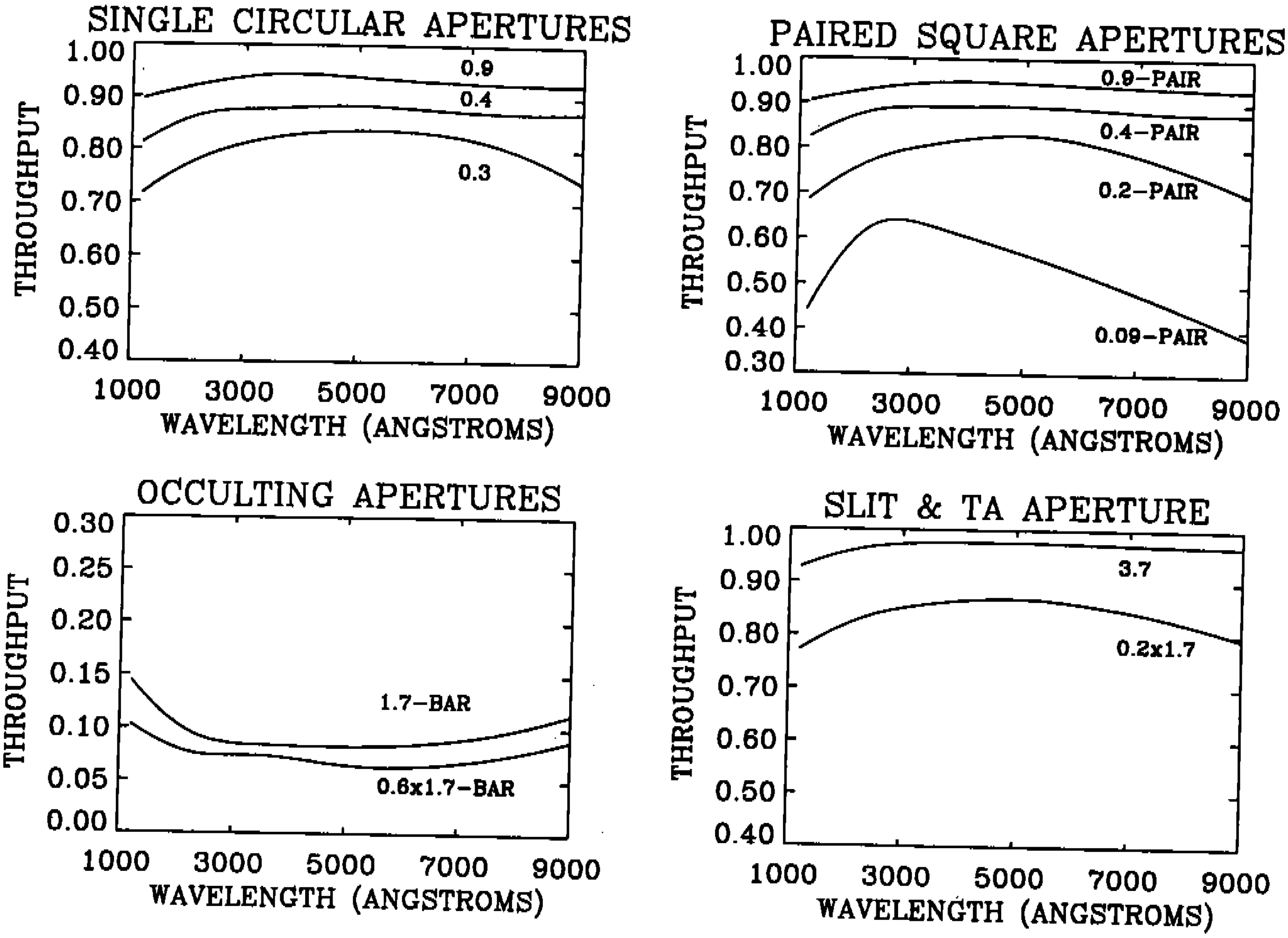

Figure 1.2.2: Fraction of light transmitted by the apertures after deployment of COSTAR for a perfectly centered point source.

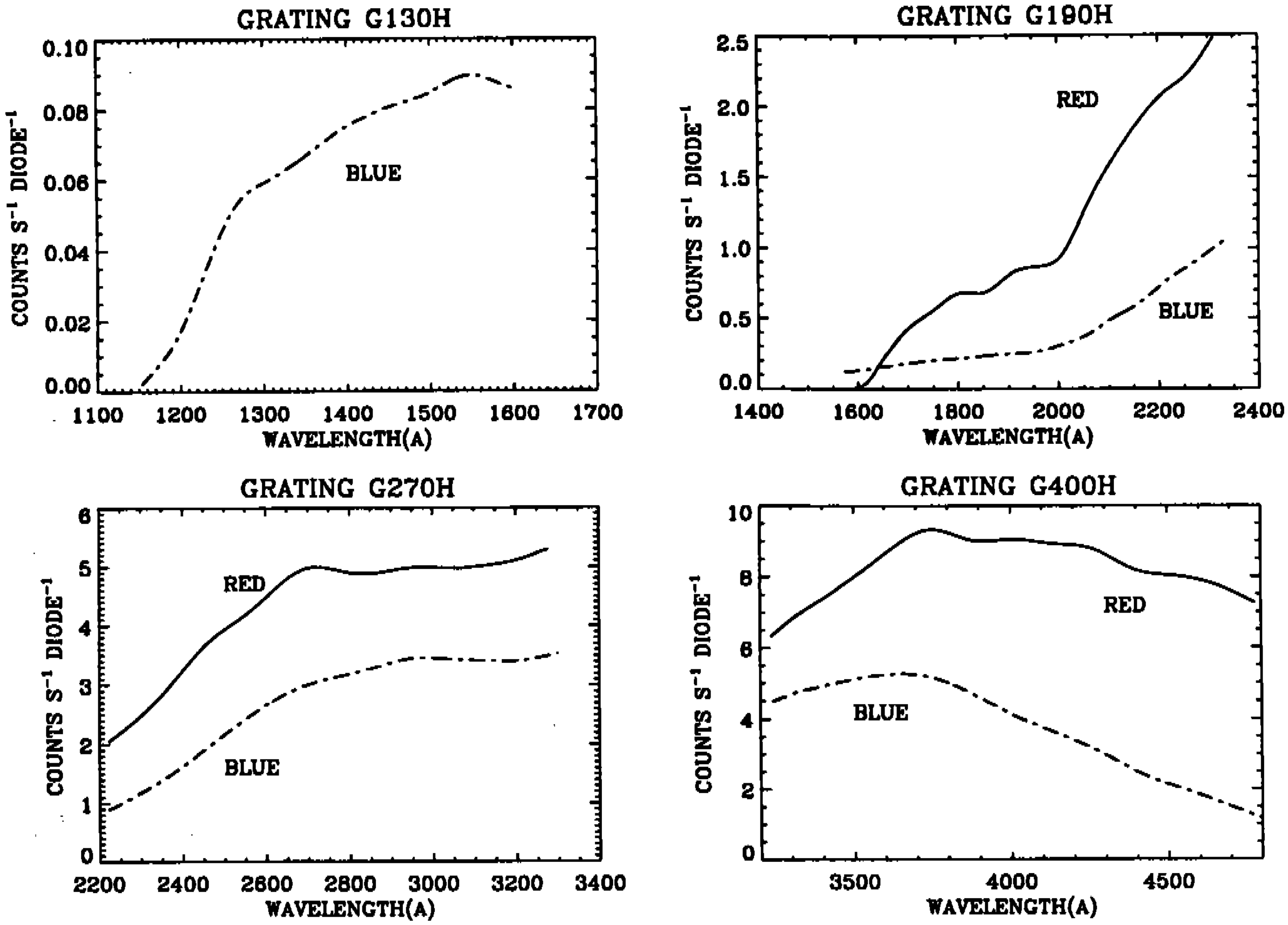

Figure 1.2.3: Detected counts-s^{-1}-diode^{-1} for the post-COSTAR FOS 0.9″ (**1.0**) aperture. Input spectrum is $F_\lambda = 1 \times 10^{-14}$ erg-cm^{-2}-s^{-1}-Å^{-1} ($F_\nu \propto \nu^{-2}$; V = 13.9).

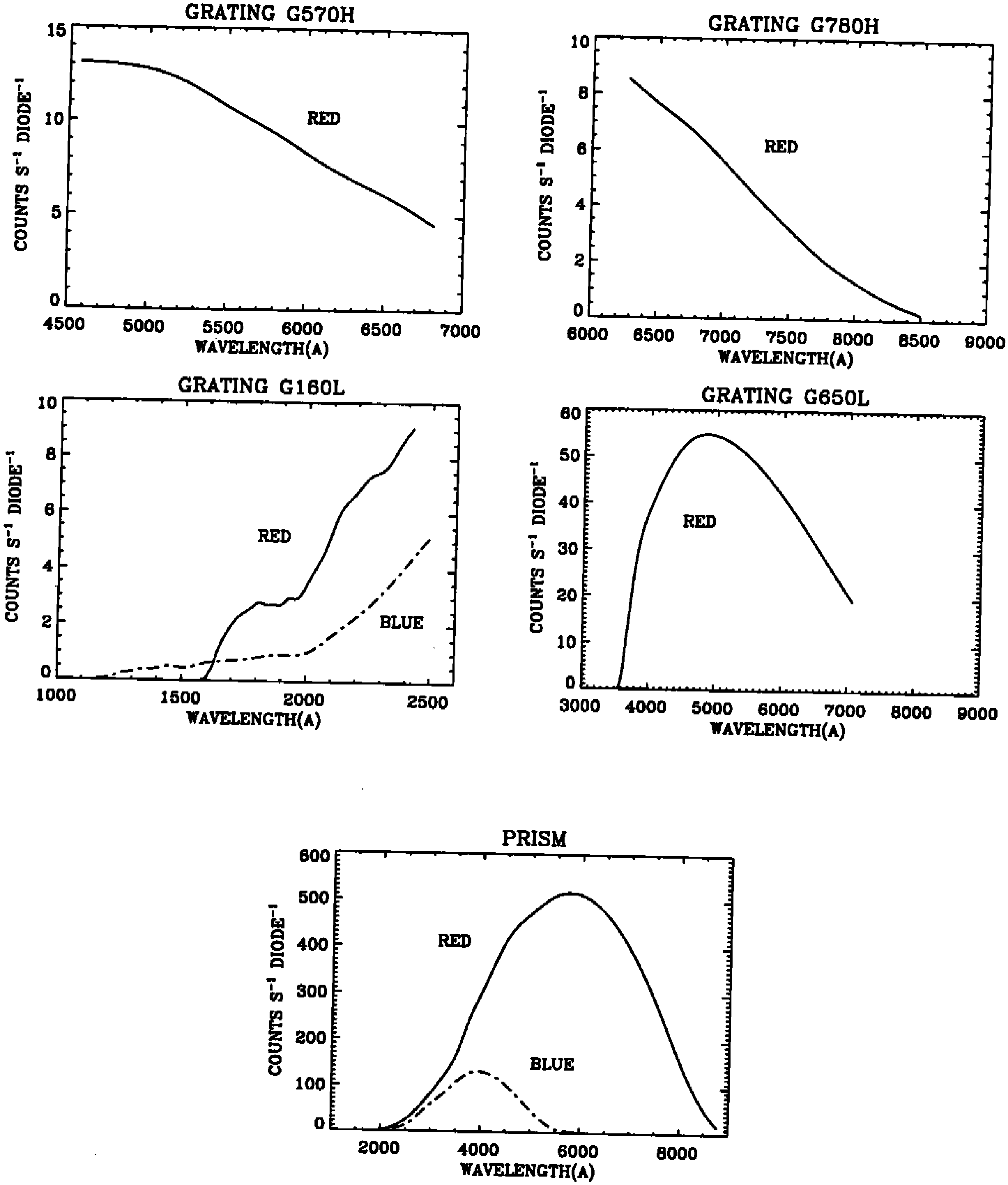

Figure 1.2.3 (cont.): Detected counts-s^{-1}-diode^{-1} for the post-COSTAR FOS 0.9″ (1.0) aperture. Input spectrum is $F_\lambda = 1 \times 10^{-14}$ erg-cm^{-2}-s^{-1}-Å^{-1} ($F_\nu \propto \nu^{-2}$; V = 13.9).

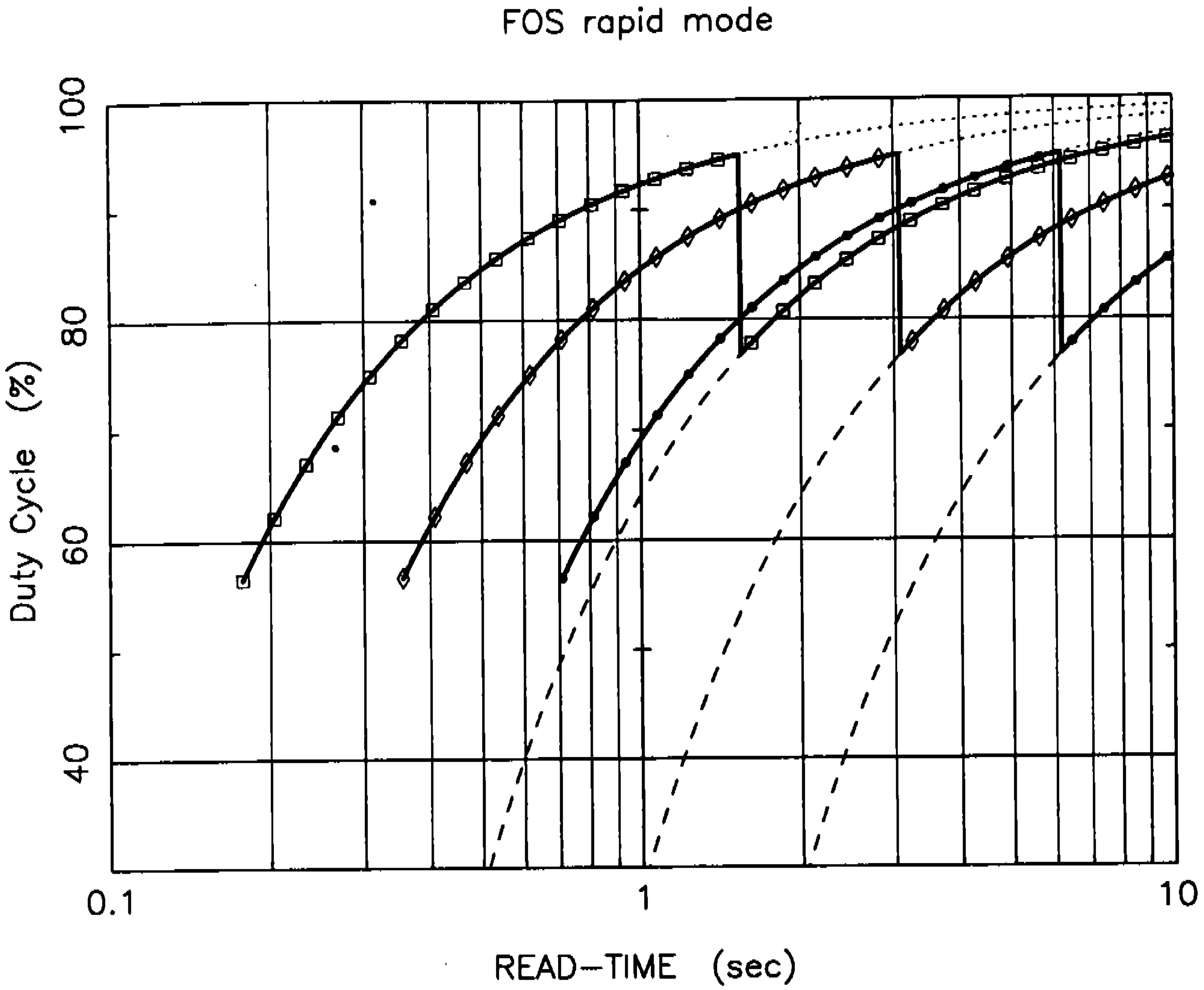

Figure 1.4.1: Percentage of time spent accumulating data in RAPID mode as a function of READ-TIME, telemetry rate, where the high telemetry rate (365kHz) is marked by a solid line and the low rate (32kHz) is marked by the dashed line, and SUBSTEP, where SUBSTEP=1 is marked by squares, SUBSTEP=2 is marked by diamonds, and SUBSTEP=4 is marked by filled dots.

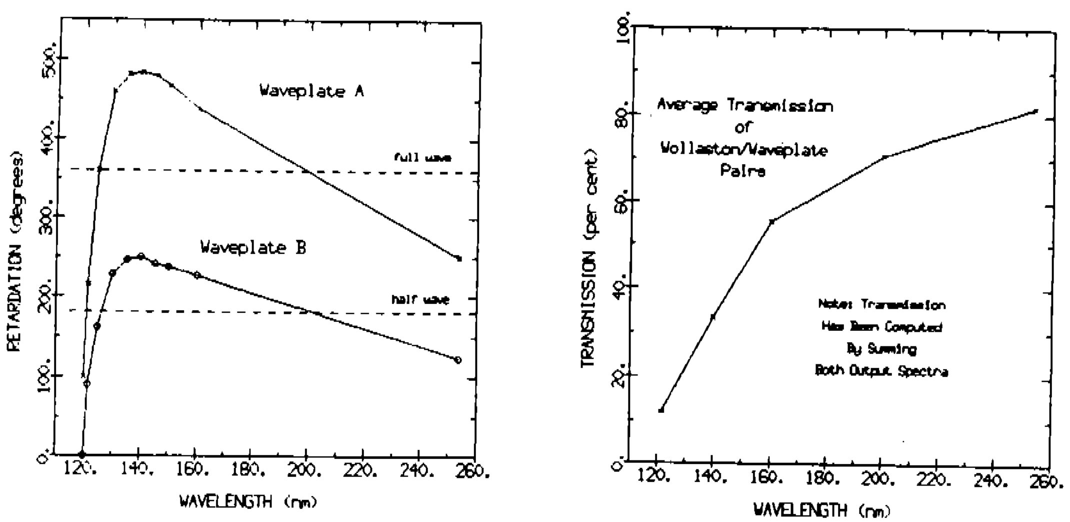

Figure 1.5.1: FOS waveplate retardation (left) and polarimeter transmission (Allen & Angel, 1982).

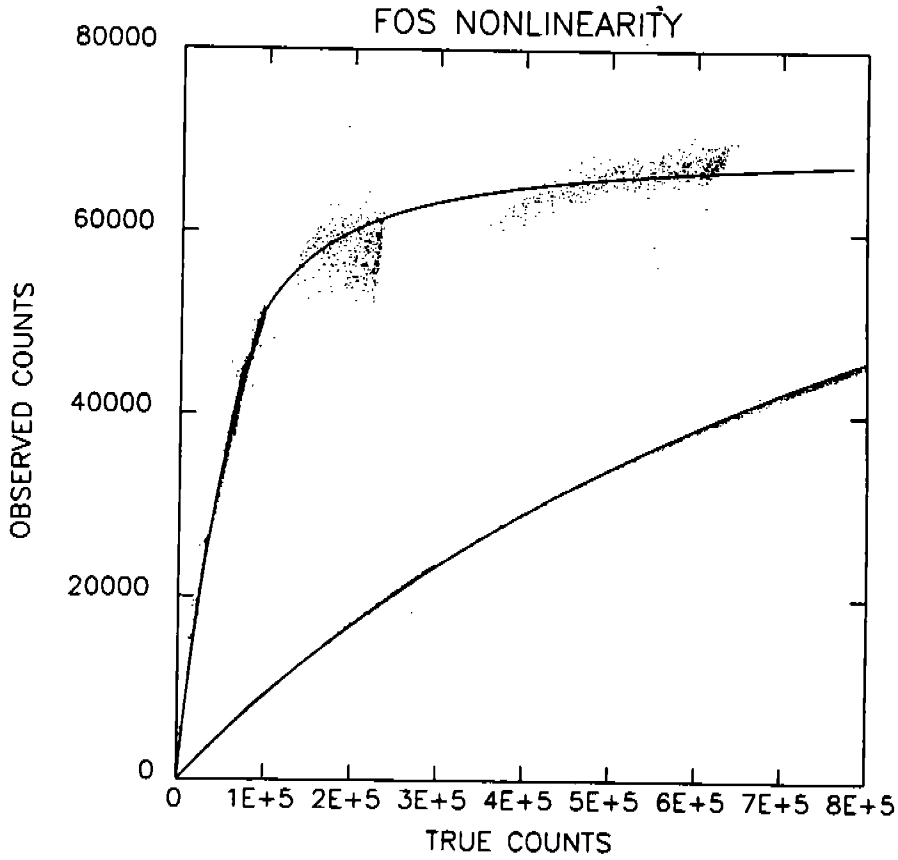

Figure 1.6.1: Measured count rate versus true count rate (Lindler & Bohlin 1986). The lower curve is a plot of the upper curve expanded by 10 in the x-direction.

Table 1.0.1

FOS INSTRUMENT CAPABILITIES

Wavelength coverage[1]	FOS/BL: 1150Å to 5400Å in several grating settings.
	FOS/RD: 1620Å to 8500Å in several grating settings.
Spectral resolution	High: $\lambda/\Delta\lambda \approx 1300$.
	Low: $\lambda/\Delta\lambda \approx 250$.
Time resolution	$\Delta t \geq 0.036$ seconds.
Acquisition aperture	$3.7'' \times 3.7''$ (4.3).
Science apertures[2]	Largest: $3.7'' \times 1.2''$ (4.3).
	Smallest: $0.09''$ square paired (0.1-PAIR).
Brightest stars observable [3]	$V \approx 8$ for B0V, $V \approx 6$ for G2V.
Dark count rate	FOS/BL: 0.007 counts s^{-1} diode^{-1}.
	FOS/RD: 0.01 counts s^{-1} diode^{-1}.
Example exposure times[4]	$F_{1300} = 2.5 \times 10^{-13}$, SNR=20/(1.0Å), t=180s.
$0.9''$ aperture	$F_{2800} = 1.3 \times 10^{-13}$, SNR=20/(2.0Å), t=5.8s (FOS/BL).
	$F_{2800} = 1.3 \times 10^{-13}$, SNR=20/(2.0Å), t=4.0s (FOS/RD).

[1] See Table 1.1.1 for grating dispersions and wavelength coverage.
[2] See Table 1.1.2 for available apertures.
[3] See Table 1.3.1 for brightest objects observable, which are strongly dependent on spectral type and grating.
[4] See Section 1.2 for exposure time calculations, and Table 1.2.1 for count rates for objects with a variety of spectral types. The example given here is for 3C273.

Table 1.1.1
FOS Dispersers

Grating	Diode No. at Low λ	Low λ (Å)	Diode No. at High λ	High λ (Å)	Δλ (Å-Diode^{-1})	Blocking Filter
Blue Digicon						
G130H	53	1140[1]	516[2]	1606	1.00	--
G190H	1	1573	516	2330[3]	1.47	--
G270H	1	2221	516	3301	2.09	SiO_2
G400H	1	3240	516	4822	3.07	WG 305
G570H	1	4574	516	6872[4]	4.45	WG 375
G160L	319	1140[1]	516	2508[3]	6.87	--
G650L	295	3540	373	9022[4]	25.11	WG 375
PRISM[5]	333	1500[6]	29	6000[4]	--	--
Red Digicon*						
G190H	503	1590[7]	1	2312	-1.45	--
G270H	516	2222	1	3277	-2.05	SiO_2
G400H	516	3235	1	4781	-3.00	WG 305
G570H	516	4569	1	6818	-4.37	WG 375
G780H	516	6270	126	8500[8]	-5.72	OG 530
G160L	124	1571[5]	1	2424	-6.64	--
G650L	211	3540	67	7075	-25.44	WG 375
PRISM[5]	237	1850	497	8950[8]	--	--

1. The blue Digicon's MgF_2 faceplate absorbs light shortward of 1140 Å.
2. The photocathode electron image typically is deflected across 5 diodes, effectively adding 4 diodes to the length of the diode array.
3. The second order overlaps the first order longward of 2300 Å, but its contribution is at a few percent.
4. Quantum efficiency of the blue tube is very low longward of 5500 Å.
5. Prism wavelength direction is reversed with respect to the gratings of the same detector.
6. The sapphire prism absorbs light shortward of 1650 Å.
7. The red Digicon's fused silica faceplate strongly absorbs light shortward of 1650 Å.
8. Quantum efficiency of the red detector is very low longward of 8600 Å.

* Wavelength direction is reversed for the red side relative to the blue side.

Table 1.1.2
FOS Apertures

Designation (Header Designation)	Number	Shape	Size (")	Separation (")	Special Purpose
0.3 (B-2)	Single	Round	0.26 dia	NA	Spectroscopy and Spectropolarimetry
0.5 (B-1)	Single	Round	0.43 dia	NA	Spectroscopy and Spectropolarimetry
1.0 (B-3)	Single	Round	0.86 dia	NA	Spectroscopy and Spectropolarimetry
0.1-PAIR (A-4)	Pair	Square	0.09	2.57	Object and Sky
0.25-PAIR (A-3)	Pair	Square	0.21	2.57	Object and Sky
0.5-PAIR (A-2)	Pair	Square	0.43	2.57	Object and Sky
1.0-PAIR (C-1)	Pair	Square	0.86	2.57	Extended Objects
0.25 x 2.0 (C-2)	Single	Rectangular	0.21 x 1.71	NA	High Spectral Resolution
0.7 x 2.0-BAR (C-4)	Single	Rectangular	0.60 x 1.71	NA	Surrounding Nebulosity
2.0-BAR (C-3)	Single	Square	1.71	NA	Surrounding Nebulosity
BLANK (B-4)	NA	NA	NA	NA	Dark and Particle Events
4.3 (A-1)	Single	Square	3.66 x 3.71	NA	Target Acquisition and Spectroscopy
Failsafe	Pair	Square	0.43 and 3.7	NA	Target Acquisition and Spectroscopy

The first dimension of rectangular apertures is along the dispersion direction, and the second dimension is perpendicular to the dispersion direction. The two apertures with the suffix designation "BAR" are bisected by an occulting bar which is 0.26" wide in the direction perpendicular to the dispersion.

Table 1.1.3
FOS Line Widths (FWHM) as a Function of Aperture Size

Designation	Size (″)	Aperture Filled with Uniform Source G130H (Blue) FWHM	Aperture Filled with Uniform Source G570H (Red) FWHM	Point Source at 3400Å FWHM
0.3	0.26 (circular)	1.00 ±.01	0.95 ±.02	0.92
0.5	0.43(circular)	1.27 ±.04	1.20 ±.01	0.93
1.0	0.86(circular)	2.29 ±.02	2.23 ±.01	0.96
0.1-PAIR	0.09(square)	0.97 ±.03	0.92 ±.02	0.91
0.25-PAIR	0.21(square)	0.98 ±.01	0.96 ±.01	0.92
0.5-PAIR	0.43(square)	1.30 ±.04	1.34 ±.02	0.94
1.0-PAIR	0.86(square)	2.65 ±.02	2.71 ±.02	0.96
0.25 X 2.0	0.21 X 1.71(slit)	0.99 ±.01	0.96 ±.01	0.92
0.7 X 2.0-BAR	0.60 X 1.71	1.83 ±.02	1.90 ±.01	1.26
2.0-BAR	1.71	5.28 ±.07	5.43 ±.04	1.34
4.3	3.66 X 3.71	12.2 ±0.1	12.2 ±0.1	0.96

The FWHM are given in units of diodes. A diode is 0.30″ wide and 1.21″ high.

Table 1.2.1

FOS Observed Counts Sec^{-1} $Diode^{-1}$ (N_λ) for Point Sources at Wavelength λ (Å)

Flux Distribution	Inputs	Equation for N_λ (counts- sec^{-1} $diode^{-1}$)
1. Continuum	F_λ(ergs cm^{-2} s^{-1} $Å^{-1}$)	$2.28 \times 10^{12} F_\lambda D_\lambda E_\lambda T_\lambda$
2. Monochromatic	I_λ(ergs cm^{-2} s^{-1})	$2.28 \times 10^{12} I_\lambda E_\lambda T_\lambda$
3. Normalized Continuum	$\frac{F_\lambda}{F_{5556}}$, m_{5556}	$7720 \frac{F_\lambda}{F_{5556}} \lambda \Delta\lambda E_\lambda T_\lambda 10^{-0.4 m_{5556}}$
4. Planck Function	T_{eff}(K), m_{5556}	$4.09 \times 10^{22} \left(\frac{e^{\frac{25897}{T}} - 1}{e^{\frac{1.4388 \times 10^8}{\lambda T}} - 1} \right) \Delta\lambda \frac{E_\lambda T_\lambda 10^{-0.4 m_{5556}}}{\lambda^4}$
5. Continuum	F_λ(ergs cm^{-2} s^{-1} hz^{-1})	$6.83 \times 10^{30} \frac{F_\lambda \Delta\lambda E_\lambda T_\lambda}{\lambda}$
6. Normalized Continuum	$\frac{F_\nu}{F_{\nu, 5556}}$, m_{5556}	$2.38 \times 10^{11} \frac{F_\nu}{F_{\nu, 5556}} \frac{\Delta\lambda E_\lambda T_\lambda}{\lambda} 10^{-0.4 m_{5556}}$
7. Power Law $\nu^{-\alpha}$	α, m_{5556}	$2.38 \times 10^{11} \left(\frac{\lambda}{5556} \right)^{\alpha} \left(\frac{\Delta\lambda E_\lambda T_\lambda}{\lambda} \right) 10^{-0.4 m_{5556}}$

E_λ = (Net HST Reflectivity) x (FOS Efficiency at Wavelength λ (Å)) x (COSTAR efficiency). See Figure 1.2.1.
T_λ = Throughput of aperture at Wavelength λ (Å) as simulated based on Telescope Image Modelling software (Burrows and Hasan 1991). See Figure 1.2.2.
D_λ = Number of Angstroms per diode at Wavelength λ (Å). See Table 1.1.1.

Note that the relevant count rate to derive SNR per resolution element is N_λ (counts- sec^{-1} $diode^{-1}$). A resolution element is one diode, regardless of sub-stepping.

Table 1.2.2
Simulated counts-sec^{-1}-$diode^{-1}$ for unreddened objects in the 0.9″ (**1.0**) aperture at 15th magnitude in V.

Blue Detector

Spectral Type	G130H (λ_{peak}=1600 Å)	G190H (λ_{peak}=2300 Å)	G270H (λ_{peak}=2650 Å)	G400H (λ_{peak}=3250 Å)	G570H (λ_{peak}=4600 Å)	G160L (λ_{peak}=2440 Å)	G650L (λ_{peak}=4000 Å)	PRISM (λ_{peak}=4000 Å)
B0V	1.6	5.1	13	14	2.0	26	18	2.2×10^2
A5V	-	0.19	0.9	1.9	1.4	0.9	7.9	90
G2V	-	-	0.14	1.3	1.1	0.08	3.5	48
ν^{-1}	0.14	0.87	2.6	4.2	1.2	5.0	7.0	81
ν^{-2}	0.05	0.37	1.3	2.5	1.0	2.3	5.1	55

Red Detector

Disperser (λ_{peak})	G190H (λ_{peak}=2300 Å)	G270H (λ_{peak}=2650 Å)	G400H (λ_{peak}=3600 Å)	G570H (λ_{peak}=4600 Å)	G780H (λ_{peak}=6300 Å)	G160L (λ_{peak}=2400 Å)	G650L (λ_{peak}=4400 Å)	PRISM (λ_{peak}=4000 Å)
B0V	14	20	16	11	2.3	40	41	3.0×10^2
A5V	0.54	1.2	2.7	8.1	2.6	1.4	26	1.6×10^2
G2V	-	0.20	1.9	6.3	3.5	0.10	18	92
ν^{-1}	2.4	4.1	5.4	6.9	3.6	6.8	20	1.4×10^2
ν^{-2}	1.0	2.1	3.6	5.8	4.0	2.8	17	1.1×10^2

Table 1.3.1

Brightness Limits[1]

Spectral Type	Red Side Brightness Limits									
	$B-V$	G190H	G270H	G400H	G570H	G780H	G160L	G650L	PRISM	MIRROR
07V	−0.32	9.3	9.8	9.0	7.9	5.7	10.3	8.2	10.5	14.8
B0V	−0.30	9.1	9.5	9.0	7.9	5.6	10.1	8.1	10.3	14.6
B1.5V	−0.25	8.8	9.4	8.8	7.9	5.7	10.0	8.1	10.2	14.5
B3V	−0.20	8.1	8.7	8.6	7.9	5.7	9.5	8.1	9.8	14.0
B6V	−0.15	7.9	8.6	8.4	7.8	5.7	9.3	8.0	9.6	13.8
B8V	−0.11	7.1	7.9	8.4	7.8	5.7	9.0	8.0	9.3	13.5
A1V	+0.01	5.9	7.0	8.0	7.8	5.8	8.6	7.9	8.9	13.1
A2V	+0.05	5.7	6.8	8.0	7.8	5.8	8.5	7.9	8.8	13.0
A6V	+0.17	5.1	6.5	7.9	7.8	5.8	8.4	7.8	8.7	12.9
A7V	+0.20	5.0	6.4	7.8	7.8	5.9	8.3	7.8	8.7	12.8
A9V	+0.28	4.4	6.2	7.7	7.8	6.0	8.2	7.7	8.6	12.7
F0V	+0.30	4.2	6.1	7.7	7.7	6.0	8.2	7.7	8.5	12.7
F5V	+0.44	3.6	6.1	7.5	7.7	6.1	8.1	7.6	8.5	12.6
F7V	+0.48	2.9	5.6	7.4	7.7	6.1	8.0	7.6	8.3	12.5
F8V	+0.52	2.7	5.4	7.3	7.7	6.1	8.0	7.6	8.3	12.5
G2V	+0.63	2.1	5.3	7.3	7.7	6.2	7.9	7.6	8.3	12.4
G6V	+0.70	—	5.2	7.2	7.7	6.2	7.9	7.5	8.2	12.4
K0V	+0.81	—	4.3	7.0	7.7	6.2	7.8	7.5	8.1	12.3
K0III	+1.00	—	3.4	6.6	7.6	6.3	7.7	7.5	8.0	12.2
K5V	+1.15	—	3.5	6.3	7.6	6.4	7.6	7.4	7.9	12.1
K4III	+1.39	—	2.1	6.0	7.5	6.5	7.5	7.3	7.8	12.0
M2I	+1.71	—	—	5.5	7.4	6.5	7.3	7.2	7.6	11.8
α[2] $= 1$		6.9	7.9	8.0	7.8	6.4	8.8	7.8	9.1	13.3
α[2] $= 2$		5.8	7.1	7.6	7.7	6.7	8.4	7.7	8.8	12.9
α[2] $= -2$	−0.46	10.2	10.3	9.2	8.0	5.8	10.9	8.2	10.8	15.4
$T = 50{,}000°$		9.6	9.9	9.0	7.9	5.7	10.4	8.2	10.5	14.9

[1] The FOS can be damaged if illuminated by sources that are too bright. If illuminated by targets brighter than the V magnitude limits given here, the instrument will go into safe mode, shutting its aperture door and stopping operations. Table 1.3.1 is for objects observed in the 3.6″ (4.3) aperture.

[2] Where $F_\nu \propto \nu^{-\alpha}$.

Table 1.3.1. *Continued.*

Spectral Type	Blue Side Brightness Limits								
	G130H	G190H	G270H	G400H	G570H	G160L	G650L	PRISM	MIRROR
07V	7.2	8.5	9.3	8.4	5.0	9.8	6.5	10.0	14.3
B0V	7.0	8.3	9.1	8.3	5.0	9.7	6.4	9.8	14.2
B1.5V	6.6	8.0	9.0	8.2	4.9	9.5	6.3	9.7	14.0
B3V	5.8	7.3	8.3	7.9	4.9	8.9	6.3	9.2	13.4
B6V	5.4	7.1	8.2	7.7	4.9	8.7	6.1	9.0	13.2
B8V	4.5	6.2	7.5	7.6	4.9	8.2	6.2	8.6	12.7
A1V	2.3	5.1	6.5	7.2	4.8	7.5	6.0	8.0	12.0
A2V	—	4.8	6.4	7.2	4.8	7.4	6.0	7.9	11.9
A6V	—	4.2	6.1	7.1	4.7	7.2	5.8	7.8	11.7
A7V	—	4.2	6.1	7.0	4.7	7.2	5.8	7.7	11.7
A9V	—	3.5	5.9	6.9	4.7	7.1	5.7	7.6	11.6
F0V	—	3.4	5.8	6.8	4.6	7.0	5.6	7.5	11.5
F5V	—	2.9	5.7	6.7	4.6	6.9	5.5	7.4	11.4
F7V	—	—	5.3	6.6	4.5	6.7	5.4	7.2	11.2
F8V	—	—	5.1	6.5	4.5	6.6	5.3	7.1	11.1
G2V	—	—	5.0	6.5	4.5	6.5	5.3	7.1	11.0
G6V	—	—	4.9	6.3	4.4	6.4	5.2	7.0	10.9
K0V	—	—	4.1	6.1	4.4	6.1	5.1	6.7	10.6
K0III	—	—	3.1	5.7	4.3	5.7	4.8	6.3	10.2
K5V	—	—	3.2	5.3	4.2	5.4	4.6	6.0	9.9
K4III	—	—	—	4.9	4.0	5.0	4.3	5.6	9.5
M2I	—	—	—	4.4	3.8	4.6	4.0	5.2	9.1
$\alpha^1 = 1$	4.2	6.1	7.5	7.3	4.6	8.0	5.7	8.4	12.5
$\alpha^1 = 2$	2.8	5.0	6.7	6.9	4.5	7.4	5.4	7.9	11.9
$\alpha^1 = -2$	8.6	9.4	9.8	8.6	5.0	10.6	6.6	10.4	15.1
$T = 50{,}000°$	7.5	8.8	9.4	8.4	5.0	10.0	6.4	10.0	14.5

[1] Where $F_\nu \propto \nu^{-\alpha}$.

2. OBSERVING MODES

The procedures for creating a Phase II proposal are being reviewed and revised as this handbook is written. We strongly recommend that users check the Phase II documentation carefully, and that users check STEIS for updates and revisions to the Handbook.

2.1 Acquiring the Target

The HST pointing is accurate and reliable. The most common source of error in target acquisition is incorrect user-supplied coordinates. To demonstrate the accuracy of the HST pointing achieved after guide star acquisition, Figure 2.1.0 shows the slews performed to center the target in the science aperture after FOS target acquisition, for observations taken after early 1991. The position $V_2 = 0.0$ and $V_3 = 0.0$ in Figure 2.1.0 corresponds to perfect initial pointing. Figure 2.1.0 shows that, using positions derived from GASP, about 70% of the blind pointings with correct coordinates fall within $1''$ of the aperture center. However, an onboard target acquisition is still necessary with the FOS to center the target in the science aperture.

Interactive acquisition mode (set with the `SPECIAL REQUIREMENT INT ACQ`) and three on-board acquisition modes (`ACQ/BINARY`, `ACQ/PEAK`, and `ACQ/FIRMWARE`) are described below. During an onboard acquisition, the FOS performs the acquisition, calculates the small offset required to center the target in a science aperture, and makes the offset. In contrast, during an interactive acquisition there must be a real time contact with HST, and the observer must be present at the ST ScI to interpret the image. Because of the probability of confusion when looking at an FOS white light picture, we believe that in nearly all cases a WFPC2 assisted target acquisition will be a better scientific choice than an interactive FOS acquisition (`INT ACQ`). However, `ACQ` does also provide an important means of verifying, after the fact, where the FOS aperture was positioned on the target during a science exposure, for both WFPC2 early acquisition and for onboard acquisitions of targets in complex fields.

The FOS acquisition aperture is $3.7'' \times 3.7''$ square (`4.3`). In order to have a 95% chance of placing a star in this aperture, the star *must* have an RMS positional error with respect to the guide stars of less than $1.0''$.

Additional acquisitions are not necessary when switching from the red side to the blue side for the $0.9''$ (`1.0`) or larger apertures, since the aperture positions are known accurately. Once a target has been acquired into a large science aperture and observed with one detector, a slew can be performed to place the target directly into the large aperture for the other detector. Such "side-switch" slews would not be accurate enough to place objects in the $0.2'' \times 1.2''$ slit (`0.25X2.0`) or the $0.3''$ aperture (`0.3`), however. In these cases an additional `ACQ/PEAK` is required as summarized in Tables 2.1.1, 2.1.3, and 2.1.3 (see also section 2.1.3 and examples in Appendix F).

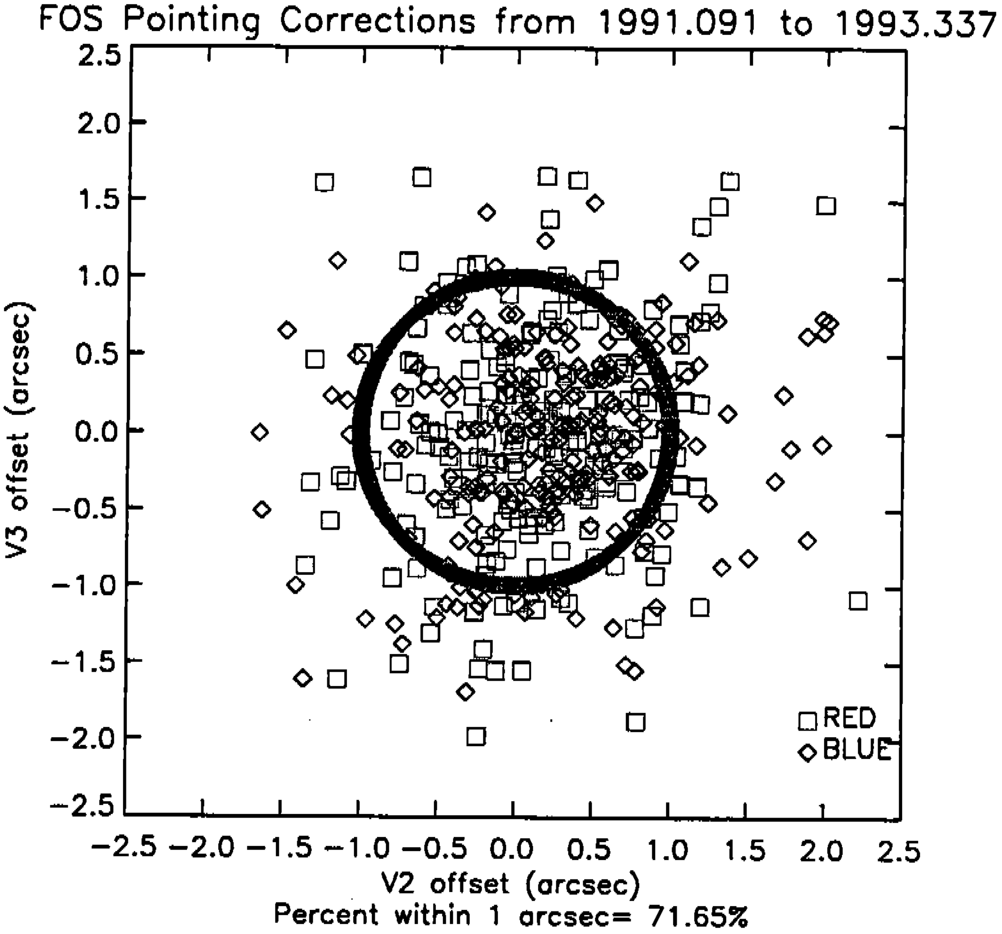

Figure 2.1.0: Slews performed after FOS target acquisition (after guide star acquisition) to center the target in the science aperture. The average red side offset, based on 128 acquisitions, is: V2 = 0.08″ ± 0.05″, V3 = −0.05″ ± 0.06″. The average blue side offset, based on 148 acquisitions, is: V2 = 0.15″ ± 0.05″, V3 = −0.06″ ± 0.05″. Seventy percent of the pointings after guide star acquisitions are within 1″ of the target.

Table 2.1.1
Recommended FOS Acquisition Sequences for
Acquisitions starting with ACQ/BINARY

Science Aperture	First Acq	Second Acq	Dimension X x Y	Acquisition Aperture
4.3	ACQ/BINARY	–		
1.0	ACQ/BINARY	–		
0.5	ACQ/BINARY	ACQ/PEAK	3X3	0.5
0.3	ACQ/BINARY	ACQ/PEAK	4X4	0.3
SLIT	ACQ/BINARY	ACQ/PEAK	9X1	SLIT

Table 2.1.2
Peak-Up Acquisition Based on Science Aperture
(for objects that can only be acquired with peak-up)

Aperture to be Used	Number of Stages	First	Second Stage	Third Stage	Fourth Stage	Throughput[1]
4.3	2	A	B			100%
4.3	3	A	B	C		100%
1.0	3	A	B	C		97%
0.5	3	A	B	C		95%
0.3	4	A	B	C	D OR E	94%
0.1	4	A	B	C	E	43%
SLIT[2]	4	A	B	C	F	93%

[1] Ratio of throughput given the centering error associated with the acquisition, over throughput with perfect centering. [2] SLIT pointing uncertainty is larger in the direction prependicular to dispersion than parallel to dispersion for the acquisition sequence given. Note that all FOS calibration acquisitions use 4-stage peak-ups A,B,C, and D; therefore, if precision flat fields are required, such a 4-stage peak-up should be used regardless of science aperture.

Table 2.1.3
Reference for Table 2.1.2

Type	Aperture	Search-Size-x	Search-Size-y	Scan-Step-x	Scan-Step-y	Critical?	Centering Error	Overhead Time
A	4.3	1	3	—	1.204	N	0.6″	6.6min
B	1.0	6	2	0.602	0.602	N	0.43″	12.9min
C	0.3	5	5	0.172	0.172	N	0.12″	22min
D	0.3	5	5	0.05	0.05	Y	0.04″	22min
E	0.1-PAIR-A	5	5	0.05	0.05	Y	0.04″	22min
F	SLIT	7	1	0.057	—	Y	0.04″	9.4min

Side-switching will be allowed ONLY for those objects where the total time (both sides combined) is less than 6 orbits. ST ScI reserves the right to change the order of the sides (and gratings) to schedule the observation most efficiently.

Three rules apply to any side-switching specification:

1. Specify the target acquisition (TA) exposures on the Exposure Logsheet for one side, while in a comment specifying the parameters such as exposure time, FAINT, BRIGHT, and spectral element for the other side of FOS. Such a specification will allow easy change of order of the detectors. If the proposer feels the TA must be performed with a specific detector, this must be stated in the General Form, question 5.
2. The special requirement GROUP NOGAP should be used in the Exposure Logsheet to link all exposures of the target.

3. If the proposer has a *scientific* need to obtain the observations in a specific grating order, the special requirement SEQ NO GAP should be used.

See the Exposure Logsheet lines 3.0 through 4.3 (Appendix F) for an example of a side-switching specification.

2.1.1 ACQ/BINARY

ACQ/BINARY is the method of choice for targets with well known energy distributions, but *should not be used for variable sources, sources of unknown color, or sources extended by much more than 1 diode, or 0.3″.* The method has a restricted dynamic range of brightness. Specifically, target brightness uncertainty should be less than 0.5 magnitudes for the use of ACQ/BINARY. Objects of poorly known color should be acquired with ACQ/PEAK.

During an ACQ/BINARY, the camera mirror reimages the FOS focal plane onto the Digicon. Acquisition of the target is performed not by moving the telescope, but by deflecting the image of the target acquisition aperture on the photocathode until the target has been placed on the Y edge of the diode array. ACQ/BINARY finds first the number of stars in the $3.7'' \times 3.7''$ acquisition aperture (designation 4.3) by integrating at three different positions in the Y-direction. The program locates the target in one of the three strips, measures its count rate, and locates the target in the X direction. The algorithm then positions the target on a Y–edge of the diode array by deflecting the image across the diode array through a geometrically decreasing sequence of Y–deflections until the observed count rate from the star is half that when the object is positioned fully on the diode array. ACQ/BINARY is the preferred acquisition mode for point sources.

Although ACQ/BINARY is designed to obtain the Nth brightest star in a crowded field by setting the optional parameter NTHSTAR, acquisitions in crowded fields have not been attempted.

There should be about 300 counts in the peak pixel for each Y-step that is on-target for Binary Search to succeed. If the number of counts in the peak is significantly larger than 300, the tolerances for when the target is on the edge of the diode array become very small since they are based on $\sqrt{N}$ statistics. Typical centering error after Binary Search is $\lesssim 0.15''$. If the Binary Search algorithm fails to converge on a position with half the counts of the original target, the telescope slews to the last position of binary search, *i.e.*, to the X position of the target and the last Y-deflection.

A target must lie within the range of counts specified by the Optional Parameters BRIGHT and FAINT. We recommend that BRIGHT and FAINT be set to allow for targets 10 times brighter and 5 times fainter than expected. Since the maximum number of Y-steps in Binary Search is 11, the default values for the parameters are BRIGHT $= 300 \times 11 \times 10 = 33{,}000$ and FAINT $= 300 \times 11/5 = 660$.

An Example of an ACQ/BINARY on an offset star followed by an FOS observation of the target star is given on lines 1 and 2 of the sample Logsheets in Appendix F.

2.1.2 ACQ/PEAK

During ACQ/PEAK the telescope slews and integrates at a series of positions on the sky with a science aperture in place. At the end of the slew sequence the telescope is returned to the position with the most counts; no positional interpolation is performed. In the case of an ACQ/PEAK into a barred aperture, or when using the Optional Parameter TYPE=DOWN, the telescope is returned to the position with the fewest counts. ACQ/PEAK is a relatively inefficient

procedure because a minimum of $\sim$ 42 seconds per dwell is required for the telescope to perform the required small angle maneuvers. Tables 2.1.2 and 2.1.3 list the recommended combinations of peak-ups for acquisition of targets according the the size of the science aperture, along with the errors in position, and the throughput errors associated with those positional errors. Table 2.1.3 lists the overhead times involved in each stage of an ACQ/PEAK.
• **Example** A peak-up into the 0.26″ (0.3) aperture would require a 1X3 peak-up into the 3.7″ × 3.7″ (4.3), followed by a 6X2 peak-up into the 0.86″ (1.0) aperture, followed by a 5X5 peak-up into the 0.26″ (0.3) aperture. The overhead time required for this three stage peak-up is 41.50 minutes.

This mode is used for objects too bright to acquire with the camera mirror in place, for objects too variable to acquire with ACQ/BINARY, for centering targets in the smallest apertures, and for positioning bright point sources on the bars of the occulting apertures in order to observe any surrounding nebulosity. For bright object acquisitions, the science grating is put in place before the acquisition. Examples of ACQ/PEAK are given on lines 10.3 through 13.3 of the sample Exposure Logsheets in Appendix F. Tables 2.1.1, 2.1,2, and 2.1.3 summarize recommended ACQ/PEAK sequences.

To acquire objects into the smallest FOS apertures (0.26″ (0.3), 0.2″ (0.25-PAIR), 0.09″ (0.1-PAIR), and 0.2″X 1.7″ slit (0.25 X 2.0)), first use a normal ACQ/BINARY acquisition, followed by a "critical" ACQ/PEAK into the science aperture (see Tables 2.1.1, 2.1.2, and 2.1.3). (For objects too bright to observe with the camera mirror in place, use instead a series of non-critical peak-ups as shown in Table 2.1.2, followed by a "critical" peak-up into the small science aperture.) The "critical" ACQ/PEAK must have a high number of counts to place the target in the center of these smallest apertures ($\approx$ 10000) and spacing between dwells of order $D/5$, where D is the diameter of the Peak Up aperture. See Table 2.1.6 below for exposure times. The non-critical ACQ/PEAK requires shorter exposure time and spacing between dwells of order D/2. An example is given in Logsheet lines 3 through 4.1 in Appendix F.

Count rates must not exceed the safety limits for the mirror or the grating selected (see Table 1.3.1 and Table 2.1.4).

An N by M pattern with steps of size X.X, Y.Y can be specified by setting SEARCH-SIZE-X=N, SEARCH-SIZE-Y=M, and SCAN-STEP-X=X.X, SCAN-STEP-Y=Y.Y. Examples are given in the Exposure Logsheets lines 10.3 through 13.3 in Appendix F.

2.1.3 INT ACQ

The mode ACQ, when used with the SPECIAL REQUIREMENT ''INT ACQ FOR", maps the acquisition aperture and sends the image to the ground in real time. The apparent elongation of stars in the y-direction caused by the shape of the diodes (0.26″ × 1.21″) is removed on the ground by multiplying the picture by an appropriate matrix. After the picture has been restored, the astronomer measures the position of the target on the image. The small offset required to move the target to the center of one of the science apertures is calculated and uplinked to the telescope; after the slew is performed the science observations begin.

A modified form of interactive acquisition, the dispersed-light interactive acquisition utilizing IMAGE mode, may be employed for acquisition of sources in which spectral features of known wavelength are prominent. This method has proven quite useful for planetary satellite acquisitions. Spacecraft overheads for this procedure are no different than the overheads for conventional INT/ACQ.

2.1.4 ACQ: Confirmatory

ACQ can also be used after another type of acquisition to provide a picture which shows where HST is pointed in FOS detector coordinates. The Exposure Logsheets provide an example (lines 5–8) of an ACQ/BINARY of an offset star followed by an offset onto the nucleus of M81. In this example, after the science observation is made, a (white light) picture of the aperture is taken by using ACQ to verify the aperture position.

2.1.5 ACQ/FIRMWARE

ACQ/FIRMWARE is an engineering mode that maps the camera-mirror image of the aperture in X and Y with small, selectable Y increments. The FOS microprocessor filters the aperture map and then finds the Y-positions of the peaks by fitting triangles through the data. Firmware is less efficient than Binary Search, and fails if more than one object is found within the range of counts set by the observer (BRIGHT and FAINT). This mode is not generally recommended.

2.1.6 Early Acquisition Using WFPC2

We recommend using WFPC2 assisted target acquisition when there will be more than two stars in the 3.7″ (4.3) acquisition aperture or when there will be intensity variations across the acquisition aperture which are larger than a few percent of the mean background intensity. A WFPC2 image of the field is taken several months in advance of the science observation. The positions of the target and an offset star are measured in the image and then (at least 2 months later) the positions are updated on the Exposure Logsheet, and the offset star is acquired with ACQ/BINARY and finally the FOS aperture is offset onto the target. There is only about a 30% chance that the same guide stars will be in the Fine Guidance Sensors (FGS) when the subsequent FOS observations are made. With new guide stars, the 1σ uncertainty in any position is 0.3″. Uncertainty in position of the telescope when slewing by 1′ due to the spacecraft roll is of order 0.05″. The Wide Field Camera II is made up of three chips of size 1.25′ on a side and a fourth chip 0.6′ on a side. Offsets larger than 30″ should be discussed with the User Support Branch.

The first step in a WFPC2 assisted target acquisition is to use a SPECIAL REQUIREMENT on the Exposure Logsheets to specify the exposure as an EARLY ACQ which must be taken at least two months before the FOS observations (see lines 5 through 8 on the exposure logsheet in Appendix F). The camera, exposure time, filter, and centering of the target in the image should be chosen such that the picture will show both the target and an isolated (no other star within 5″) offset star which is brighter than $m_V = 20$ and more than 1 magnitude brighter than the background (magnitudes per square arcsecond). In order to insure that an appropriate offset star will be in the WFPC2 image, the centering of the target in the WFPC2 field should be chosen by measuring a plate or CCD image. The Target List for the FOS exposures should provide the offset star with nominal coordinates and with position given as TBD-EARLY. (See example lines 4 and 5 on the Target List in Appendix F.) The Target List also should list the position of the offset star as RA-OFF, DEC-OFF, and FROM the target. Alternatively, the offsets can be given as XI-OFF and ETA-OFF, or R, PA, see the Phase II Proposal Instructions Section 5.1.4.3 on Positional Offsets.

After the WFPC2 exposure has been taken and the data have been received, the next step is to get the picture onto an image display so you can i), choose an offset star, ii) measure its right ascension and declination, and iii) measure the right ascension and declination of the target relative to the offset star. An STSDAS task (stsdas.wfpc.metric) is available currently to extract pointing and roll angle information from the WFPC header and to convert WFPC pixels to right ascension and declination. Upon calibration, the task "metric" will also be available for WFPC2. If this program is not available, you will need to patch your WFPC2 image into the Guide Star Catalog reference frame. Based on your choice of an offset star, the ST ScI will choose a pair of guide stars for the FOS observations which will stay in the "pickles" during the move from the offset star to the target. The probability that a suitable pair of guide stars can be found increases as the separation of the offset star and the target decreases. So, choose the offset star as close as possible to the target (but not so close as to violate the background rule in the preceding paragraph). The final step is to send the position of the offset star and the positional offsets to the ST ScI to update the proposal information for your succeeding FOS observations.

2.1.7 Examples

The following section gives examples for acquiring different types of astronomical objects based on the strengths and weaknesses of the various target acquisition methods.

- **Example: Single Stars**

Stars with visual magnitudes brighter than about 12^{th} are too bright for FOS acquisitions with the camera mirror, and observations of objects that bright will safe the instrument. The exact limit depends on the spectral type of the star and on the detector as shown in Table 2.1.4 below. For a more complete list see Table 1.3.1.

Table 2.1.4

FOS Visual Magnitude Limits with Camera Mirror

	O7V	B0V	B3V	A1V	A6V	G2V	K0III	ν^{-1}	ν^{-2}
Red Side Limit	14.8	14.6	14.0	13.1	12.9	12.4	12.2	13.3	12.9
Blue Side Limit	14.3	14.2	13.4	12.0	11.7	11.0	10.2	12.5	11.9

Stars that are too bright for ACQ/BINARY can be acquired by using ACQ/PEAK with one of the high dispersion gratings instead of the camera mirror (see lines 10.3 through 10.6 on the Exposure Logsheets in Appendix F). If the visual magnitude of a single star or point source is fainter than limits given in Table 2.1.4 above, if the star does not vary by more than 0.5 magnitudes, and if the colors are known, use ACQ/BINARY for the acquisition.

- **Example: Stars Projected on Bright Backgrounds**

ACQ/BINARY can find successfully a star projected on a uniform background provided the target acquisition integration time is long enough to give $\sim$ 300 peak counts from the star and the star is at least a magnitude brighter than the background surface brightness in magnitudes per square arcsecond. If star magnitude and the background magnitude differ by less than 1 magnitude, the star can still be acquired with ACQ/BINARY by increasing the integration time. Alternatively, the acquisition can be accomplished by using an early acquisition with WFPC2, followed two months later by an FOS acquisition and blind offset.

A different problem arises when the background varies across the acquisition aperture. Because the logic in the ACQ/BINARY program drives the star to the edge of the diode array by finding the position which gives half the maximum number of counts, any change in the background in the Y-direction will bias the derived Y-position of the star. Simulations of acquisitions of stars projected onto bright galaxies such as NGC 3379 show that the shot noise in the star will determine the accuracy (rather than the spatially-variable background), provided the star is at least 15″ from the center of the galaxy.

- **Example: Diffuse Sources and Complex Fields**

The FOS onboard acquisition methods were designed to acquire point sources. Consequently, diffuse sources and complex fields must be observed by first acquiring a star and then offsetting to the desired position in the source. The most accurate positioning of the FOS aperture on the source will be accomplished by using an early WFPC2 assisted target acquisition. In many programs, the interesting positions in the source will be chosen on the basis of WFPC2 images. If the imaging program is planned as described in the section on WFPC2 assisted TAs, the science images can be used for the acquisition.

- **Example: Nebulosity Around Bright Point Sources**

The optimal FOS aperture position for a bright point source surrounded by nebulosity will depend on the distribution and brightness of the nebulosity relative to the point source. If high spatial resolution images show that the nebulosity has a scale length of a few tenths of an arcsecond and is relatively symmetrical around the source, then the signal-to-noise ratio may be maximized by placing the stellar source on the occulting bar of one of the occulting apertures and observing simultaneously the nebulosity on both sides of the occulting bar. When using this approach, you should first use Binary Search to position the source near the center of the occulting aperture. The second step is to use a Peak Down in the Y-direction to position the stellar source on the occulting bar. An example is given in lines 11, 12, and 13 of the Exposure Logsheet in Appendix F.

If high resolution images show that the nebulosity is rather asymmetrical, the best approach may be to observe the nebulosity with one of the small circular apertures. In that case the bright stellar source should be acquired with ACQ/BINARY, followed by an ACQ/PEAK, followed by an offset onto the nebulosity.

- **Example: ACQ/PEAK**

ACQ/PEAK is now the method of choice for targets with variability of order 0.5 magnitudes or greater. This method utilizes a spatial scan series of exposures to locate the target. The position with the maximum signal is chosen; no positional interpolation is performed. This method must be used also for targets brighter than about V=13 (see Table 1.3.1).

For a planetary object, an area of sky larger than the TA aperture (3.7″ × 3.7″, 4.3) may have to be searched, plus the object may be too bright to acquire with ACQ/BINARY. By using the target acquisition aperture, an effective aperture of size 3.7″ × 1.2″ (designation 4.3) is available and an area of 7.4″ × 7.4″ can be searched. The first two steps of the ACQ/PEAK are to perform a 2 × 6 dwell pattern with the (effective) 3.7″ × 1.2″ aperture (4.3). Then the ACQ/PEAK sequence outlined in Tables 2.1.1, 2.1.2, and 2.1.3 for the appropriate aperture can be used.

The most time efficient way to acquire a bright target with the FOS is to use the 3.7″ × 1.2″ (4.3) aperture in a 1 × 3 dwell pattern, followed by a 6 × 2 dwell pattern into a 0.9″ (1.0) aperture. The third step depends on the science to be done. As with the example given above, for an object to be centered into the 0.9″ (1.0) aperture, a non-critical ACQ/PEAK can be performed into the 0.4″ (0.5) aperture. These types of acquisitions are shown on lines 10.3 through 13.3 on the Exposure Logsheet in Appendix F and summarized in Tables 2.1.1, 2.1.2, and 2.1.3.

2.1.8 Acquisition Exposure Times

There should be about 300 counts in the peak of the Y-step that is centered on the star in an ACQ/BINARY exposure. The maximum number of Y-steps which can be taken during ACQ/BINARY is 11. Table 2.1.6 summarizes the total exposure time for an ACQ/BINARY, *i.e.*, the time per Y-step multiplied by 11, for various types of stars. *The exposure times in Table 2.1.6, scaled to the magnitude of the target, are the times that should be entered in the Exposure Logsheets.* There is a minimum integration time that can be entered on the Exposure Logsheet. The minimum is constrained by the FOS livetime limit given in Table 2.1.5. If the exposure time must be larger than that calculated from Table 2.1.6 to accommodate the minimum time, the values for the optional parameters BRIGHT and FAINT must be set to reflect the total number of counts expected.

$$\mathrm{BRIGHT} = 33,000 \times \frac{\mathrm{TIME}_{\mathrm{Table\ 2.1.5}}}{\mathrm{TIME}_{\mathrm{Table\ 2.1.6}}}$$

$$\mathrm{FAINT} = 660 \times \frac{\mathrm{TIME}_{\mathrm{Table\ 2.1.5}}}{\mathrm{TIME}_{\mathrm{Table\ 2.1.6}}}$$

For example, for a red side ACQ/BINARY of a 12^{th} magnitude offset K0III star, 0.29s is the exposure time derived from Table 2.1.6, but the minimum exposure time is 0.66s. The default values of BRIGHT and FAINT must then be multiplied by the factor 0.66/0.29 = 2.28, so that BRIGHT = 75,100 and FAINT = 1500.

The peak-up exposure times in Table 2.1.6 are calculated to produce 1000 counts in the peak of the target image, which is the number of counts recommended for the non-critical ACQ/PEAK described above. The ACQ/PEAK sensitivity has considerable wavelength and aperture size dependence. A critical ACQ/PEAK into small apertures requires 10,000 counts total to achieve a centering error that corresponds to a signal loss of less than about 2% for the apertures smaller than 0.3″. For a critical peak up, the values in Table 2.1.6 relating to peak up must be multiplied by a factor of 10.

The times in Table 2.1.6 do not include the overhead involved in the initial setup of parameters or the analysis time, since that overhead should not be included on the Exposure Logsheet specifications. The overhead times for the lengthy ACQ/PEAK mode is given in Table 2.1.3.

Extrapolations of acquisition exposure times for sources fainter than V=19.5 should not be extrapolated from Table 2.1.6 because of the background noise.

2.2 Taking Spectra: ACCUM and RAPID Spectropolarimetry: STEP-PATT = POLSCAN

Examples of exposure logsheets are included for ACCUM mode (see lines 3.0 through 4.3 in Appendix F) and RAPID mode (see lines 11.0 through 13.0).

In RAPID mode, when a wavelength range is specified, that range will be used whether or not there is room in memory for a larger region. Therefore, specifying a wavelength range is not a good idea unless absolutely necessary, because it restricts the wavelength region that is read out. The full wavelength region is often useful. For example, the background can be determined directly from the diode array for gratings G130H, G160L, G190H, G650L, G780H, and PRISM. The diodes below the lowest wavelength, given in Table 1.1.1, can be used to average the actual background rate. The zero order can be monitored for G160L if all diodes are read out. If the observer needs *only* a specific wavelength range to be read out, then that range should be specified in with the keyword WAVELENGTH (column 8) of the Phase II exposure logsheet. Otherwise, the largest possible wavelength range will be automatically observed that is compatible with the READ-TIME requested.

The use of STEP-PATT = POLSCAN is demonstrated in the exposure logsheet lines 14.0 through 19.0. As mentioned in Section 1.5, only the G270H grating may be available for polarimetric observations post-COSTAR; even with the G270H, full utility has not yet been demonstrated post-COSTAR.

Table 2.1.5

Minimum Exposure Times to be Entered in Exposure Logsheets

ACQ/BINARY	0.66 sec
ACQ/FIRMWARE	0.96 sec
ACQ/PEAK	0.003 sec
ACQ	3.84 sec

Table 2.1.6
FOS Exposure Times ($V = 15$ unreddened)—Red Side

Spectral Type	$B-V$	Peak/up G190H	Peak/up G270H	Peak/up G400H	Peak/up G570H	Peak/up G780H	Peak/up G650L	Peak/up PRISM	Peak/up MIRROR	ACQ/BIN
07V	−0.32	0.2	0.1	0.2	0.5	3.3	0.3	0.1	0.1	0.39
B0V	−0.30	0.2	0.1	0.2	0.5	3.6	0.4	0.1	0.1	0.46
B1.5V	−0.25	0.3	0.1	0.3	0.5	3.5	0.4	0.1	0.1	0.53
B3V	−0.20	0.5	0.3	0.3	0.5	3.4	0.4	0.1	0.1	0.8
B6V	−0.15	0.6	0.3	0.3	0.5	3.6	0.5	0.1	0.1	1.0
B8V	−0.11	1.2	0.6	0.4	0.5	3.3	0.5	0.1	0.2	1.3
A1V	+0.01	3.5	1.2	0.5	0.5	3.2	0.5	0.2	0.2	2.0
A2V	+0.05	4.2	1.4	0.5	0.5	3.2	0.5	0.2	0.2	2.1
A6V	+0.17	7.3	2.0	0.5	0.5	3.0	0.5	0.2	0.2	2.4
A7V	+0.20	7.6	2.1	0.5	0.6	2.8	0.5	0.2	0.2	2.4
A9V	+0.28	12	2.3	0.6	0.6	2.8	0.6	0.2	0.3	2.7
F0V	+0.30	14	2.5	0.6	0.6	2.8	0.6	0.2	0.2	2.8
F5V	+0.44	32	2.7	0.6	0.6	2.4	0.6	0.3	0.2	3.0
F7V	+0.48	45	3.8	0.7	0.6	2.3	0.6	0.3	0.2	3.3
F8V	+0.52	50	4.6	0.7	0.6	2.3	0.6	0.3	0.3	3.4
G2V	+0.63	95	5.8	0.8	0.6	2.2	0.6	0.3	0.3	3.5
G6V	+0.70	—	5.9	0.9	0.6	2.2	0.7	0.3	0.3	3.7
K0V	+0.81	—	13	1.0	0.6	2.0	0.7	0.3	0.4	4.0
K0III	+1.00	—	30	1.5	0.6	1.9	0.7	0.4	0.4	4.5
K5V	+1.15	—	28	2.0	0.6	1.8	0.8	0.4	0.4	4.9
K4III	+1.39	—	—	2.8	0.7	1.7	0.8	0.5	0.5	5.4
M2I	+1.71	—	—	4.0	0.7	1.7	0.9	0.6	0.5	6.2
$\alpha = 1$		1.5	0.5	0.5	0.5	1.7	0.5	0.2	0.2	1.5
$\alpha = 2$		4.0	1.1	0.6	0.6	1.4	0.6	0.3	0.2	2.2
$\alpha = -2$	−0.46	0.2	0.1	0.2	0.4	3.2	0.3	0.1	0.1	0.23
$t = 50{,}000°$		0.2	0.2	0.3	0.5	3.0	0.4	0.1	0.1	0.35

FOS Exposure Times ($V = 15$ unreddened)—Blue Side

Spectral Type	Peak/up G130H	Peak/up G190H	Peak/up G270H	Peak/up G400H	Peak/up G570H	Peak/up G650L	Peak/up PRISM	Peak/up MIRROR	ACQ/BIN
07V	1.3	0.5	0.2	0.3	5.9	1.6	0.1	0.1	0.80
B0V	1.5	0.6	0.2	0.3	6.1	1.6	0.1	0.1	0.90
B1.5V	2.1	0.8	0.2	0.3	6.7	1.8	0.1	0.1	1.1
B3V	4.6	1.5	0.3	0.4	6.2	1.9	0.2	0.1	1.8
B6V	6.6	1.8	0.4	0.5	7.0	2.1	0.2	0.2	2.2
B8V	14	3.9	0.8	0.6	7.0	2.1	0.2	0.2	3.4
A1V	—	11	1.8	0.8	7.4	2.5	0.4	0.4	6.1
A2V	—	13	2.3	0.8	7.1	2.5	0.4	0.4	6.9
A6V	—	25	2.9	0.9	8.2	2.9	0.5	0.5	8.1
A7V	—	26	3.0	1.0	8.2	3.0	0.5	0.5	8.6
A9V	—	41	3.4	1.1	8.2	3.4	0.5	0.6	9.7
F0V	—	43	3.7	1.1	8.7	3.4	0.6	0.6	10.
F5V	—	68.	3.9	1.3	9.0	4.0	0.6	0.7	12.
F7V	—	—	5.7	1.4	9.2	4.3	0.8	0.8	14.
F8V	—	—	6.9	1.5	9.2	4.4	0.8	0.9	15.
G2V	—	—	7.7	1.6	9.2	4.6	0.9	1.0	16.
G6V	—	—	7.9	1.7	9.4	5.2	1.0	1.1	18.
K0V	—	—	19.	2.1	11.	5.8	1.3	1.4	22.
K0III	—	—	39	3.2	11	7.3	2.0	2.0	33
K5V	—	—	40	4.5	13	9.0	2.5	2.6	44
K4III	—	—	—	6.6	16.	12	3.5	4.0	65.
M2I	—	—	—	11.	19.	16.	5.0	5.6	92.
$\alpha = 1$	20.	4.2	0.8	0.7	8.6	3.2	0.3	0.3	4.2
$\alpha = 2$	60.	12.	1.6	1.1	9.6	4.2	0.4	0.5	7.3
$\alpha = -2$	0.4	0.2	0.1	0.2	5.6	1.4	0.1	0.1	0.44
$T = 50{,}000°$	1.0	0.4	0.2	0.3	6.5	1.6	0.1	0.1	0.70

Notes to Table 2.1.6

Note: Exposure time must be multiplied by $10^{0.4(V-15)}$.

[1] Optimal exposure times for ACQ/BINARY and ACQ/FIRMWARE are calculated to detect 300 peak counts in the peak pixel of the target.

[2] ACQ/PEAK into the 0.26″ (0.3) aperture requires 10000 total counts.

[3] Exposure times for ACQ/PEAK into all apertures excluding the slit are calculated to detect 1000 total counts for non-critical acquisitions. For critical centering into apertures smaller than 0.3″, multiply the exposure times by a factor of 10. **Note that the exposure time for ACQ/PEAK must be multiplied by the inverse throughput of the aperture used** (T_λ, **see Figure 1.2.2**). Although the exact factor depends on the input spectrum, the approximate multiplicative factors are 1.1 for the 0.9″ apertures (1.0), 1.2 for the 0.4″ apertures (0.5), and 1.25 for the 0.26″ aperture (0.3).

3. INSTRUMENT PERFORMANCE AND CALIBRATIONS

For additional information on instrument performance, see *Calibrating the Hubble Space Telescope: Proceedings of a Workshop*, ed. Blades & Osmer (1994) and Part VI of the *HST Data Handbook*, ed. Baum (1994). Both documents are available on-line via STEIS (see section 4 for information on accessing STEIS).

3.1 Wavelength Calibrations

All FOS wavelengths are vacuum wavelengths, both below 2000Å and above.

Wavelength offsets between the internal calibration lamp and a known external point source are based on observations of the dwarf emission line star AU Mic, that have been corrected for geomagnetically induced image drift (Kriss, Blair, & Davidsen 1992). On the red side, the mean offset between internal and external source is $+0.176 \pm 0.105$ diodes. On the blue side, the mean offset is -0.102 ± 0.100 diodes. These offsets are *not included* in the pipeline reduction wavelength calibration. With the observed dispersion reported by Kriss, Blair, & Davidsen, velocity measurements based on single lines in FOS spectra have a limiting accuracy of roughly 20 km s^{-1} if wavelength calibrations are obtained at the same time, with no filter-grating wheel motion (*i.e.*, NO GAP), and if the target is well centered in the science aperture. (See Appendix D for line lists and spectra of the comparison lamps for each detector/disperser combination.) If simultaneous wavelength calibrations are not obtained, the non-repeatability of order 0.3 diodes in the positioning of the filter–grating wheel will dominate the errors in the zero point of the wavelength scale (Hartig 1989).

3.2 Absolute Photometry

The post-refurbishment absolute photometric calibrations are performed by observing some or all of the standard stars G191B2B (WD0501+527), BD+28D4211, BD+75D325, HZ–44, and BD+33D2642 in the large ($3.7'' \times 1.2''$, 4.3) aperture. As of the writing of this handbook, there is little information on time dependence of the sensitivity.

3.3 Flat Fields

Observations of two hot spectrophotometric standard stars (G191B2B and BD+28D4211) are used to produce spectral flat fields for all usable FOS detector/disperser combinations. A highly precise target acquisition strategy (4-stage ACQ/PEAK with pointing uncertainty of 0.03 arcsec) is used for these observations so that filter-grating wheel repeatability (0.10 arcsec) is the dominant source of uncertainty in photocathode sampling. All post-refurbishment flat fields will be derived via the so-called superflat technique (see Lindler *et al.*- CAL/FOS-088; flat field article by Keyes in HST Calibration Workshop, ed. Blades &d Osmer (1994); see also Part VI, Chapter 16 in the HST Data Handbook, ed. Baum (1994)).

Appendix G provides figures showing preliminary flat field structure for all usable FOS detector/disperser combinations derived from SMOV epoch (March, 1994) superflat observations. These figures are provided as an approximate guide since analysis of the observations is not complete at the time of the writing of this handbook. However, no additional strong (greater than 5% deviation from unity) features are expected to appear.

It must be emphasized that FOS flat field corrections are intended to remove **photocathode granularity** typically on the scale of 10 pixels or less. If high precision flat fields are required for scientific objectives, observers should attempt to attain the same pointing accuracy (described above) used for FOS flat field calibration observations so that the science target illuminates the same portion of the photocathode as was sampled by the calibration observations.

During Cycle 4 several observations will be made to attempt to quantify the change in flat field granularity structure as a function of target mis-centering perpendicular to dispersion. Most pixel ranges in typical flat fields display deviations of 1–2% about the mean value of unity or about a local running mean, however, some substantial (5–50%) features do occur. Fragmentary evidence from pre-refurbishment flats indicates that photocathode granularity in these strong features can change by 25% on the scale of a diode height (1.2 arcsec). Should such a feature occur in the vicinity of an important spectral line and target centering be less accurate than that of the flat field calibration observation, then the observed flux could be affected by a currently unknown amount. We note that there is such a feature in the 1500–1550 A. range (affects C IV resonance doublet) of the FOS/BLUE G160L spectrum.

Normally one epoch of flat field measurement is made per cycle for each detector/disperser combination to be used, however in the pre-refurbishment era some substantial temporal variation in FOS/RED G190H, G160L, and, to a lesser extent, G270H flat fields was observed. These changes were most profound in the first two and one-half years after launch; little variation has been noted since November, 1992. Nonetheless, these gratings will continue to be monitored at additional periodic intervals.

Some time dependence has been observed in the red side flat fields. Red side data taken after January 1992 and before refurbishment can be flat fielded with the data most appropriate to the observation. The STSDAS task getreffile will refer the user to the appropriate flat field. Red side data taken between October 1990 and January 1992 will be difficult to flat field because of the lack of time–dependent flat fields available between 1990 and 1992. The time dependence (or lack thereof) of the post–refurbishment flat fields has not been established at the writing of this handbook.

3.4 Sky Lines

The lines of geocoronal Ly $\alpha\lambda1216$ and OI $\lambda1304$ appear regularly in FOS spectra, with a width determined by the size of the aperture (see Table 1.1.3). Occasionally, when observing on the daylight side of the orbit, the additional sky lines of OI $\lambda1355$ and of OII $\lambda2470$ can also be seen. The second order Ly $\alpha\lambda1216$ appears sometimes in the G160L grating.

4. SIMULATING FOS

A simulator developed by K. Horne is available in the Space Telescope Science Data Analysis System (STSDAS) in the package synphot. Details about the STSDAS synphot package can be found in the Synphot User's Guide, by H. Bushouse, Sep. 1993, STScI, and in Appendix D of the HST Data Handbook (1994, Baum). The synphot data, which is not part of standard STSDAS, must be retrieved and installed to run synphot, as described in Appendix D.

• **Logging on to STEIS**. To log onto STEIS, type **ftp stsci.edu** or **ftp 130.167.1.2.** If prompted for Name, enter **anonymous.** Otherwise enter **user anonymous**. The password is your full email address. You are now in a UNIX-FTP environment. Enter **get README** to transfer the instructions to your home account. Most information relevant to data reduction is located within the `/instrument_news` and the `cdbs` directories. (For detailed information on STEIS, see the HST Data Handbook, Part XI, Chapter B, ed. Baum 1994.)

Synphot can be used to "observe" an arbitrary input spectrum with any FOS configuration to produce a predicted spectrum of detector counts s^{-1} diode^{-1}. This can be done using one of several tasks in the synphot package, including countrate, calcspec, and plspec. The operation of each of these tasks involves specifying the desired FOS observing mode, the input spectrum, and the form of the output spectrum. The choice as to which task to use depends on the desired results. For producing spectra in units of counts s^{-1} diode^{-1} the countrate task is the easiest to use and its input parameters are set up to mimic those found on FOS exposure log sheets.

For example, to reproduce the countrate spectrum shown in Figure 1.2.3 for the FOS blue side with grating G190H and the 1.0 aperture, the parameters for the countrate task would be set as given in Table 4.1. Note the inclusion of the argument "costar" in the aperture parameter, which is necessary for the task to use the aperture throughput data that are appropriate for the PSF and plate scale provided by COSTAR. In this example the input spectrum is specified using the unit function, which produces a spectrum that has constant flux as a function of wavelength. The two arguments for the unit function specify the flux level and units (in this case 1.0×10^{-14} ergs s^{-1} cm^{-2} Å^{-1} or "flam").

The task evaluates the spectrum on a wavelength grid that is automatically selected to match the dispersion (Ångstroms diode^{-1}) of the chosen observing mode. The computed spectrum will be written to the STSDAS table "spectrum.tab", which will contain two columns of wavelength and flux values, where the wavelengths will be in units of Ångstroms and the spectrum in units of counts diode^{-1}. With exptime=1, as in this example, the flux units are then essentially counts s^{-1} diode^{-1}. The spectral data in this table can be plotted using, for example, the STSDAS task sgraph (e.g. sgraph "spectrum.tab wavelength flux").

In addition to the unit function used in this example, synphot also has built-in blackbody and power-law functions that can be used to synthesize spectra of those forms. For example, in the countrate task you could set "synspec = bb(8000)" and "synmag = 14.5 V" to synthesize an 8000 K blackbody spectrum that is normalized to a V magnitude of 14.5. You could also specify "synspec = pl(3500,2)" and "synmag = 13.9 V" to obtain a power-law spectrum of the form F(ν) proportional to ν^{-2} (which has constant flux in wavelength space), normalized to a V magnitude of 13.9.

The userspec parameter can also be set to read spectral data from an existing table, such as data you may already have for a particular object. There are several spectral atlases available on STEIS that you can use as input to Synphot. Current holdings include a library of HST standard star spectra, Kurucz model atmospheres, a spectrum synthesis atlas from

G. Bruzual, the Bruzual-Persson-Gunn-Stryker spectral atlas which has wavelength coverage from the near-UV to the near-IR, and the optical stellar atlas from Jacoby, Hunter, & Christian (1985). See Appendix B of the Synphot User's Guide for information on how to obtain these data.

Table 4.1: Example parameters in Synphot countrate task to simulate an FOS observation of a flat-spectrum source with flux=1.0 x 10^{-14} ergs s^{-1} cm^{-2} $Å^{-1}$, as in Figure 1.2.3.

Parameter	Setting	Definition
output	spectrum.tab	Output table name
instrument	fos	Science instrument
detector	blue	Detector used
spec_elem	g190h	Spectral elements used
aperture	1.0,costar	Aperture / field of view
cenwave	INDEF	Central wavelength (HRS only)
userspec	unit(1.e-14,flam)	User supplied input spectrum
synspec		Synthetic spectrum
synmag		Magnitude of synthetic spectrum
refwave	INDEF	Reference wavelength
reddening	0.	Interstellar reddening in E(B-V)
exptime	1.	Exposure time in seconds
verbose	yes	Print results to STDOUT?
count_tot	INDEF	Estimated total counts
count_ref	INDEF	Estimated counts at reference wavelength
refdata		Reference data

Acknowledgements

I would like to thank Ralph Bohlin, Ian Evans, Ron Gilliland, Tony Keyes, Anuradha Koratkar and Rex Saffer for their careful reading of the Handbook. I would also like to thank Tony Keyes for updating the FOS simulator, for producing both bright limits and target acquisition times, and for making many useful suggestions. I would like to thank Cindy Taylor for producing most of the tables and the plots. I would like to thank Howard Bushouse, Jen Christensen, Anne Gonnella, Keith Horne, Buell Jannuzi, Pete Reppert, Sue Simkin, William Welsh, Rogier Windhorst, and Meg Urry for providing comments, criticisms, and corrections.

5. REFERENCES

Allen, R.G., & Angel, J.R.P. 1982, *FOS Spectropolarimeter Performance, FOS Instrument Handbook*, Version 1, ST ScI, page C-1.

Allen, R.G., & Smith, P.S. 1992, *FOS Polarimetry Calibrations*, Instrument Science Report CAL/FOS-078.

Baum, S. 1994, ed. *HST Data Handbook*, ST ScI.

Bazell, D. 1990, *Synphot Users Guide*, ST ScI.

Blades, J.C., Osmer, S.J. 1994, ed. *Calibrating the Hubble Space Telescope: Proceedings of a Workshop*, ST ScI.

Burrows, C., & Hasan, H. 1991, *Telescope Image Modelling User Manual*, ST ScI.

Bushouse, H. 1993, Synphot User's Guide, STScI.

Caldwell, J., & Cunningham, C.C. 1992, *Grating Scatter in the FOS and the GHRS*, Science Verification 1343 Interim Report.

Ford, H.C. 1985, *FOS Instrument Handbook*, ST ScI.

Harms, R.J. 1982, *The Space Telescope Observatory*, ed. D.N.B. Hall, (Special Session of Commission 44, IAU General Assembly, Patras, Greece, August, 1982; NASA CP-2244).

Harms, R.J., Angel, R., Bartko, F., Beaver, E., Bloomquist, W., Bohlin,R., Burbidge, E.M., Davidsen, A.,F., Flemming, J.C., Ford, H., & Margon, B. 1979, *SPIE*, **183**, 74.

Hartig, G.F. 1989, *Faint Object Spectrograph Instrument Handbook Supplement No. 1*, ST ScI.

Hartig, G.F. 1989, *FOS Filter-Grating Wheel Repeatability: Dependence on Motor Selection*, Instrument Science Report CAL/FOS-060.

Jacoby, G., Hunter, D., and Christian, C., 1984, ApJS, 56, 257.

Kriss, G.A., Blair, W.P., & Davidsen, A.F. 1991, *In-Flight FOS Wavelength Calibration – Template Spectra*, Instrument Science Report CAL/FOS-067.

Kriss, G.A., Blair, W.P., & Davidsen, A.F. 1992, *Internal/External Offsets in the FOS Wavelength Calibration*, Instrument Science Report CAL/FOS-070.

Lindler, D., & Bohlin, R. 1986, *FOS Linearity Corrections*, Instrument Science Report CAL/FOS-025.

Morris, S.L., Weymann, R.J., Savage, B.D., & Gilliland, R.L. 1991 *Ap. J. (Letters)*, **377**, L21.

Mount, G., & Rottman, G. 1981, *The Solar spectral irradiance 1200–3184Å near solar maximum: July 15, 1980*, J. Geophys. Res. **86**, 9193.

Neill, J.D., Bohlin, R.C., & Hartig, G. 1992, *Photometric Calibration of the Faint Object Spectrograph*, Instrument Science Report CAL/FOS-077

Rosenblatt, E.I., Baity, W.A., Beaver, E.A., Cohen, R.D., Junkkarinen, V.T., Linsky, J.B., and Lyons, R.W. 1992, *An Analysis of FOS Background Dark Noise*, Instrument Science Report CAL/FOS-071.

Wegener, R., Caldwell, J., Owne, T., Kim, S.J., Encrenaz, T., & Comber, M. 1985 *The Jovian Stratosphere in the Ultraviolet, Icarus*, **63**, 222.

Welsh, W.F., Chance, D., & Keyes, C.D. 1994 *High Speed Spectroscopy Using the FOS in Rapid Mode*, Instrument Science Report in preparation.

APPENDIX A.

Taking Data with FOS

Two sets of nomenclature are used to describe the taking of FOS data—those used in the exposure logsheets to command observations, and those used in the FOS data headers. Table A.1 gives the translation between the two, together with defaults and definitions.

FOS observations are performed in a nested manner, with the innermost nest being the livetime of the instrument plus the deadtime (LT + DT). Table A.1 lists the parameters in the order in which FOS observations are nested. Standard spectra are taken by sub-stepping the diode array along the dispersion in the X direction, and then by performing the sub-stepping five times over adjacent diodes to minimize the impact of dead diodes. The sequence is then

$$(\mathrm{LD} + \mathrm{DT}) \times 4 \times 5.$$

The minimum livetime is 0.003 seconds. The minimum livetime plus deadtime is 0.030 seconds. Using the minimum livetime results in very inefficient observations, since data are being taken only $0.003/0.03 = 0.1$ of the time.

The user has access only to those parameters that can be set in the exposure logsheet. For example, the user cannot set the livetime, but the user can set the product of livetime and INTS (STEP-TIME = LT× INTS). Likewise, the user cannot explicitly set the deadtime, but in PERIOD mode, the user can set the ratio of livetime to deadtime (DATA-RATIO = LT/DT).

For the most common mode, ACCUM, an FOS integration is constructed in the order (LT+DT), INTS, NXSTEPS, OVERSCAN, YSTEPS, NPATT, and finally NREAD. The total elapsed time of an integration is then given by

$$\Delta t = (\mathrm{LT} + \mathrm{DT}) \times \mathrm{INTS} \times \mathrm{NXSTEPS} \times \mathrm{OVERSCAN} \times \mathrm{YSTEPS} \times \mathrm{NPATT} \times \mathrm{NREAD}.$$

where NXSTEPS = SUB-STEP, and YSTEPS = Y-SIZE. This equation also gives the elapsed time for the observation, which for standard ACCUM mode is equal to

$$\Delta t = (\mathrm{LT} + \mathrm{DT}) \times \mathrm{INTS} \times 4 \times 5 \times 1 \times \mathrm{NPATT} \times \mathrm{NREAD}.$$

The number of patterns, NPATT, is set after the setting of sub-step (NXSTEPS), OVSERSCAN, and YSTEP, to achieve the exposure time requested. When NPATT has reached the maximum that it can be set to (256), then INTS is incremented. Obviously, this must be done in an optimal way to ensure that the efficiency ($\propto$ LT/DT) remains high. The maximum value for INTS is also 256.

For a RAPID observation, an FOS integration is built up in a slightly different order; (LT+DT), INTS, NXSTEP, OVERSCAN, YSTEPS, NPATT, and finally NMCLEARS. The total elapsed time of the observation is

$$\Delta t = (\mathrm{LT} + \mathrm{DT}) \times \mathrm{INTS} \times \mathrm{NXSTEP} \times \mathrm{OVERSCAN} \times \mathrm{YSTEPS} \times \mathrm{NPATT} \times \mathrm{NMCLEARS}.$$

which is usually equal to

$$\Delta t = (\mathrm{LT} + \mathrm{DT}) \times \mathrm{INTS} \times 4 \times 5 \times 1 \times \mathrm{NPATT} \times \mathrm{NMCLEARS}.$$

However, the sub-stepping, the overscan values, and the wavelength range can be lowered in RAPID to accommodate shorter time between the taking of spectra.

For a PERIOD observation, an FOS integration is built up of

$$\Delta t = (\mathrm{LT} + \mathrm{DT}) \times \mathrm{INTS} \times \mathrm{NXSTEP} \times \mathrm{OVERSCAN} \times \mathrm{YSTEPS} \times \mathrm{SLICES} \times \mathrm{NPATT}$$

where SLICES = BINS. As with RAPID, x step and overscan values can be lowered to result in a greater number of SLICES (BINS).

These equations give the elapsed time of an observation and so they can be used to calculate the actual start time of any observation, by subtracting them from the first packet time (FPKTTIME) which is given in the group parameter at the beginning of every group of "multi-group" data.

$$\text{Start Time} = \mathrm{FPKTTIME} - \Delta t$$

The start time of the entire observation is also given in the data header as EXPSTART. All times in the header, including the first packet time, and the start time, are given in units of Modified Julian Date, which is the Julian date minus 2400000.5. The Modified Julian Date for 1993 is given by:

$$\mathrm{MJD} = 48987.0 + \text{day of year} + \text{fraction of day from } 0^h UT.$$

Table A.1

FOS Observing Parameters
Listed in Order of Execution

Exposure Logsheet	FOS Header	Default	Definition
—	LIVETIME	0.500 sec	(LT) Time FOS is integrating.
—	DEADTIME	0.010 sec	(DT) Overhead time.
—	INTS	—	Number of times to execute (LT+DT)
SUB-STEP	NXSTEP	4	Number of steps of size diode/NXSTEP in direction of dispersion.
COMB	OVERSCAN*	YES	Whether or not to execute x stepping to remove the effects of dead diodes. For COMB= YES, MUL=5. For COMB= NO, MUL=1.
Y-SIZE	YSTEPS	1	Number of steps perpendicular to dispersion.
BINS	SLICE	5	For PERIOD only, equal to 1 otherwise. Number of bins to divide one period into.
—	NPATT	—	Number of times to execute the pattern so as to achieve the exposure time.
—	NREAD	—	For ACCUM only, equal to 1 otherwise. For readouts short enough to correct for GIMP
—	NMCLEARS	—	For RAPID only, equal to 1 otherwise. Number of times to clear data so as to read new data.

* The FOS header value for OVERSCAN is equal to the value for MUL.

Table A.1. *Continued*
Additional FOS Observing Parameters

Exp.Log.	FOS	Default	Definition
STEP-TIME	LT×INTS	0.5	Available in RAPID and PERIOD.
DATA-RATIO	LT/DT	Maximum	Available in PERIOD only.

APPENDIX B.

Dead Diode Tables

C. Taylor

Occasionally one of the 512 diodes on the red or the blue side becomes very noisy, or ceases to collect data. Since launch, the FOS has lost 3 diodes on the blue side and 2 diodes on the red side. In addition, several diodes on each side have become noisy and have been disabled. When a diode goes bad in orbit, there is a delay before that diode behavior is discovered, and another delay time before that diode is disabled so that its effect is removed from the data. Table B.1 lists the current (as of December 6, 1993) disabled diodes. Table B.2 lists the history of the diodes that have been disabled, when they were discovered to be bad, and when they were removed from action. The channels are numbered in this table from 0 to 511, while they are numbered in the STSDAS tasks from 1 to 512.

Table B.1

FOS DEAD AND NOISY CHANNEL SUMMARY[1]

BLUE DETECTOR

DISABLED Dead Channels	DISABLED Noisy Channels	DISABLED Cross-Wired Channels	ENABLED But Possibly Noisy
49	31	47	8
101	73	55	138
223	144		139
284	201		209/210
292	218		421
409	225		426
441	235		
471	241		
	268		
	398		
	415		
	427		
	451		
	465		
	472		
	497		
8	16	2	6

Total Blue Disabled: 26

RED DETECTOR

DISABLED Dead Channels	DISABLED Noisy Channels	ENABLED But Possibly Noisy
2	110	153
6	189	142
29	285	174
197	380	258/259
212	381	261
308	405	410
486	409	
	412	
7	8	6

Total Red Disabled: 15

1. Diode Range is 0-511.

Table B.2
FOS DEAD AND NOISY CHANNELS HISTORY[1]

BLUE DETECTOR

DISABLED Dead Channels	DATE Died	DATE Disabled
49	2/17/88	2/17/88
101	8/28/91	12/14/91
223	4/6/88	4/6/88
284	2/17/88	2/17/88
292	9/7/93	10/11/93
409	2/17/88	2/17/88
441	6/20/91	8/3/91
471	6/1/91	8/3/91

DISABLED Noisy Channels	DATE Noticed	DATE Disabled
31	3/11/88	11/1/90
73	Prelaunch	Prelaunch
144	3/17/93	5/3/93
201	Prelaunch	Prelaunch
218	Prelaunch	Prelaunch
225	Prelaunch, ?	5/18/90,(enabled 6/11/90),11/1/90
235	10/1/90	11/1/90
241	10/3/90	11/1/90
268	Prelaunch	Prelaunch
398	12/90	2/20/91
415	Prelaunch,10/92	Prelaunch,(enabled 2/20/91), 2/15/93
427	Prelaunch, 3/5/92	Prelaunch,(enabled 2/20/91),4/13/92
451	Prelaunch	Prelaunch
465	Prelaunch	Prelaunch
472	Prelaunch	Prelaunch
497	3/11/88	11/1/90
219	Prelaunch	Prelaunch,ENABLED 2/20/91

RED DETECTOR

DISABLED Dead Channels	DATE Died	DATE Disabled
2	Prelaunch	Prelaunch
6	Prelaunch	Prelaunch
29	10/27/91	1/7/92
197	12/90	2/20/91
212	Prelaunch	Prelaunch
308	10/12/93	
486	Prelaunch	Prelaunch

DISABLED Noisy Channels	DATE Noticed	DATE Disabled
110	7/16/90	9/14/90
189	9/91	12/14/91
285	Prelaunch	Prelaunch (formerly DEAD)
380	7/91	8/3/92
381	Prelaunch,5/93	Prelaunch,(enabled 8/27/90),10/11/93
405	Prelaunch	Prelaunch
409	Prelaunch	Prelaunch
412	11/91	10/11/93
235	Prelaunch	Prelaunch,ENABLED 8/27/90
261	Prelaunch	Prelaunch,ENABLED 8/27/90
344	Prelaunch	Prelaunch,ENABLED 8/27/90

1. Diode Range is 0-511.

APPENDIX C.

Grating Scatter

M. Rosa
Space Telescope European Coordinating Facility,
Garching bei Munchen, Germany

1. Dispersion and diffraction of light in the FOS

The FOS is a single pass spectrometer with blazed, ruled gratings. Both the blue and the red side detectors cover wide spectral ranges. Therefore, the FOS is subject to "scattered" light which has its origin primarily in the diffraction patterns of the gratings and the entrance apertures, as well as the micro roughness of gratings due to their ruled surfaces. These limitations are brought about by physical principles.

Additional scattering due to contamination of optical surfaces or unbaffled stray light worsens the situation. However, the analysis of laboratory and in-flight FOS data shows that the actual instrument performance is very close to the performance anticipated from ideal optical surfaces. Therefore, the contamination of observations by scattered light can be predicted with reasonable accuracy.

For illustration of the above arguments, let the target spectrum be the model atmosphere appropriate for the Sun (Kurucz 1993), observed in the FOS BLUE G190H mode through the 0.9 arcsec round aperture. The detector covers a range of $\pm$ 1.47 degrees of the diffracted angle, corresponding to the wavelength range 1573 Å to 2330 Å . The 3 panels of Figure C.1 cover the range -10 to $+23$ degrees in diffracted angles (0 Å to 7800 Å in first order). Figure C.1 shows, in logarithmic count rates (offset by $+1$ in the y direction),

- the "ideal" spectrum as observed by an unphysical instrument that relates wavelengths one-to-one to diffracted angles;
- the "grating" spectrum as dispersed by the blazed grating; orders visible on the graph are 0, 1 and 2;
- the "model observations", *i.e.*, the ddispersed spectrum convolved with the additional scattering imposed by the finite size aperture, the ruled surface of the grating and a minute amount of dust on the optical surfaces.

The shapes of the zero order peaks in the lower panel of Figure C.1 reflect the actual line spread function (LSF). The far wings of this LSF carry light from the peak of the original distribution into domains where the target spectrum, filtered by the total throughput of all optical elements and the detector efficiency, produces very few intrinsic counts. In addition this LSF moves photons from the zero order peak into the adjacent parts of the 1st order seen by the detector—although the zero order peak itself is correctly baffled.

In Figure C.2 are shown the actual observed count rates for the star 16 Cyg B, very similar to the Sun, overlaid with the "ideal" and the "model" observations from Figure C.1. For a solar-like target spectrum, the scattered light component ranges between 0.999 and 0.01 of the observed signal in the BLUE G190H mode.

2. Predicting the contamination

UV observations of intrinsically red spectra are subject to severe contamination. A rough idea of the contamination can be obtained from Table C.1, where the log of the count ratio

(Scattered+Intrinsic/Intrinsic) is listed for a variety of target spectra and high dispersion FOS modes.

As a guide to the wavelength range where scattered light will dominate over the signal for a given target spectrum, one determines the signal count rate spectrum:

$$N_\lambda = F_\lambda * E_\lambda$$

where N_λ is the count rate per diode, F_λ is the incident spectrum, and E_λ is the efficiency as a function of wavelength for the spectral range (FOS mode) of interest, and for the adjacent modes (wavelength ranges) towards the red. Scattered light will dominate the signal in regions were N_λ falls off more rapidily than the LSF. The medium range (10–500 diode) wings of the LSF can be approximated by an inverse square function (diode-diode$_0$)$^{-2}$, the conversion from λ space into diode space is provided in Table 1.1.1 (FOS Dispersers).

In order to accurately predict the contamination by scattered light for a given grating/detector/aperture combination, an appropriate estimate of the intrinsic energy distribution of the target is required; and the properties of all optical components have to be taken into account in detail. Software to model the resultant count rate spectra will soon be made available in the IRAF/STSDAS FOS analysis package.

3. Advice to proposers

- UV spectra shortward of 2500 Å of very red targets may be obtained almost free of scattered red light in the low resolution modes of the GHRS.
- Use the BLUE digicon for very red targets (later than K3) for G190H observations to reduce the amount of far red scattered photons.
- Consult table C.1 to find the wavelength range where the scattered light starts to dominate. Observations of continuum sources shortward of this range are absolutely useless, unless the intrinsic spectra flatten off. For example, the coronal emission in α Ori (M0Iab) can be traced in a G130H spectrum, but a quantitative assessment is impossible.
- Contaminated data with a ratio of scattered counts over intrinsic counts of up to 5 can likely be corrected **provided** the intrinsic target spectrum is known for longer wavelengths, **and provided** the exposure times are chosen such as to give enough S/N for the weak signal in the total of signal+scattered counts. It is also advisable to obtain a target spectrum at longer wavelengths, at least with the adjacent FOS range.

Additional References

Ayres,T.R.: 1993, "Scattered Light in the G130H and G190H Modes of the HST FOS" , CAL/FOS–0115, STScI

Caldwell, J. and Cunningham, C.C : 1992, Science Verification 1343 Interim Report

Kinney,A.L., Bohlin,R.C.: 1993, "Background due to scattered light", CAL/FOS–0103, STScI

Rosa, M.R.: 1993, "Scattered light in the FOS: An Assessment using science data" , CAL/FOS–0114, STScI = ST-ECF Newsletter No. 20, p. 16

Stroke, G.W.: 1967, "Diffraction Gratings", in *Encyclopedia of Physics - Handbuch der Physik*, S.Flügge (ed.), Springer, Berlin, p.427–754

Table C.1
Logarithmic ratios of count rates (Scattered+Intrinsic)/(Intrinsic) for unreddened stars. FOS, blue detector

A0 V G130H		G5 V G190H		K 3 III G270H	
λ	log[(S+I)/I)]	λ	log[(S+I)/I)]	λ	log[(S+I)/I])
1170	0.98	1600	2.92	2250	1.49
1215	1.73	1700	1.00	2350	1.15
1250	0.18	1800	0.41	2500	0.52
1300	0.02	1900	0.19	2700	0.24
1400	0.01	2000	0.07	3000	0.02
1600	0.00	2300	0.01	3300	0.00

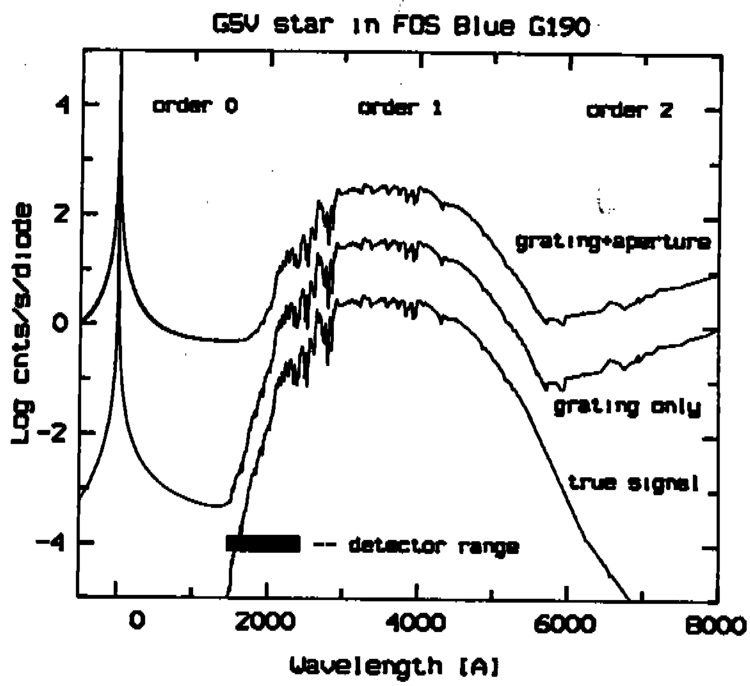

Figure C.1: FOS Blue G190H Count rate spectra for a G5 V model atmosphere in the detector plane. See text. Note that the real detector only covers the wavelength range marked by a thick bar.

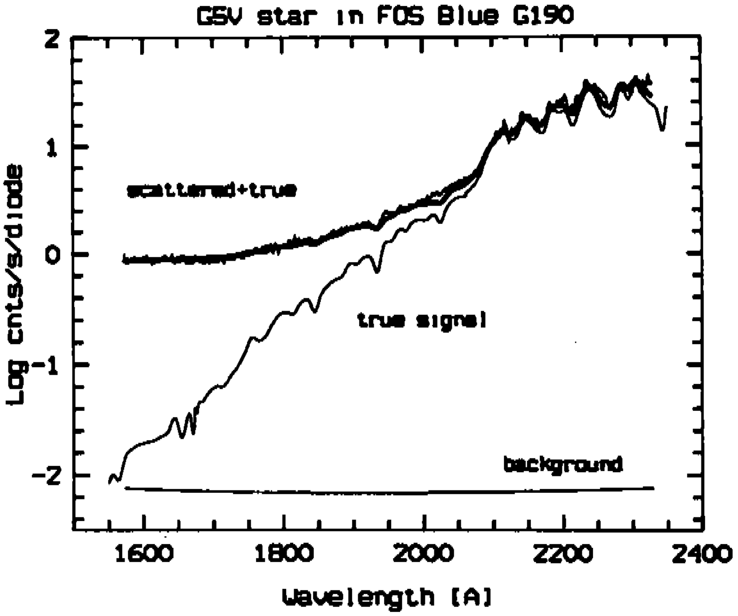

Figure C.2: FOS Blue G190H data for the G5 V star 16 Cyg B. The count rate spectrum due to intrinsic photons and the composite of intrinsic and scattered photons are overlaid.

Appendix D

FOS Wavelength Comparison Spectra

Charles D. (Tony) Keyes

This appendix provides maps of the FOS Pt-Cr-Ne comparison spectrum for each FOS detector/disperser combination except the prism. The spectra are plotted as count-rates versus wavelength in Figures D.1 through D.14. Table D.1 contains a listing of the vacuum wavelength and element-of-origin for 159 potentially usable FOS comparison lines in the spectral range 1200-8800 Angstroms. The wavelength of each of these lines is indicated by a diamond symbol in the figures. Please note that some of the lines marked on any particular plot may not be used in actual FOS dispersion-relation calibration computations.

Table D.1: Wavelength and Identification of FOS Comparison Lines

Vacuum Wavelength	Element	Vacuum Wavelength	Element	Vacuum Wavelength	Element
1238.852	Pt	1907.494	Ne	2390.262	Pt
1248.610	Pt	1911.710	Pt	2440.797	Pt
1271.793	Pt	1916.083	Ne	2487.919	Pt
1309.496	Pt	2037.089	Pt	2509.195	Pt
1327.432	??	2050.097	??	2603.913	Pt
1378.956	Pt	2076.139	Pt	2628.815	Pt
1382.046	Pt	2129.283	Pt	2640.132	Pt
1410.135	??	2144.922	Pt	2651.641	Pt
1482.826	Pt	2165.872	Pt	2703.205	Pt
1494.726	Pt	2175.352	Pt	2706.696	Pt
1509.272	Pt	2191.000	Pt	2734.770	Pt
1524.704	Pt	2235.610	Pt	2763.736	Ne
1530.199	??	2246.215	??	2772.490	Pt
1534.894	Pt	2263.363	Pt	2810.327	Cr
1554.929	Pt	2269.542	Pt	2876.693	Pt
1574.322	Pt	2275.083	Pt	2890.137	Cr
1581.399	??	2293.085	Pt	2894.720	Pt
1621.718	Pt	2311.668	Pt	2930.652	Pt
1688.358	Ne	2319.007	Pt	2956.594	Ne
1723.158	Pt	2340.894	Pt	2964.156	Ne
1867.100	Pt	2357.825	Pt	2987.111	Cr
1883.079	Pt	2378.002	Pt	2998.845	Pt

Table D.1: Wavelength and Identification of FOS Comparison Lines

Vacuum Wavelength	Element	Vacuum Wavelength	Element	Vacuum Wavelength	Element
3022.460	Cr	3970.873	Cr	5946.479	Ne
3089.126	??	3977.795	Cr	6031.672	Ne
3204.966	??	3985.026	Cr	6076.024	Ne
3219.139	Ne	3992.249	Cr	6097.851	Ne
3245.086	Ne	4127.875	Cr	6144.763	Ne
3298.689	Ne	4255.528	Cr	6165.298	Ne
3302.810	Pt	4276.013	Cr	6219.003	Ne
3310.732	Ne	4290.938	Cr	6268.226	Ne
3324.706	Ne	4345.731	Cr	6306.536	Ne
3379.250	Ne	4352.993	Cr	6336.184	Ne
3409.107	Pt	4372.508	Cr	6384.757	Ne
3418.880	Ne	4386.202	Cr	6404.022	Ne
3448.688	Ne	4581.334	Cr	6508.330	Ne
3473.564	Ne	4602.040	Cr	6534.688	Ne
3521.476	Ne	4627.477	Cr	6600.775	Ne
3543.912	Ne	4647.452	Cr	6680.127	Ne
3569.549	Ne	4653.463	Cr	6718.897	Ne
3594.575	Cr	4757.421	Cr	6931.385	Ne
3606.349	Cr	4923.655	Cr	7034.353	Ne
3634.705	Ne	5039.156	Ne	7175.920	Ne
3665.154	Ne	5081.797	Ne	7247.170	Ne
3695.251	Ne	5117.927	Ne	7440.953	Ne
3728.140	Ne	5299.666	Ne	7490.937	Ne
3744.954	Cr	5332.264	Ne	8084.688	Ne
3778.232	Ne	5402.063	Ne	8138.653	Ne
3819.774	Pt	5411.286	Cr	8302.612	Ne
3909.867	Cr	5658.231	Ne	8379.914	Ne
3920.270	Cr	5749.896	Ne	8420.745	Ne
3929.762	Cr	5806.062	Ne	8497.699	Ne
3942.616	Cr	5854.114	Ne	8656.766	Ne
3964.811	Cr	5883.522	Ne	8783.038	Ne

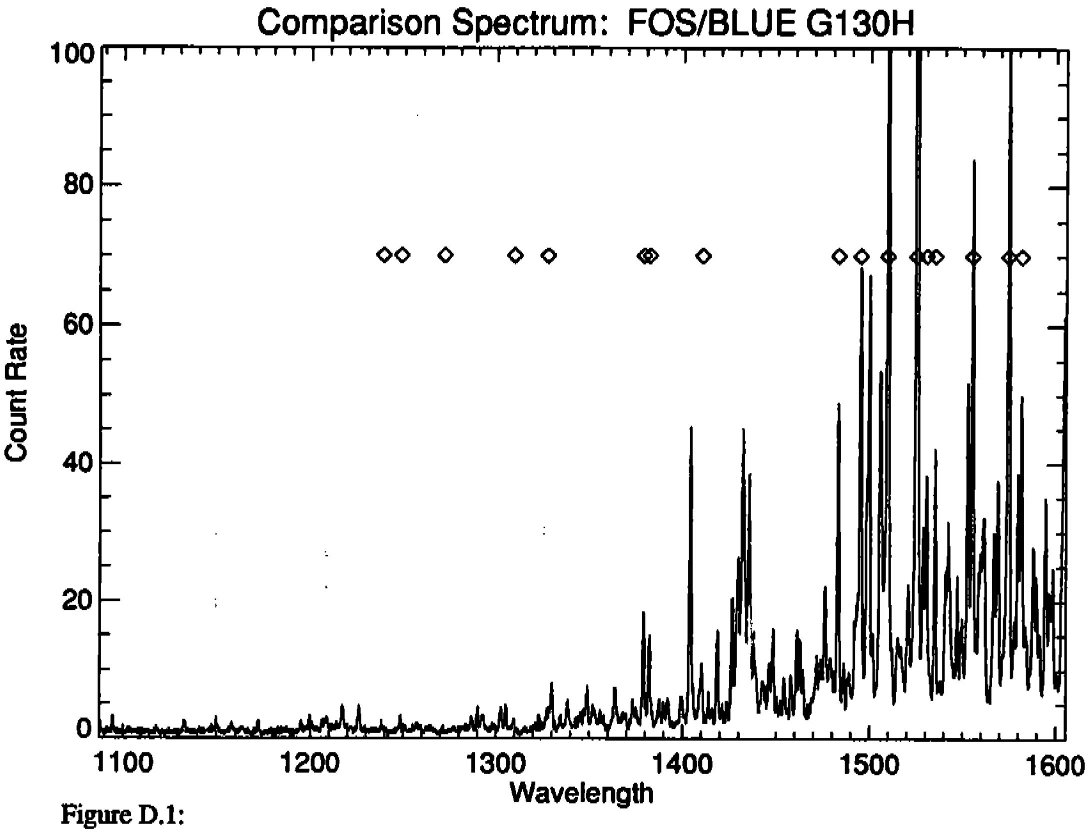

Figure D.1:

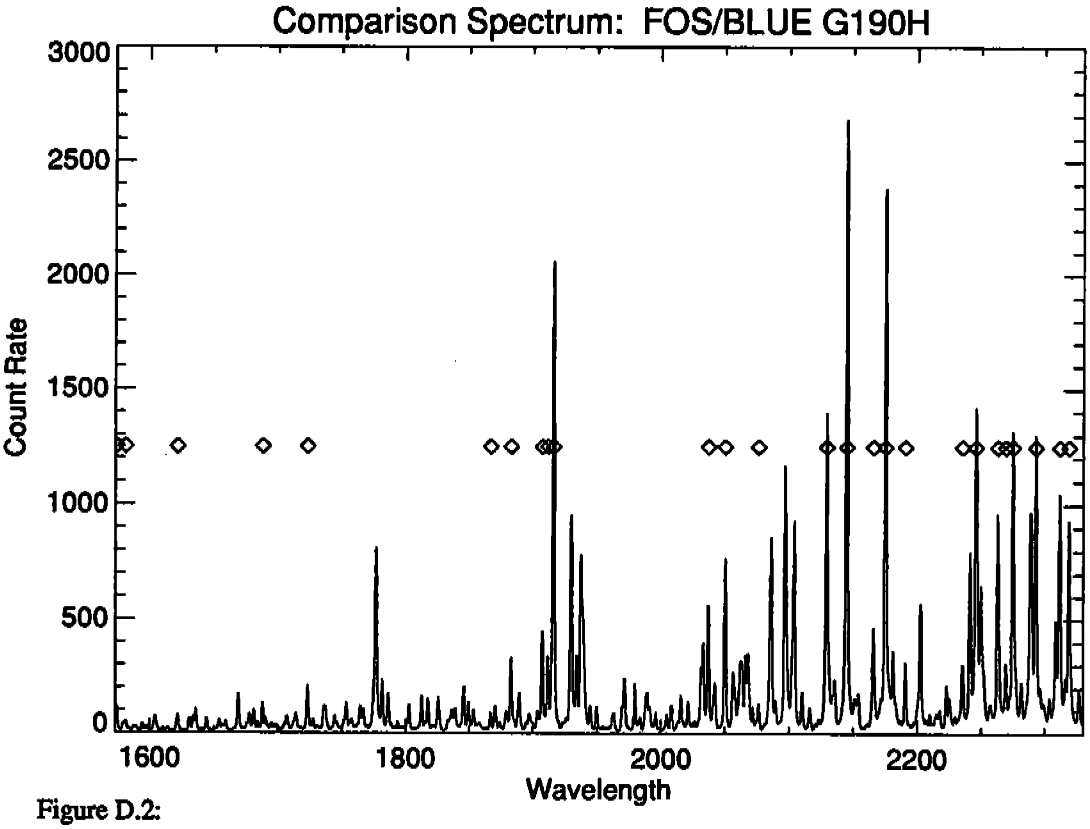

Figure D.2:

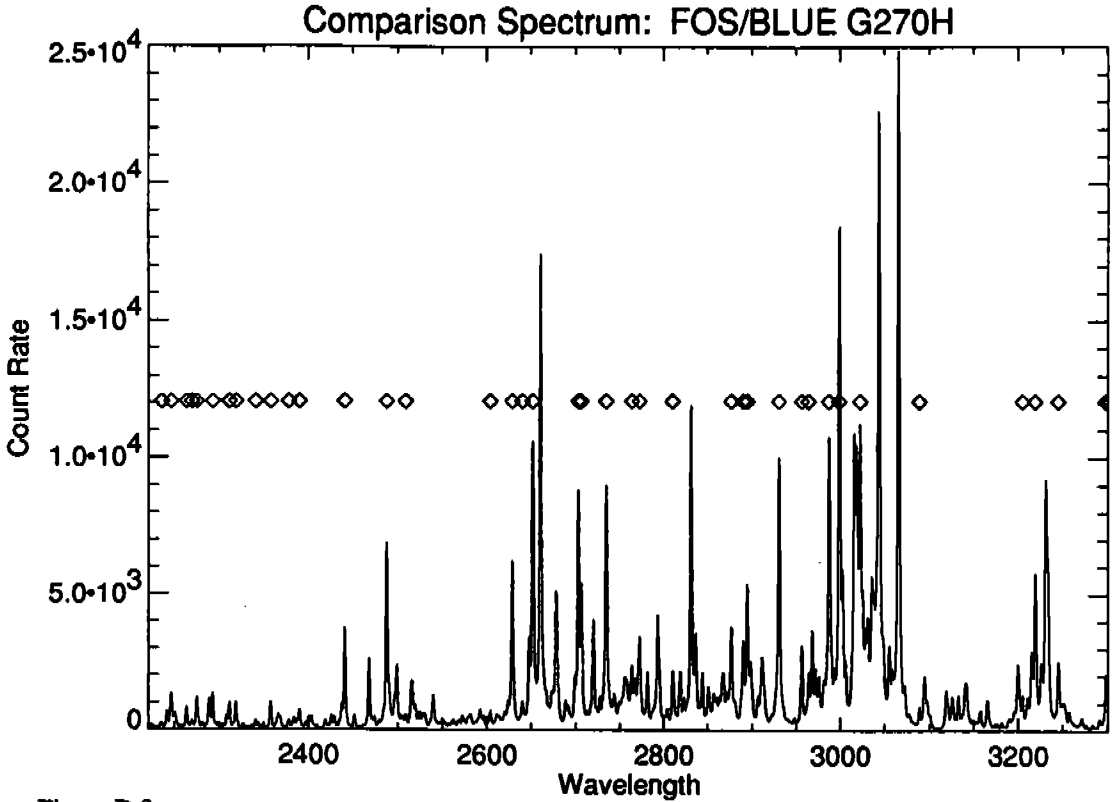

Figure D.3:

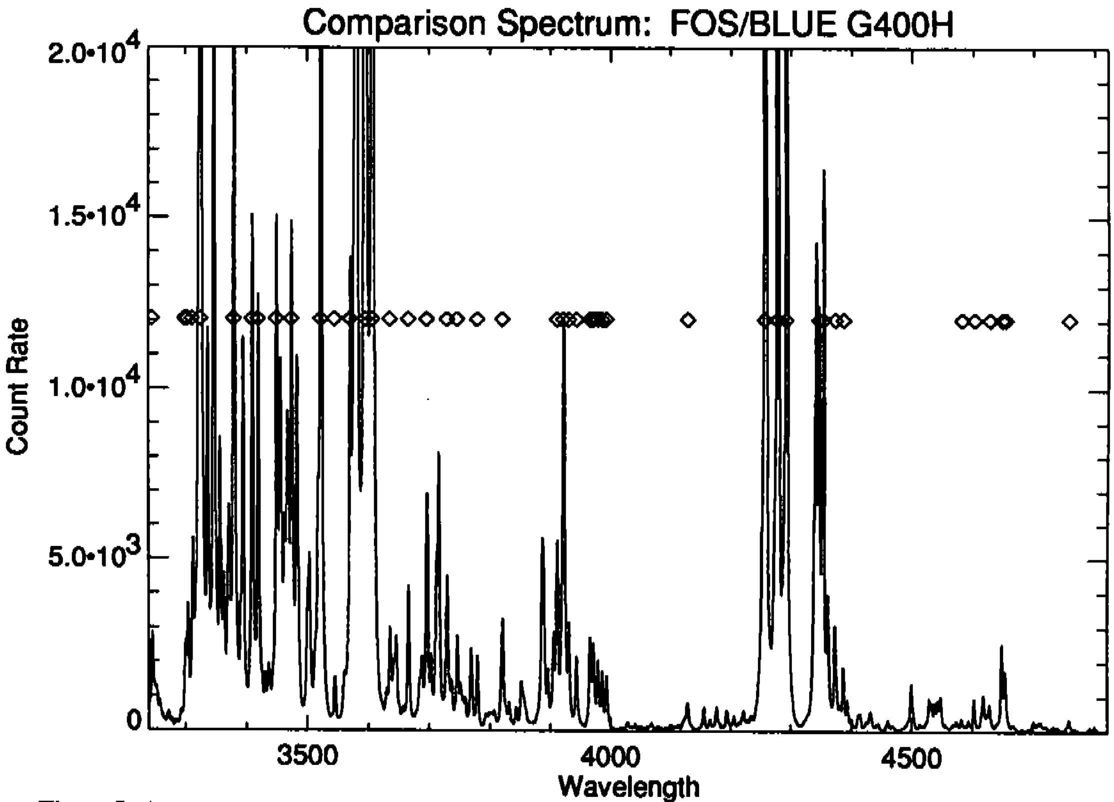

Figure D.4:

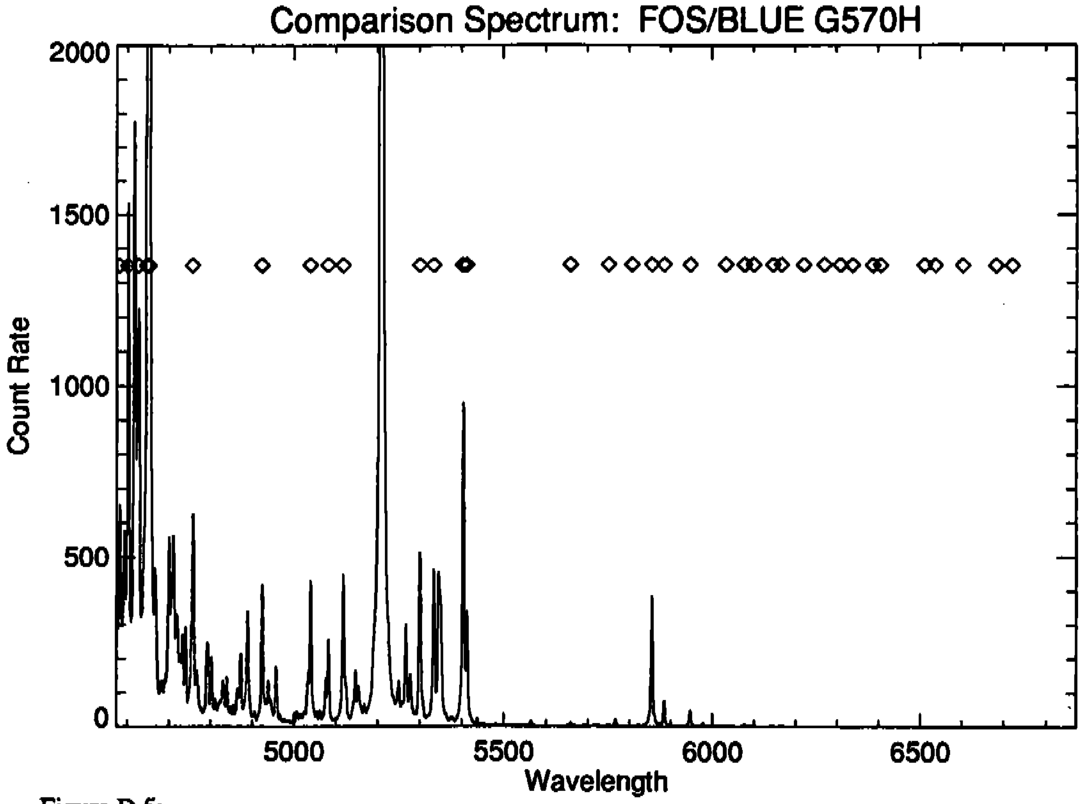

Figure D.5;

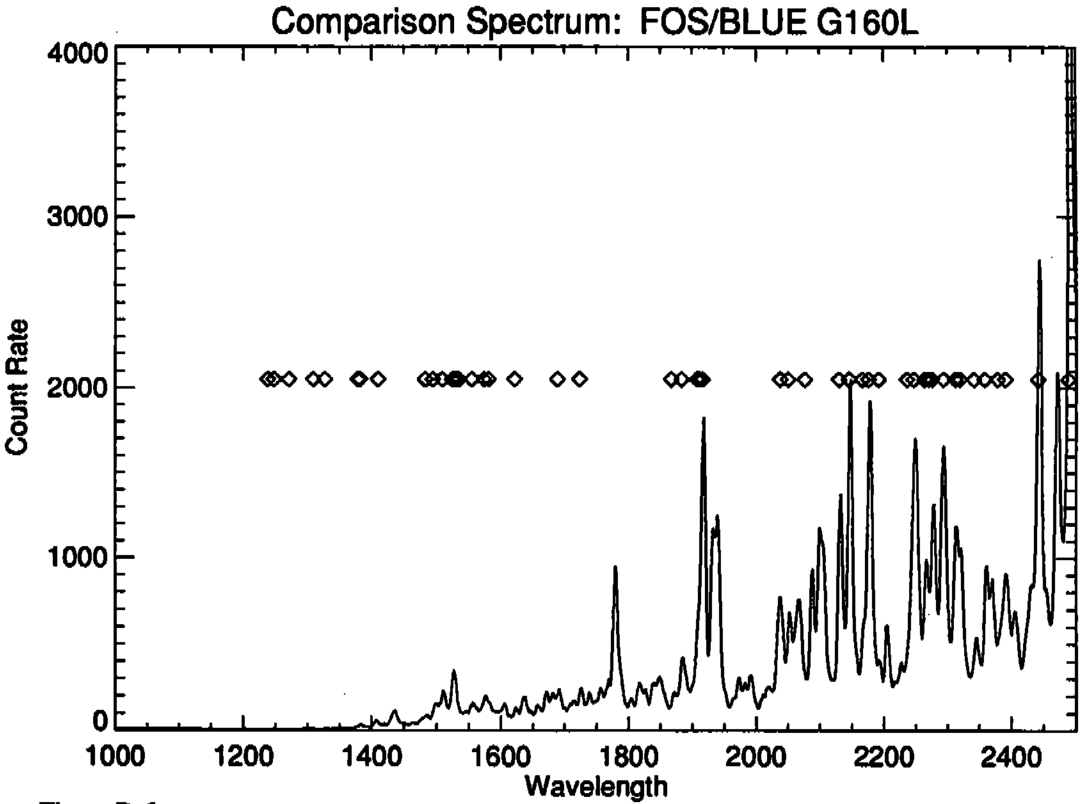

Figure D.6:

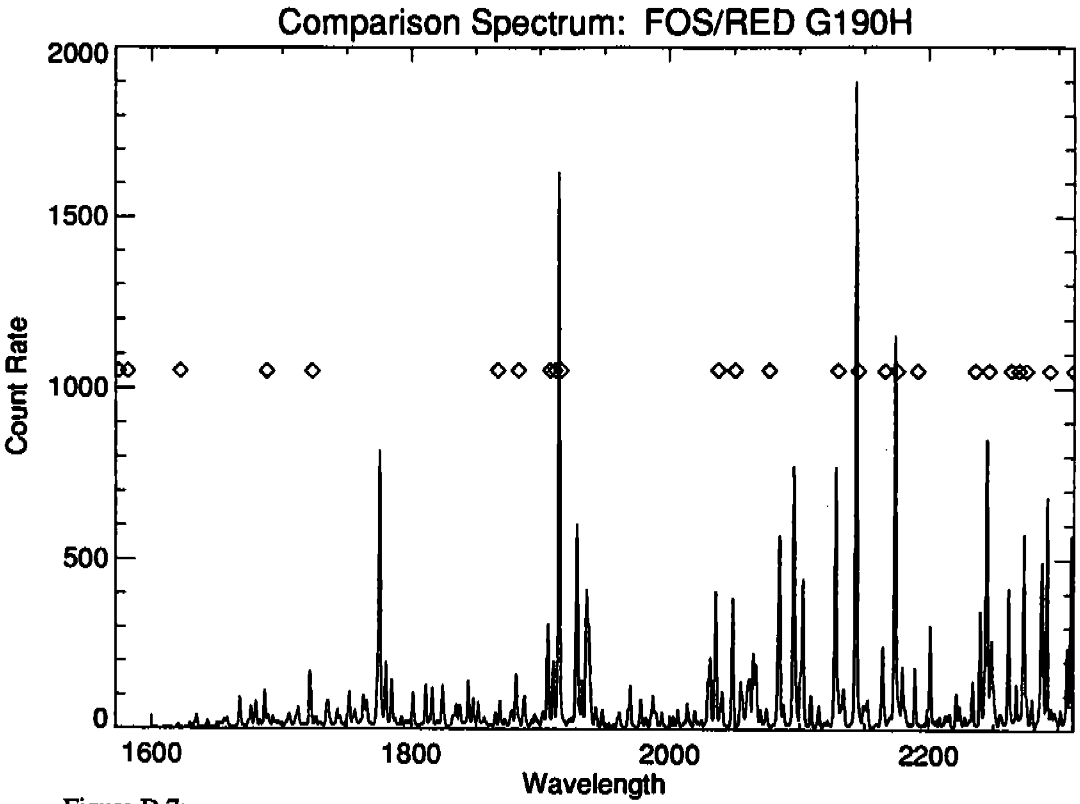

Figure D.7:

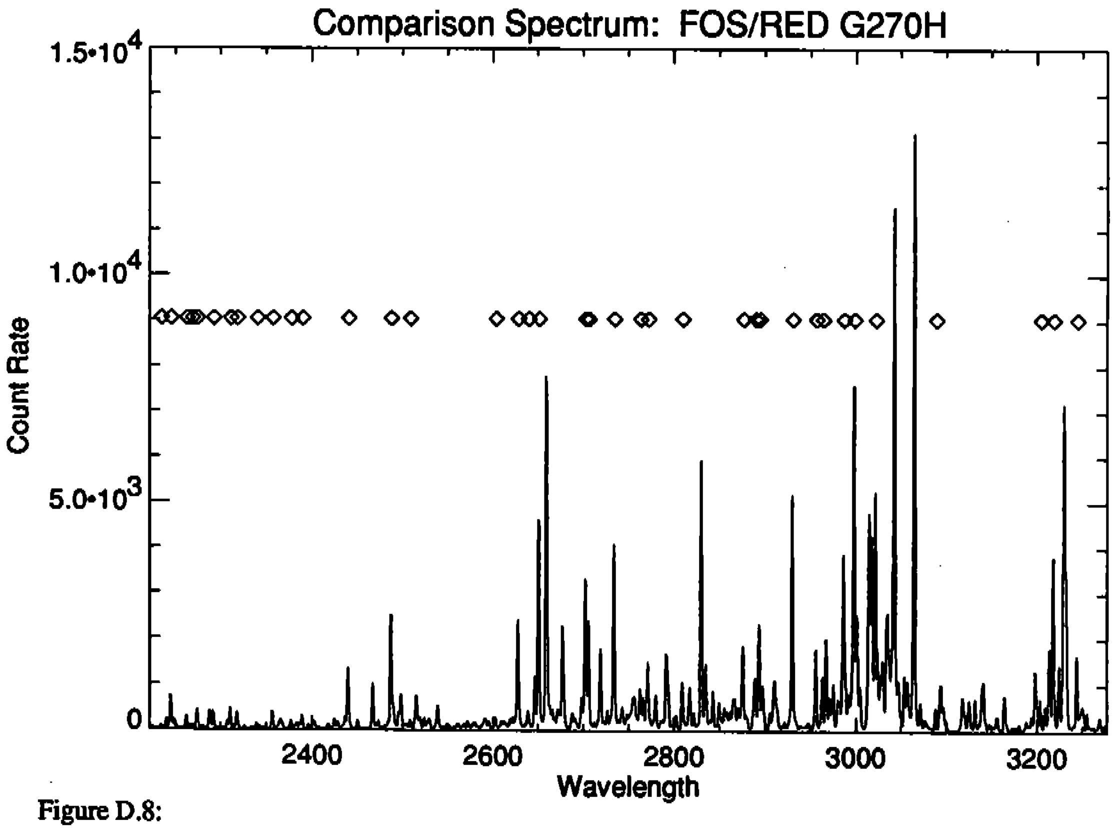

Figure D.8:

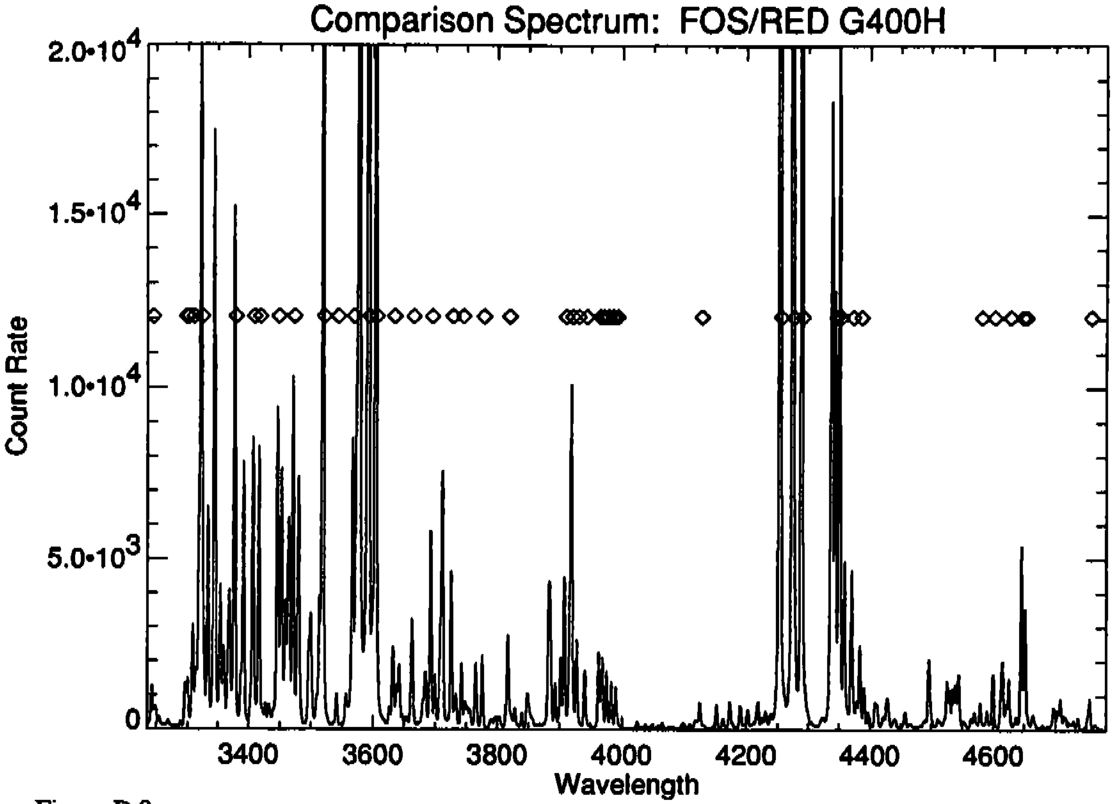

Figure D.9:

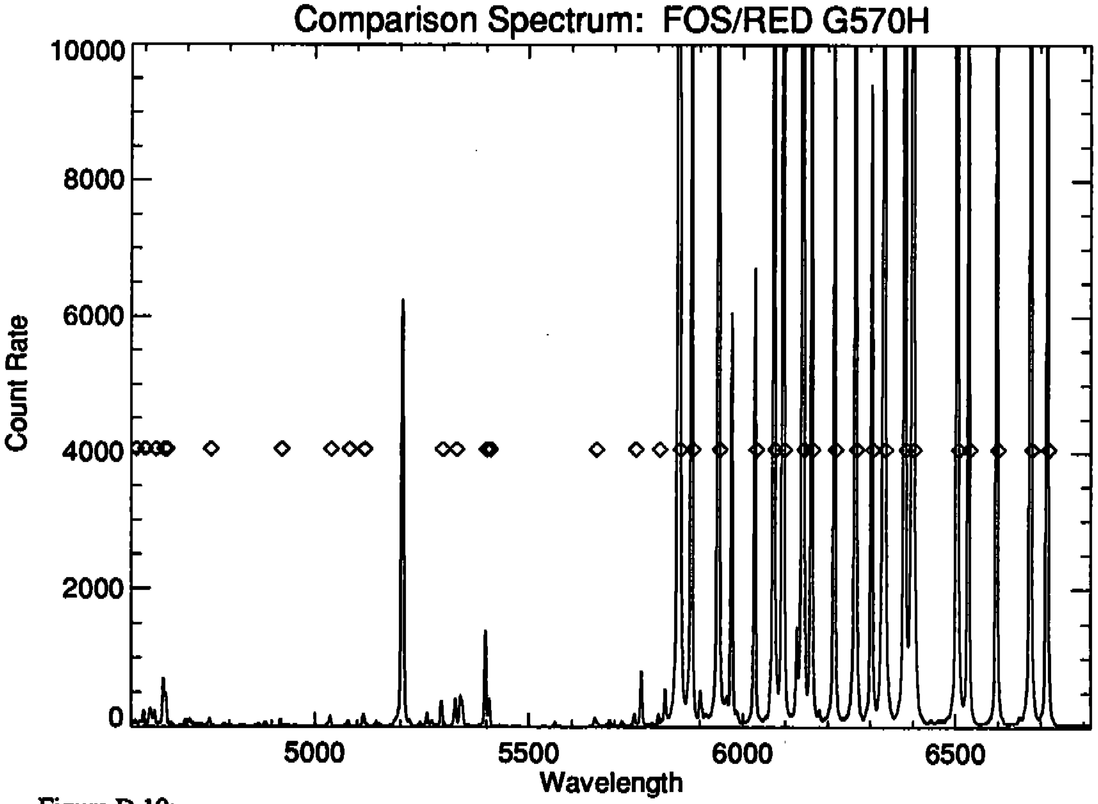

Figure D.10:

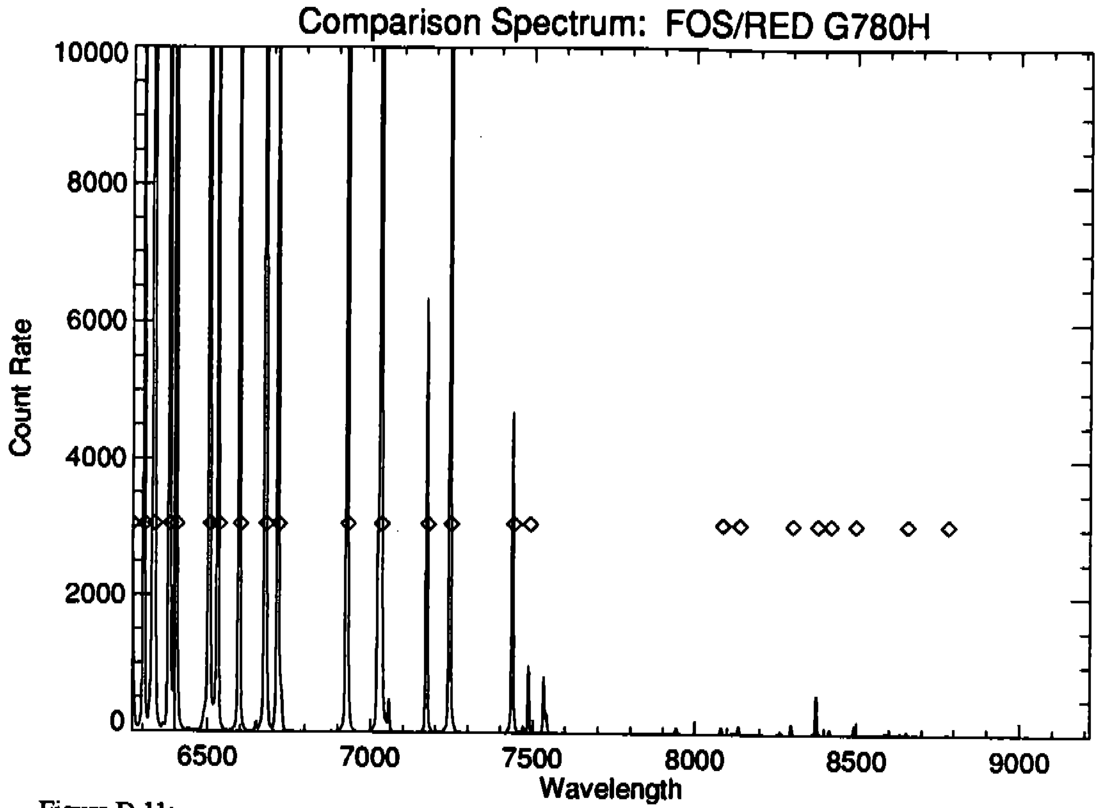

Figure D.11:

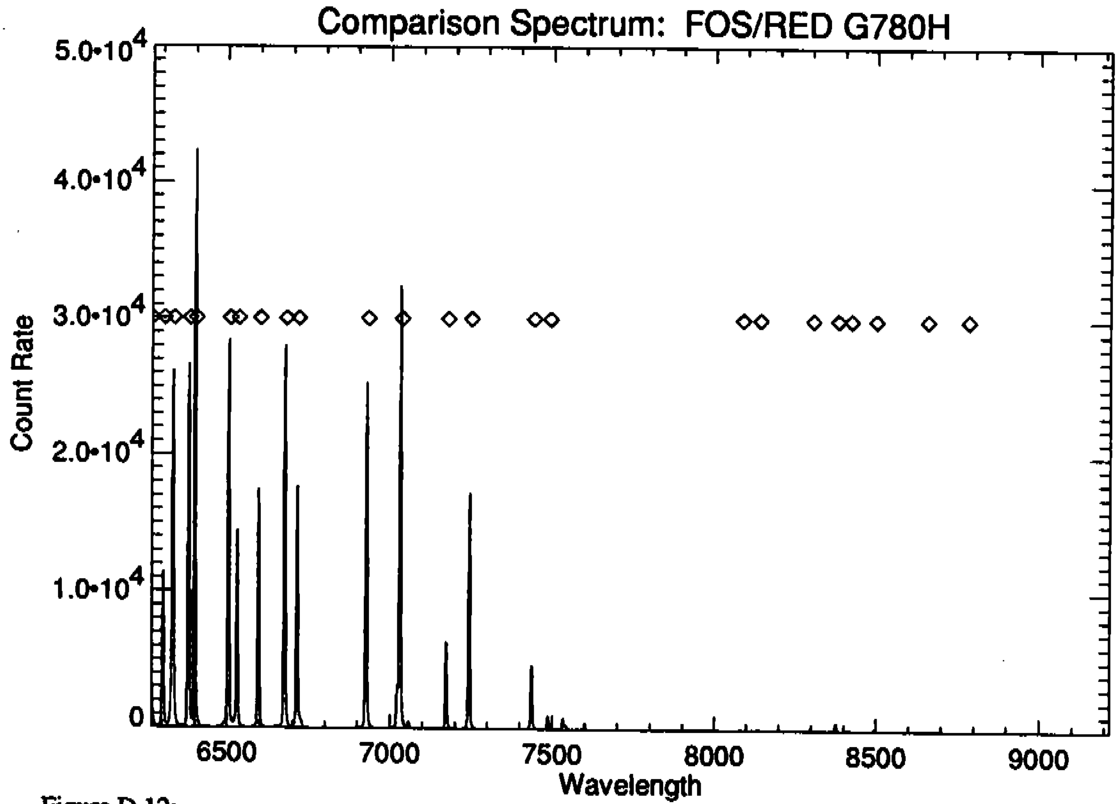

Figure D.12:

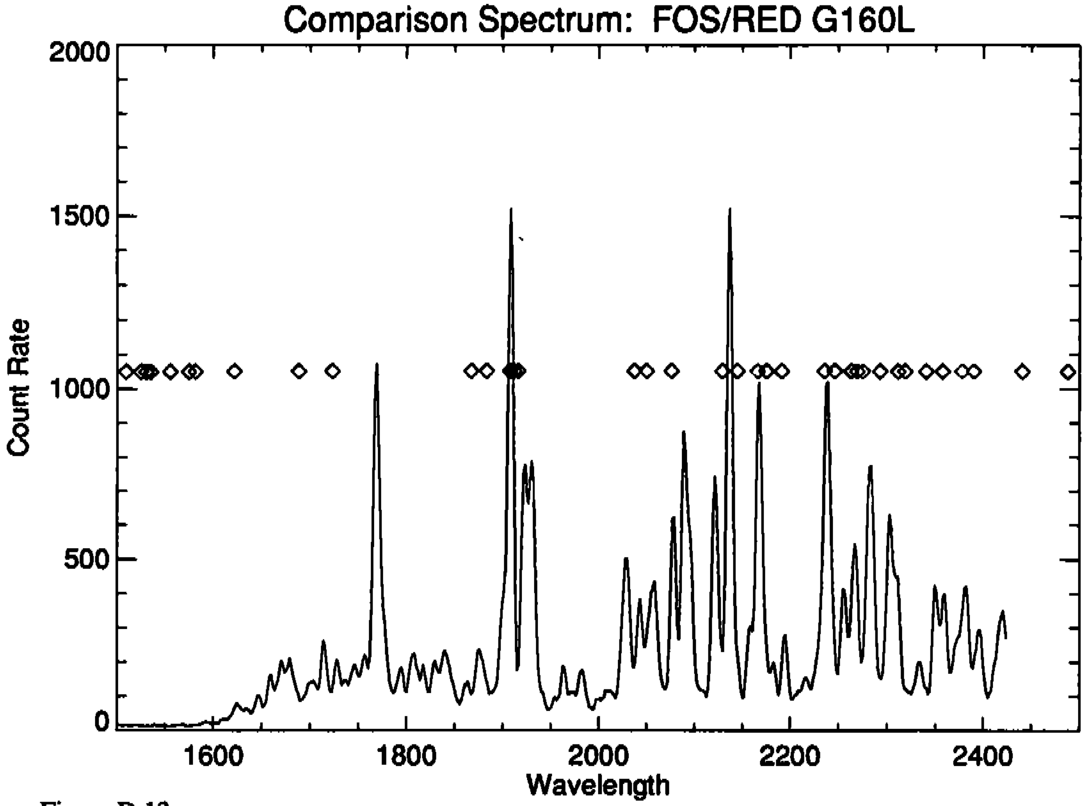

Figure D.13:

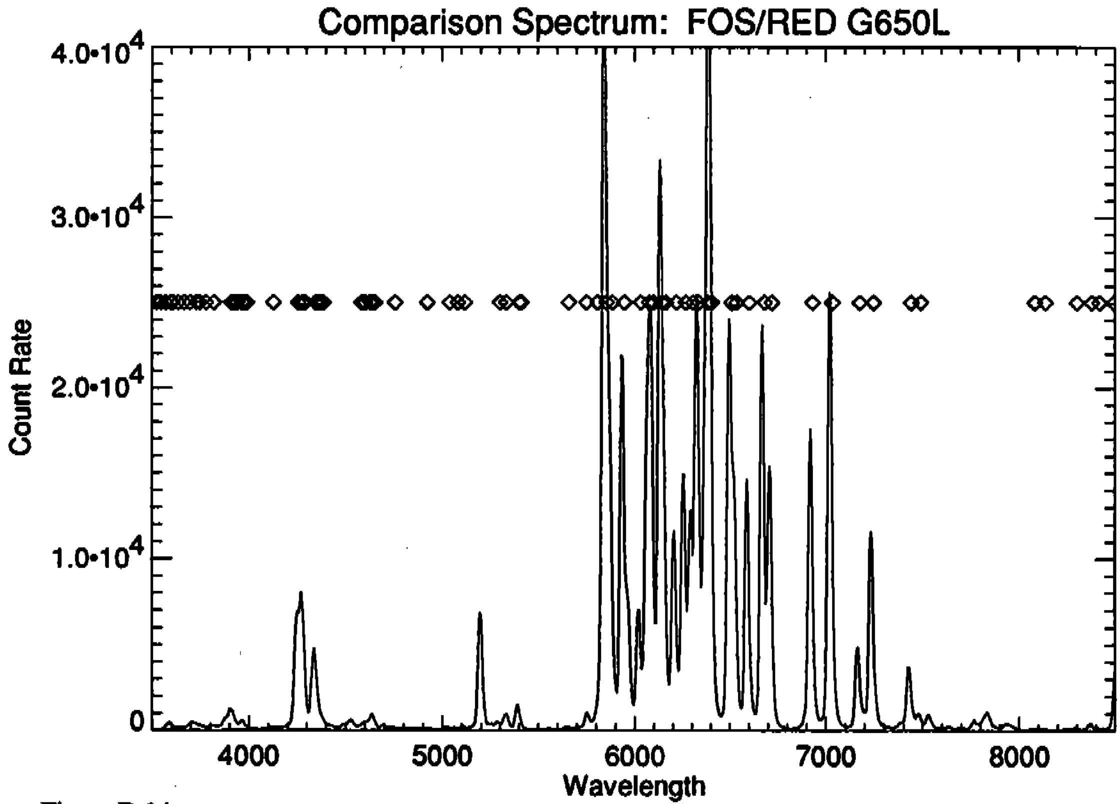

Figure D.14:

APPENDIX E

Faint Object Spectrograph Instrument Science Reports

April 1, 1994

060 FOS Filter-Grating Wheel Repeatability: Dependence on Motor Selection , G. Hartig - 5/89
067 In-Flight FOS Wavelength Calibration - Template Spectra G.A. Kriss, W.P. Blair, and A.F. Davidsen - 2/91
068 FOS Red Detector Plate Scale and Orientation, B. Bhattacharya and G. Hartig - 11/91
069 FOS Red Detector Flat-field and Sensitivity Degradation, G. Hartig - 11/91
070 Internal/External Offsets in the FOS Wavelength Calibration G.A. Kriss, W.P. Blair, and A.F. Davidsen - February 1992
071 An Analysis of FOS Background Dark Noise - E.I. Rosenblatt, W.A. Baity, E.A. Beaver, R.D. Cohen, V.T. Junkkarinen, J.B. Linsky, and R. Lyons - 4/92
072* Aperture Calibrations During Science Verification of the FOS L. Dressel and R. Harms - May 1992 (reworked)
073 Scattered Light Characteristics of the HST FOS F. Bartko, G.S. Burks, G. A. Kriss, A.F. Davidsen, R.D. Cohen, V.T. Junkkarinen and R. Lyons - April 1992
074 On - Orbit Discriminator Settings for FOS R.D. Cohen - February 1992
075 FOS Spectral Flat Field Calibration (Science Verification Phase Data), S.F. Anderson - February 1992
076 Analysis of FOS On-Orbit Detector Background with Burst Noise Rejection, E.A. Beaver and R. W. Lyons - April 1992
077 Photometric Calibration of the FOS J. D. Neill, R. C. Bohlin, and G. Hartig - June 1992
078 FOS Polarimetry Calibration [update of CAL/FOS 055] R.G. Allen and P.S. Smith - March 1992
079 FOS Operation in the South Atlantic Anomaly W. A. Baity, E. A. Beaver, J.B. Linsky and R. W. Lyons - April 1992
080 FOS On-Orbit Background Measurements R. W. Lyons, J. B. Linsky, E.A. Beaver, W. A. Baity, and E. I. Rosenblatt - April 1992
081 FOS Onboard Target Acquisition Tests S. Caganoff, Z. Tsvetanov, and L. Armus - April 1992
082 Lab Test Results of the FOS Detector Performance in a Variable External Magnetic Field E. A. Beaver and P. Foster - June 1992

084 Photometric Calibration of the Faint Object Spectrograph and Other HST Scientific Instruments - R.C. Bohlin and J.D. Neill 7/92

085 FOS Aperture Throughput Variations with OTA Focus - D. Lindler and R. Bohlin, 8/92

086 Analysis of Photometric Standards following July 1992 FOS Overlight Stafing Event, C. J. Taylor and C. D. Keyes, 12/92

087 FOS Blue Dectector Plate Scale and Orientation; A. Koratkar, 5/93

088 FOS Flats From Super Spectra; D. Lindler, R. Bohlin, G. Hartig and C. Keyes, 3/93

089 Primary author: T. Keyes

090 FOS Flat Field Reference Files: A Quick Reference Guide to the Appropriate File for a Particular Date and Instrumental Configuration; C. Keyes and C. Taylor

091 A Rough Photometric Calibration for FOS,BLUE,G160L,ORDER0, Keith Horne and Michael Eracleous, 8/93

092 The Post COSTAR Rotation Matrices for Calculating V2,V3 Offsets in Mode 2 FOS Target Acquisition; A.P. Koratkar and O. Lupie

093 FOS Inverse Sensitivity Reference Files: A Quick Reference Guide to the Appropriate File for a Particular Date and Instrumental Configuration, Cynthia J. Taylor and Charles D. (Tony) Keyes, 6/93

094 FOS Calibration Plan for Cycle 3; Charles D. (Tony) Keyes and Anuradha Koratkar, 6/93

095 Location of FOS Polarimetry; Anuradha Koratkar and Cynthia J. Taylor, 6/93

096 Location of FOS Spectra: Cycle 1 and Cycle 2 Results, Anuradha Koratkar and Cynthia J. Taylor, 8/93

097 Light Loss in FOS as a Function of Pointing Error, R. C. Bohlin, 8/93

098 Correction of the geomagnetically-induced image motion problem on the Hubble space telescope's faint object spectograph, John E. Fitch, Dr. George F. Hartig, Dr. Edward A. Beaver and Dr. Richard G. Hier, 8/93

099 Serendipitous Background Monitoring of the Hubble Space Telescope's Faint Object Spectograph, John E. Fitch and Glenn Schneider, 8/93

100 Cycle1/Cycle2 Discriminator Settings, Cynthia J. Taylor and Anne L. Kinney, 2/94

101 authors: Roberto Gilmozzi and Ellyne Kinney

102 FOS Aperture Throughput Variations due to Focus Changes, D.L. Lindler and R.C. Bohlin, 8/93

103 Background Due to Scattered Light, A.L. Kinney and R.C. Bohlin, 9/93

104 Pre-COSTAR FOS Point Spread Functions and Line Spread Functions from Models, I.N. Evans, 9/93
105 Pre-COSTAR FOS Aperture Throughputs from Models, I.N. Evans, 9/93
106 Pre-COSTAR FOS Aperture Transmissions for Point Sources and Surface Brightness of Diffuse Sources, R. C. Bohlin, 10/93
107 Pre-COSTAR FOS Aperture Throughputs for Mis-centered Targets Derived from PSF Models, I.N. Evans, 11/93
108 FOS Calibration Plan for SMOV, A.Koratkar,C.Keyes, A.Kinney, I.Evans and C. Taylor, 11/93
109 FOS Calibration Plan for Cycle 4, A.Koratkar, A.Kinney, C.Keyes, I.Evans, and C.Taylor, 11/93
110 Location of FOS Spectra: Cycle 3, Anuradha Koratkar, 12/93
111 Positions Prepeatability of Spectra Obtained with the FOS, Lyons, R.W., Beaver, E.A., Cohen, R.D., & Junkkarinene, V.T., 2/94
114 Scattered Light in the FOS: An Assessment Using Science Data, Michael R. Rosa, 11/93
115 Scattered Light in the G130H and G190H Modes of the HST Faint Object Spectograph, 11/93
116 SMOV Report I: Location of FOS Spectra, Anuradha Koratkar, Cynthia Taylor, Anne Kinney and Charles (Tony) Keyes
117 SMOV Report II: FOS Coarse Alignment 4907, A.L. Kinney, A.P. Koratkar, O. Lupie, C.J. Taylor and C.D. Keyes
118 SMOV Report III: FOS Baseline Sensitivity, Charles (Tony) Keyes, Anne Kinney, Anuradha Koratkar, Cynthia Taylor, 1/94
119 The Faint Object Spectograph Binary Search Target Acquisition Simulator BS4, I.N. Evans, 2/94
120 FOS Aperture Transmissions for Point Sources, R.C. Bohlin, 2/94

* Draft version - not yet released.

Standard Calibration Source Instrument Science Reports

001 Updates to HST Standard Star Fluxes, R. Bohlin, & D. Lindler, July, 1992.
002 Preliminary Comparison of the HST and White Dwarf Absolute Flux Scales, R. Bohlin, December, 1993.

APPENDIX F

Exposure Logsheets

The RPS version of the Exposure Logsheets given in Appendix F can be copied from anonymous ftp (stsci.edu, or 130.167.1.2). The Logsheets are in the subdirectory proposer/documents/props_library. They are called fos_handbook5_example.

TARGET LIST a) Fixed Targets ID = version_5 [3]

1	2	3	4	5	6	7		8
Tar No	Target Name	Target Description	Target Position	Coord Eqnx	Radial Vel.	Acqui Prblm	FLX REF	Flux data
1	3C298 QUASAR	E,314	RA-OFF= 8.785' +/- 0.3", DEC-OFF= 20.9' +/- 0.3", FROM 2				1	V= 16.79, E(B-V)= 0.2
2	3C298-OFFSET	A,126	RA= 14H 16M 30S +/- 1", DEC= +6D 42' 0" +/- 1"	1950			1	V=15
Comments: A5 STAR USED FOR OFFSET.								
3	M81	E,301,919	RA= 9H 51M 30S +/- 10", DEC= +69D 18.3' +/- 10"	1950			1	V=18,E(B-V)=0.2
4	M81-OFFSET	A	RA-OFF= 0.05S +/- 1', DEC-OFF= 0' +/- 1, FROM 3, TBD-EARLY					
Comments: TO BE FOUND - OFFSET STAR.								
5	BRIGHT_STAR	A,111	RA= 2H 16M 28S +/- 1", DEC= +43D 51' 56" +/- 2"	1950			1	V=14,TYPE=B3V,E(B-V)=0.5
6	AE-AQR	A,151,154,161	RA= 20H 40M 9.02S +/- 0.5", DEC= -0D 52' 15.5" +/- 0.5", PLATE-ID=02C4	J2000			1	V= 10.8 +/- 1.1
7	0405-123	E,314	RA= 4H 5M 27.45S +/- 1", DEC= -12D 19' 31.8" +/- 1"	1950			1	V=14.82
8	MRK421	E,316	RA= 11H 1M 40.57S +/- 1", DEC= +38D 28' 43" +/- 1"	1950			1	V=13.5
9	WD0501+527 G191-B2B GSSS3734-050 6	J,705,702	RA=05H 05M 30.6S +/- 0.01S, DEC=+52D 49' 54.0" +/- 0.2"	2000			1 2 3	V = 11.78 +/- 0.02 B = 11.44 +/- 0.02 U = 10.24 +/- 0.02
Comments: THE GUIDE STAR CATALOG NAME IS GIVEN.								
Epoch of Position J 1983.10		RA proper motion (seconds of time/yr) 0.0075 +/- 0.0050	DEC Proper Motion (arcsec/yr) -0.0880 +/- 0.0050					Annual Parallax (arcsec) 0.0000 +/- 0.0000

EXPOSURE LOGSHEET

ID = version_5 [4]

1 Line Number	2 Seq Name	3 Target Name	4 Instr Config	5 Oper. Mode	6 Aper or FOV	7 Spectral Element	8 Central Waveln.	9 Optional Parameters	10 Num Exp	11 Time	12 S/N Rel. Time	13 Flx Ref	14 Pr	15 Special Requirements
1		3C298-OFFSET	FOS/RD	ACQ/BINARY	4.3	MIRROR			1	2.41S		1	3	ONBOARD ACQ FOR 2 CYCLE 5 / 1-18.1
2		3C298	FOS/RD	ACCUM	0.5	G780H	7800		1	600S	10	1	3	
Comments: SIGNAL_TO_NOISE IS PER DIODE.														
3		MRK421	FOS/RD	ACQ/BINARY	4.3	MIRROR		BRIGHT=57500 FAINT=1100	1	0.66S		1	3	ONBOARD ACQ FOR 4 GROUP 3-4.3 NO GAP
Comments: BLUE SIDE ACQ BIN- EXP=0.83 SEC. USE DEFAULT BRIGHT AND FAINT LIMITS.														
4		MRK421	FOS/RD	ACQ/PEAK	0.25x2.0	G190H		SCAN-STEP-X=.057 SEARCH-SIZE-X=9 SEARCH-SIZE-Y=1	1	0.3S			1	ONBOARD ACQ FOR 4.1-4.2
4.1		MRK421	FOS/RD	ACCUM	0.25X2.0	G190H			1	300S			1	
4.2		MRK421	FOS/BL	ACQ/PEAK	0.25x2.0	G190H		SCAN-STEP-X=.057 SEARCH-SIZE-X=9 SEARCH-SIZE-Y=1	1	0.6S			1	ONBOARD ACQ FOR 4.3
Comments: SIDE SWITCH.														
4.3		MRK421	FOS/BL	ACCUM	0.25X2.0	G130H			1	300S			1	
5		M81	WFC	IMAGE	ALL	F606W			1	60S		1	1	EARLY ACQ FOR 6-8.1
6		M81-OFFSET	FOS/BL	ACQ/BINARY	4.3	MIRROR			1	TBD		1	1	SEQ 6-8.1 NO GAP ONBOARD ACQ FOR 7-8.1
7		M81	FOS/BL	ACCUM	0.5	G190H	1900		1	3000S	10	1	1	
Comments: SIGNAL_TO_NOISE IS PER DIODE.														
8		M81	FOS/BL	ACQ	4.3	MIRROR			1	200S		1	1	
Comments: FOS ACQIMAGE OF FIELD OF VIEW.														
8.1		M81	FOS/BL	IMAGE	0.3	G400H		Y-SIZE=3 Y-SPACE=10.7 COMB=YES SUB-STEP=4	1	3600S	10		1	
Comments: SIGNAL_TO_NOISE IS PER PIXEL.														
10.3		BRIGHT_STAR	FOS/RD	ACQ/PEAK	4.3	G570H	5700	SCAN-STEP-Y=1.204 SEARCH-SIZE-X=1 SEARCH-SIZE-Y=3	1	0.17S			1	ONBOARD ACQ FOR 10.4

EXPOSURE LOGSHEET ID = version_5 [5]

1 Line Number	2 Seq Name	3 Target Name	4 Instr Config	5 Oper. Mode	6 Aper or FOV	7 Spectral Element	8 Central Waveln.	9 Optional Parameters	10 Num Exp	11 Time	12 S/N Rel. Time	13 Flx Ref	14 Pr	15 Special Requirements
10.4		BRIGHT_STAR	FOS/RD	ACQ/ PEAK	1.0	G570H	5700	SCAN-STEP- X=.602 SCAN-STEP- Y=.602 SEARCH-SIZE-X=6 SEARCH-SIZE-Y=2	1	0.18S			1	ONBOARD ACQ FOR 10.5
10.5		BRIGHT_STAR	FOS/RD	ACQ/ PEAK	0.5	G570H	5700	SCAN-STEP- X=0.30 SCAN-STEP- Y=0.30 SEARCH-SIZE-X=3 SEARCH-SIZE-Y=3	1	0.19S			1	ONBOARD ACQ FOR 10.6
10.6		BRIGHT_STAR	FOS/RD	ACCUM	1.0	G570H	5700		1	1M			1	
11		AE-AQR	FOS/BL	ACQ/ PEAK	4.3	G190H		SCAN-STEP- Y=1.204 SEARCH-SIZE-X=1 SEARCH-SIZE-Y=3	1	0.07S		1	1	ONBOARD ACQ FOR 11.1
Comments:	VARIABLE TARGET. FAINTEST V MAG USED WITH 13,000 BB IN SIMULATION. EXPECT MIN 1000 COUNTS/DWELL.													
11.1		AE-AQR	FOS/BL	ACQ/ PEAK	1.0	G190H		SCAN-STEP- X=.602 SCAN-STEP- Y=.602 SEARCH-SIZE-X=6 SEARCH-SIZE-Y=2	1	0.08S		1	1	ONBOARD ACQ FOR 11.2
11.2		AE-AQR	FOS/BL	ACQ/ PEAK	0.3	G190H		SEARCH-SIZE-X=5 SEARCH-SIZE-Y=5 SCAN-STEP- X=0.172 SCAN-STEP- Y=0.172	1	0.09S		1	1	ONBOARD ACQ FOR 11.3
11.3		AE-AQR	FOS/BL	ACQ/ PEAK	0.3	G190H		SEARCH-SIZE-X=5 SEARCH-SIZE-Y=5 SCAN-STEP- X=0.052 SCAN-STEP- Y=0.052	1	0.90S		1	1	ONBOARD ACQ FOR 12
Comments:	CRITICAL ACQ/PEAK STAGE. EXP TO PRODUCE 10000 COUNTS/DWELL.													
12		AE-AQR	FOS/BL	RAPID	0.3	G190H		READ-TIME=8	1	300M			1	

EXPOSURE LOGSHEET ID = version_5 [6]

1	2	3	4	5	6	7	8	9	10	11	12	13	14	15
Line Number	Seq Name	Target Name	Instr Config	Oper. Mode	Aper or FOV	Spectral Element	Central Waveln.	Optional Parameters	Num Exp	Time	S/N Rel. Time	Flx Ref	Pr	Special Requirements
13		WD0501+527	FOS/RD	ACQ/ PEAK	4.3	G270H		SCAN-STEP- Y=1.204 SEARCH-SIZE-X=1 SEARCH-SIZE-Y=3	1	3.0S			1	ONBOARD ACQ FOR 13.1
13.1		WD0501+527	FOS/RD	ACQ/ PEAK	1.0	G270H		SCAN-STEP- X=.602 SCAN-STEP- Y=.602 SEARCH-SIZE-X=6 SEARCH-SIZE-Y=2	1	3.0S			1	ONBOARD ACQ FOR 13.2
13.2		WD0501+527	FOS/RD	ACQ/ PEAK	0.5	G270H		SEARCH-SIZE-X=3 SEARCH-SIZE-Y=3 SCAN-STEP- X=0.30 SCAN-STEP- Y=0.30	1	3.0S		1	1	ONBOARD ACQ FOR 13.3
13.3		WD0501+527	FOS/RD	ACQ/ PEAK	0.3	G270H		SEARCH-SIZE-X=4 SEARCH-SIZE-Y=4 SCAN-STEP- X=0.125 SCAN-STEP- Y=0.125	1	3.0S		1	1	ONBOARD ACQ FOR 13.4
13.4		WD0501+527	FOS/RD	ACCUM	0.5	G270H			1	276S			1	
14		0405-123	FOS/BL	ACQ/ BINARY	4.3	MIRROR			1	2.8S	17	1 3	1	ONBOARD ACQ FOR 15 SEQ 14-15 NO GAP
15		0405-123	FOS/BL	ACCUM	4.3	G270H	2700	POLSCAN=4B	1	22M	90	1 3	1	
16		WAVE	FOS/BL	ACCUM	0.3	G270H			1	DEF			1	
17		3C298	FOS/RD	ACQ/ PEAK	4.3	G270H		SCAN-STEP- Y=1.204 SEARCH-SIZE-X=1 SEARCH-SIZE-Y=3	1	3.0S			1	ONBOARD ACQ FOR 17.1
17.1		3C298	FOS/RD	ACQ/ PEAK	1.0	G270H		SCAN-STEP- X=.602 SCAN-STEP- Y=.602 SEARCH-SIZE-X=6 SEARCH-SIZE-Y=2	1	3.3S			1	ONBOARD ACQ FOR 17.2

EXPOSURE LOGSHEET ID = version_5 [7]

1	2	3	4	5	6	7	8	9	10	11	12	13	14	15
Line Number	Seq Name	Target Name	Instr Config	Oper. Mode	Aper or FOV	Spectral Element	Central Waveln.	Optional Parameters	Num Exp	Time	S/N Rel. Time	Flx Ref	Pr	Special Requirements
17.2		3C298	FOS/RD	ACQ/ PEAK	0.3	G270H		SEARCH-SIZE-X=5 SEARCH-SIZE-Y=5 SCAN-STEP- X=0.172 SCAN-STEP- Y=0.172	1	4.2S		1	1	ONBOARD ACQ FOR 17.3
17.3		3C298	FOS/RD	ACQ/ PEAK	0.7X2.0 -BAR	G270H		TYPE=DOWN SEARCH-SIZE-X=1 SEARCH-SIZE- Y=11 SCAN-STEP- Y=0.05	1	150S		1	1	ONBOARD ACQ FOR 18

Comments: CRITICAL PEAKDOWN.

18		3C298	FOS/RD	ACCUM	0.7X2.0 -BAR	G270H			1	6000S		1	3	

Appendix G

Post-COSTAR FOS Inverse Flat Fields

Charles D. (Tony) Keyes

This appendix provides plots of the flat field granularity structure for all high dispersion FOS detector/disperser combinations. These plots are of the *inverse* flat field, which is applied as a multiplicative operator in routine PODPS pipeline processing. The inverse flats shown are preliminary versions of the first post-COSTAR flat field reference files and are based upon standard star "superflat" observations obtained in early March, 1994.

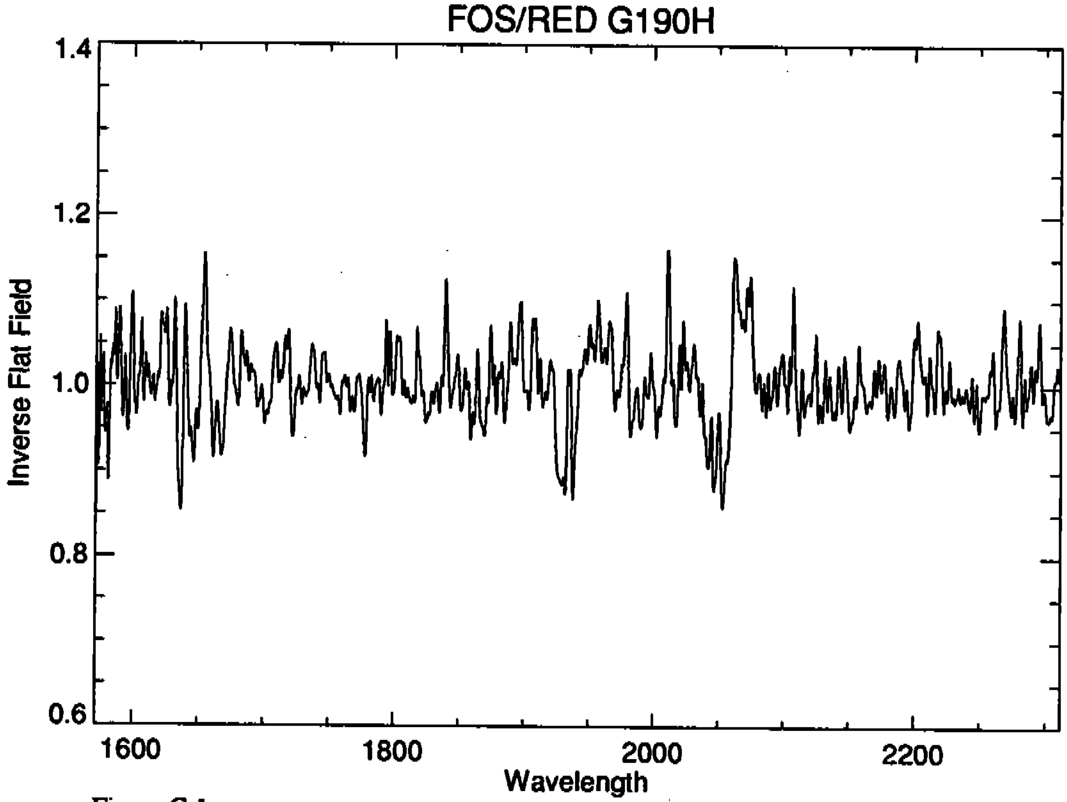

Figure G.1:

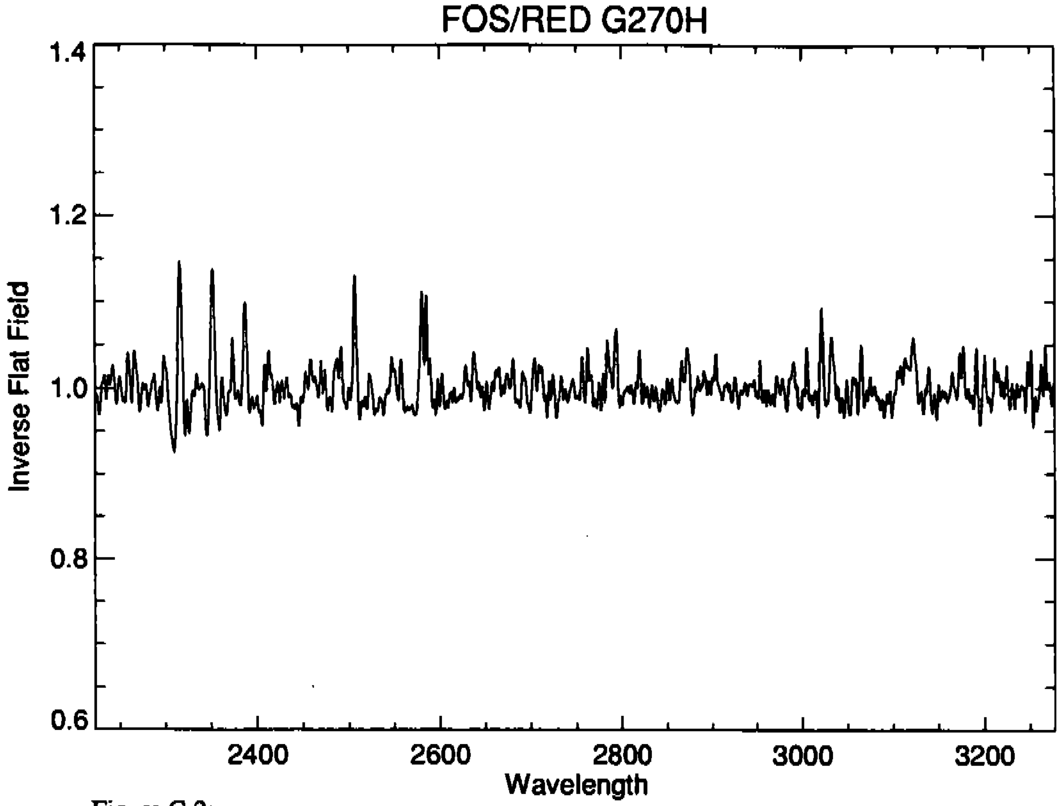

Figure G.2:

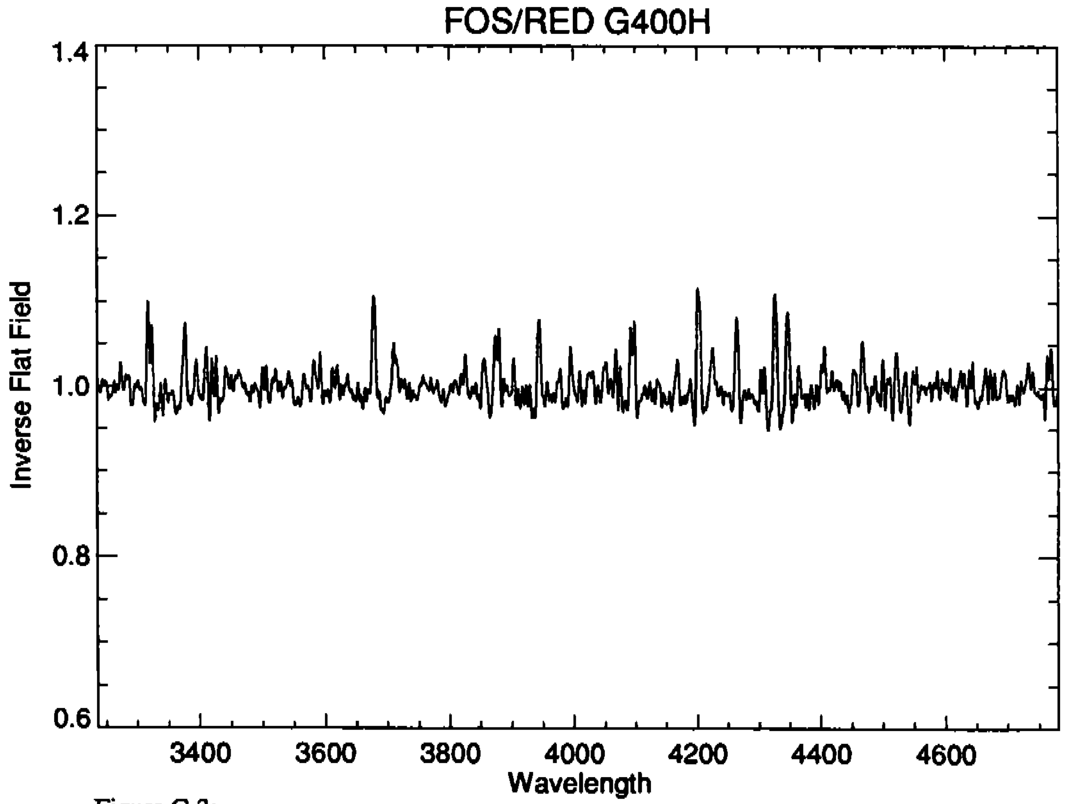

Figure G.3:

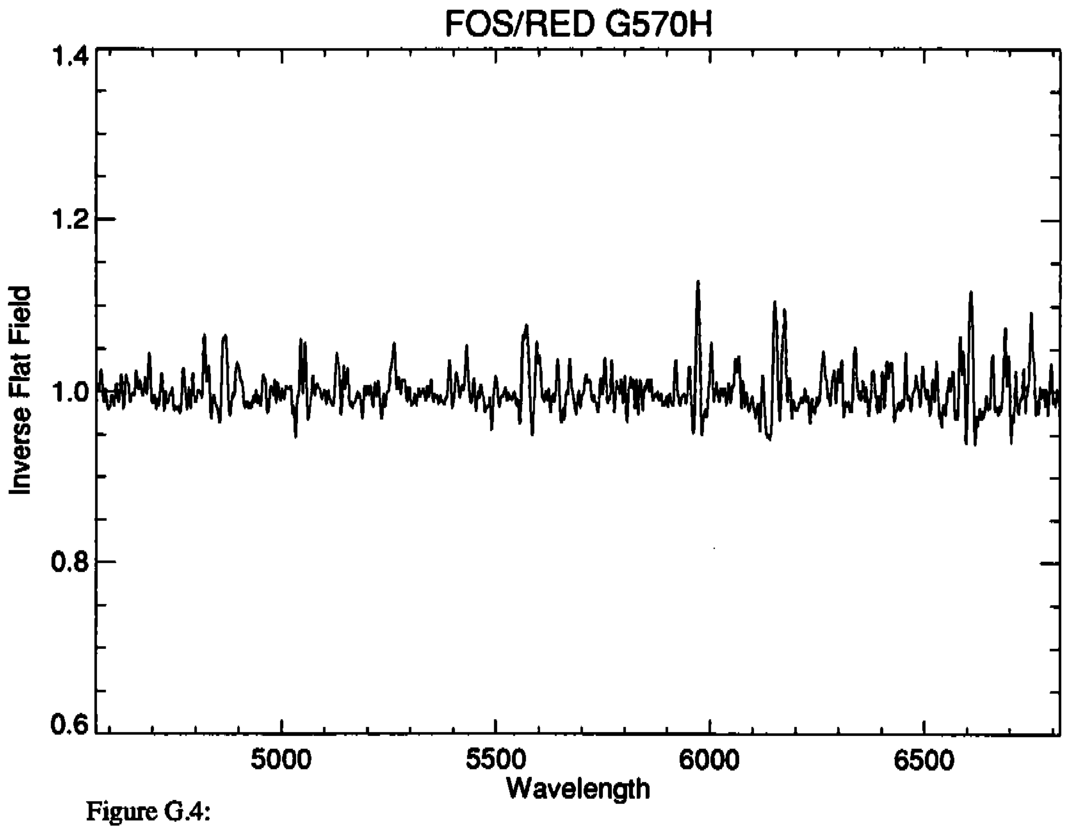

Figure G.4:

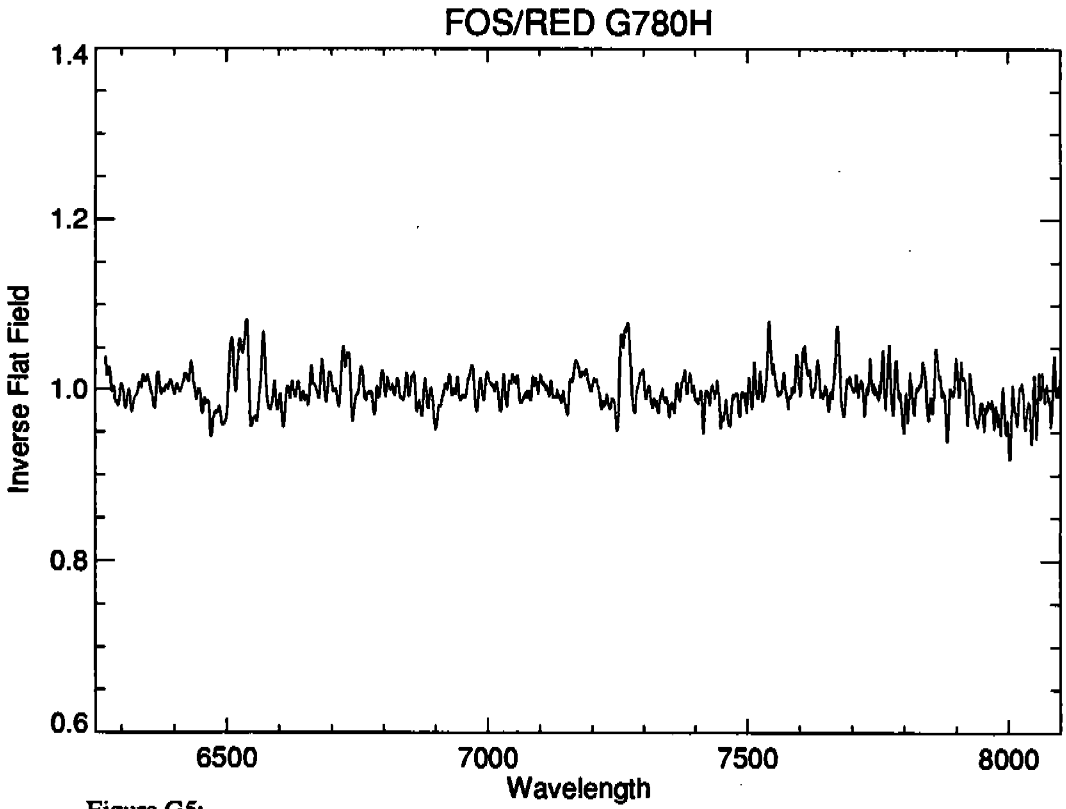

Figure G5:

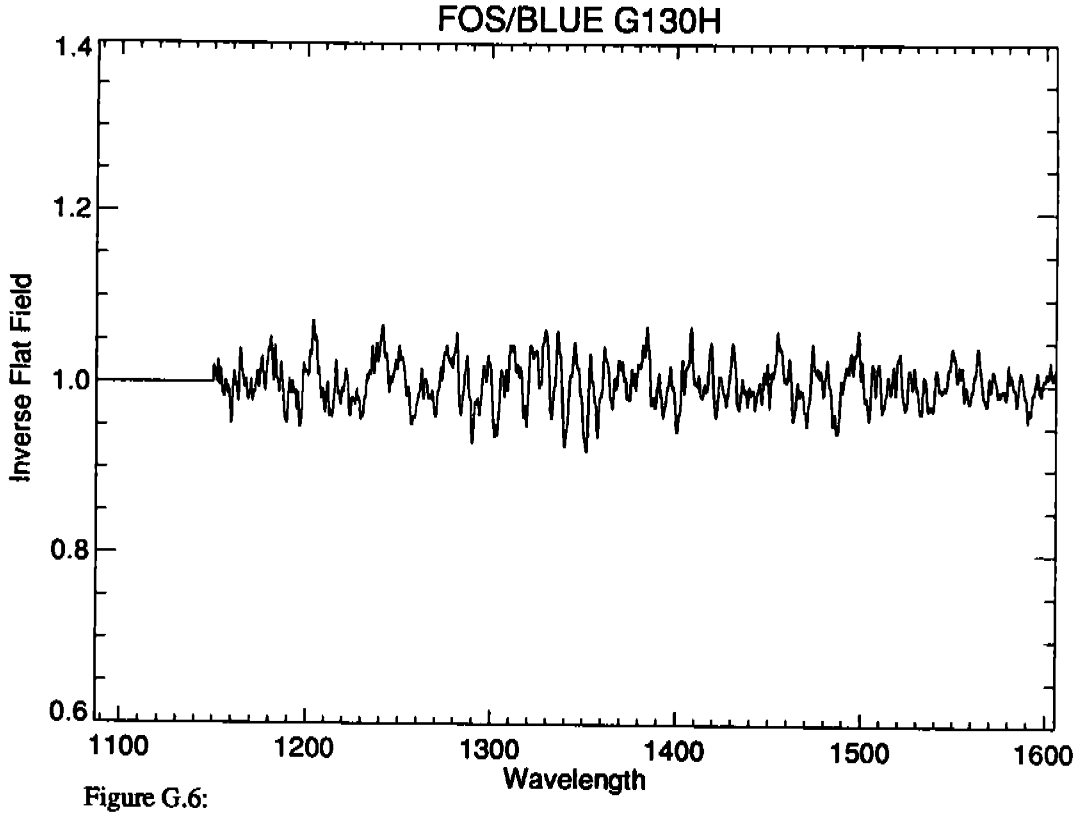

Figure G.6:

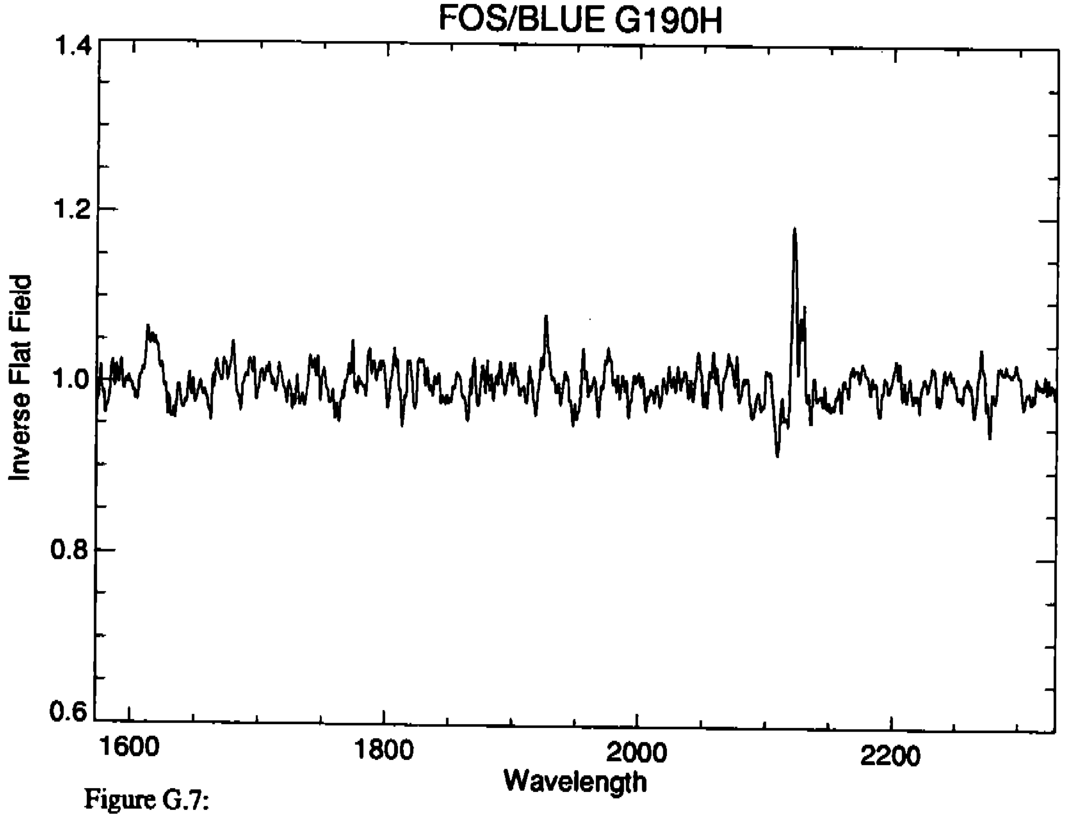

Figure G.7:

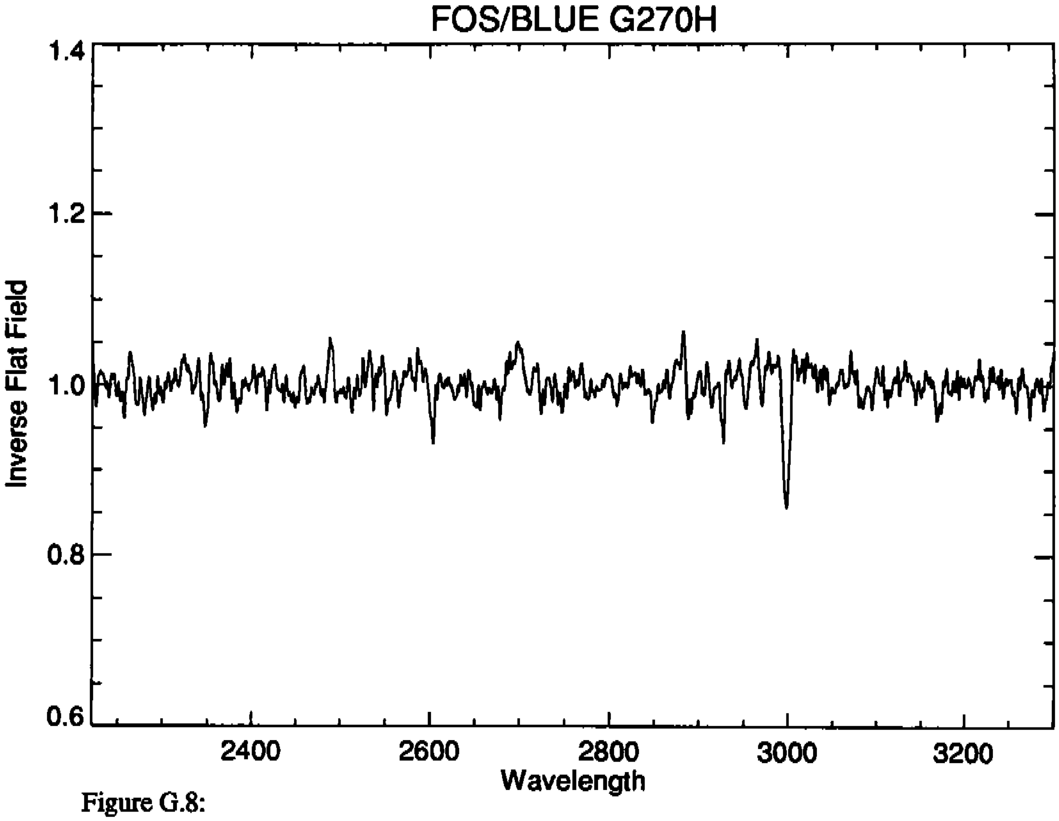

Figure G.8:

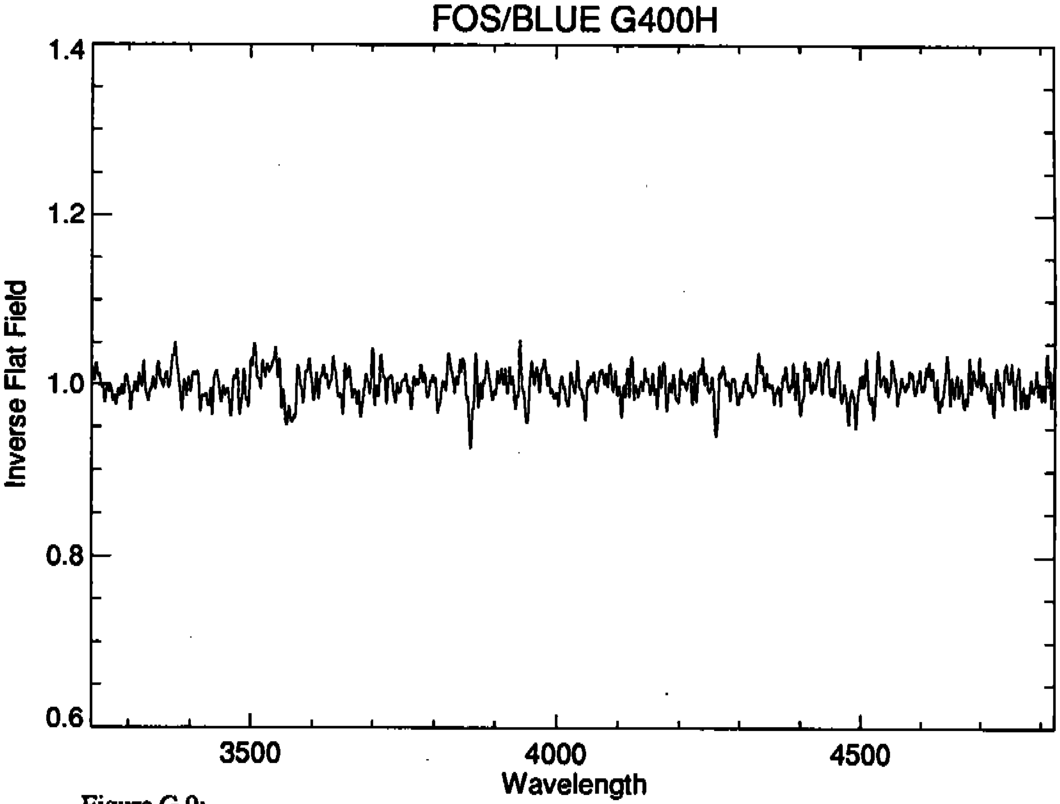

Figure G.9:

APPENDIX H

Changes to the Version 5.0 Instrument Handbook

- Figure 1.2.1. Updated HST + FOS + COSTAR efficiency.
- Figure 1.2.2. Updated aperture throughput.
- Figure 1.2.3. Updated observed counts per second per diode.
- Figure 1.4.1. Addition of duty cycle plot, for RAPID mode.
- Figure 2.1.0. Updated slews performed after FOS target acquisition.
- Figures 3.3.1, 3.3.2, and 3.3.3. Updated flat fields.

- Table 1.2.2.. Updated observed counts per second per diode.
- Table 2.1.1, 2.1.2, and 2.1.3. Updated FOS acquisition sequences.
- Table 2.1.6. Updated FOS exposure times.
- Table 4.1. Updated examples for simulation of FOS spectra.

- Appendix C, Scattered light, by M. Rosa.
- Appendix D, FOS Wavelength Comparison Spectra, by C.D.Keyes.